Exploration of Porphyrin-based Semiconductors for Negative Charge Transport Applications Using Synthetic, Spectroscopic, Potentiometric, Magnetic Resonance, and Computational Methods

by

Jeffrey Scott Rawson

Department of Chemistry
Duke University

Date:_____

Approved:

_____
Michael J. Therien, Supervisor

_____
David N. Beratan

_____
Alvin L. Crumbliss

_____
Martin C. Fischer

Dissertation submitted in partial fulfillment of
the requirements for the degree of
Doctor of Philosophy
in the Department of Chemistry in the Graduate School
of Duke University

2014

ABSTRACT

Exploration of Porphyrin-based Semiconductors for Negative Charge Transport Applications Using Synthetic, Spectroscopic, Potentiometric, Magnetic Resonance, and Computational Methods

by

Jeffrey Scott Rawson

Department of Chemistry
Duke University

Date:_____

Approved:

_____
Michael J. Therien, Supervisor

_____
David N. Beratan

_____
Alvin L. Crumbliss

_____
Martin C. Fischer

An abstract of a dissertation submitted in partial fulfillment of the requirements for the degree of Doctor of Philosophy in the Department of Chemistry in the Graduate School of Duke University

2014

Abstract

Organic π-conjugated materials are emerging as commercially relevant components in electronic applications that include transistors, light-emitting diodes, and solar cells. One requirement common to all of these functions is an aptitude for accepting and transmitting charges. It is generally agreed that the development of organic semiconductors that favor electrons as the majority carriers (n-type) lags behind the advances in hole transporting (p-type) materials. This shortcoming suggests that the design space for n-type materials is not yet well explored, presenting researchers with the opportunity to develop unconventional architectures. In this regard, it is worth noting that discrete molecular materials are demonstrating the potential to usurp the preeminent positions that π-conjugated polymers have held in these areas of organic electronics research.

This dissertation describes how an extraordinary class of molecules, *meso*-to-*meso* ethyne-bridged porphyrin arrays, has been bent to these new uses. Chapter two describes vis-NIR spectroscopic and magnetic resonance measurements revealing that these porphyrin arrays possess a remarkable aptitude for the delocalization of negative charge. In fact, the miniscule electron-lattice interactions exhibited in these rigid molecules allow them to host the most vast electron-polarons ever observed in a π-conjugated material. Chapter three describes the development of an ethyne-bridged

porphyrin-isoindigo hybrid chromophore that can take the place of fullerene derivatives in the conventional thin film solar cell architecture. Particularly noteworthy is the key role played by the 5,15-bis(heptafluoropropyl)porphyrin building block in the engineering of a chromophore that, gram for gram, is twice as absorptive as poly(3-hexyl)thiophene, exhibits a lower energy absorption onset than this polymer, and yet possesses a photoexcited singlet state sufficiently energetic to transfer a hole to this polymer. Chapter four describes synthetic efforts that expand the repertoire of readily available *meso*-heptafluoropropyl porphyrin building blocks. The findings suggest that the remaining challenges to the exploitation of these pigments will be overcome by a sufficiently firm grasp of their subtle electronic structures, and a willingness to eschew the customary strategies of chromophore assembly.

For Rachael, whose support proved to be the vital reagent that allowed me to reach this point.

For Julius, who reminds me that there is more to life than one's career.

For Hilton, who was the first person to suggest that I could actually do this.

Contents

List of Tables

List of Figures

Acknowledgements

Writing in this section is fraught with the peril that an important person might be forgotten. If you don't see your name here, please know that this is the last piece of a long document and I am exhausted; it's probably not personal. If you are a current Therien graduate student, the important insights are further on in the document, scroll down to find the answers to your questions, and for heaven's sake send me an email so I can explain more completely. If you want to learn more about porphyrin oligomer synthesis, read Paul Frail's dissertation, and if you want to learn more about porphyrin spectroscopy and electronic structure, read Tim Duncan's dissertation.

Thanks are due first to my parents. I think that at this point, you are having trouble believing that this is about to end successfully. That's understandable. You managed not to reveal any lingering doubts you might have had, and you gave me a foundation upon which I have drawn many times during this long pursuit. While I am acknowledging family, I should also mention Rachael, who suffered through my graduate education at least as much as I did. The entire Elliott clan has demonstrated remarkable understanding and support, for which I am grateful.

I am also grateful to Hilton Weiss and Simeen Sattar. When I was a student at Bard College I exhibited no particular aptitude for academic science, yet they indulgently guided me through five years that must have looked to them like a train

wreck, and only suggested once or twice that I might consider a different major. Their nurturing got me through that experience, and their encouragement prevented me from giving up on a graduate degree.

Thanks to all my senior labmates whose mentorship guided my development. Animesh, you are the handsomest man to ever work in a hood next to mine; you taught me to use the glovebox and to freeze-pump-thaw, and I am forever in your debt. Pravas, you demonstrated how to set one's sights on big picture research, and showed that sometimes This Is What It Is. Jaehong, your soulful sigh still rings in my ears; your help with the fundamentals of spectroscopy and Origin™ were invaluable. Jennifer, you were a paragon of patience in the face of infinite frustrations, and before my eyes you used the scientific method to extract sensible mechanisms from messy, shapeless rocks. Ying Ma, you seemed to draw upon an inexhaustible font of positive energy in the face of endless failed polymer functionalization reactions. "Mark" Zhenyuan Zhang, you were legendary.

Several of my junior colleagues were also very significant to my development, by granting me an opportunity to serve as a mentor and setting their own examples of resolute perseverance in the face of the imperfect. I have been amazed to see how far you have come in just a few years. Ruobing, I'll never forget the time you made a disaster, and I'll always be impressed with your ability to turn around and recover after a disappointment; never lose that smile. Ting, I envy your ability to be unfazed, and I'm

grateful for the times you boosted my confidence. Yusong, I enjoyed the similarities of our temperaments and I hope you will remain ambitious.

A few of my contemporaries cannot escape mention here. Nick, the only word that seems appropriate is 'profound', and that about sums it up. Jong and Hyejin, I know I shouldn't lump you together, but you are just so well matched; your good humor has lightened many moments. Jean-Hubert, mon frère, many of the things I would like to say to you are not printable here. You truly are my brother. We got through so much together, and we'll always have the Funk Show; take care of your breast.

I would also like to acknowledge several faculty from UNC Chapel Hill who positively impacted my time here. Wei You has been an excellent and supportive collaborator ; Tom Meyer tolerated me even though collaborations between us never worked out ; Malcolm Forbes was an inexhaustible and ever-generous font of knowledge regarding EPR instrumentation, a shining personal example, and came even to my dissertation defense, where he contributed to the committee discussion ; Shubin Liu and Cindy Schauer provided mentorship and support as I developed experience in computational chemistry.

I was fortunate to have, in effect, a second 'bonus' adviser for my graduate studies who I had essentially to myself. Paul A., your enthusiasm and strength of

personality are buoyant. The mentorship and friendship you provided were indispensible to me. Thanks so much for everything.

Finally, it would be the most grievous error if I forgot to mention my gratitude to Mike. I'll never know whether you had a hand in getting me into Duke, or if that was just a gross oversight on the part of the admissions committee, but joining your lab gave me a third chance at a PhD that I really didn't deserve. When I started, I did not understand even the origin of an electronic absorption spectrum, and I couldn't get through the abstract of one of your papers. Working in the Therien lab, I was always encouraged to dig into matters more deeply, and I was allowed to pursue new areas of knowledge instead of being pigeonholed.

1. Introduction

The purpose of this introduction is to offer a brief explanation of the terminology and the organization of this dissertation. I have chosen not to write any sort of comprehensive review, because it would become out of date quite soon after publication. Reviews of all the subjects covered in this dissertation are readily found by literature searches; more information about the synthesis of multiporphyrin arrays can be found by reading the dissertation of Paul Frail, and the dissertation of Timothy Duncan contains a comprehensive review of porphyrin spectroscopy.

1.1 Supermolecules

The chapters of this dissertation make several mentions of "supermolecules", but they do not contain an explicit definition of the term. In the context of this work, supermolecules are chromophores comprised of multiple pigment units attached to each other by ethyne bridges. The strong coupling provided by these bridges causes the π-electron systems of the individual dye motifs to merge together, so that electronic states are delocalized over the entire system. Thus, each molecule is just one chromophore, giving rise to spectroscopic and electronic behaviors that are not simple sums of the constituent parts. The canonical examples of this from within our research group are the multiporphyrin arrays,[1] the (polypyridyl)metal-porphyrin conjugates,[2] and the proquinoidal-bridged diporphyrins.[3]

The term "supermolecule" can lead to confusion with supramolecular chemistry. In fact, Lehn often used the terms supermolecule and supramolecule almost interchangeably.[4] Supramolecular chemistry is defined as the chemistry of the intermolecular bond, in which noncovalent interactions associate two or more molecules in a designed fashion. In supramolecular arrays, the electronic coupling between subunits is generally weak, and supramolecular complexes give rise to localized electronic states and behaviors that trace their geneses to individual substructures. The two distinctions between these supramolecular structures, and the compounds referred to as supermolecules in this dissertation, are thus i) supramolecular assemblies are held together noncovalently, while our supermolecules are single covalently-bonded molecules, and ii) supramolecular assemblies may feature several chromophores with individual, localized electronic structures, while our supermolecules are single chromophores with delocalized electronic structures.

1.2 Potentiometric scales and terminology

One significant theme throughout this work is the potentiometric manipulation of π-conjugated molecules to generate charged species. Chapter two describes the direct study of the anion radicals of multiporphyrin arrays; Chapter three describes two novel compounds, distinguished from each other primarily by the fact that one is capable of photooxidizing poly(3-hexyl)thiophene; Chapter four describes the synthesis of a

porphyrin whose defining characteristic is redox potentials that are unusual due to its (*meso*-heptafluoropropyl)substituents.

Throughout these chapters, electrochemically-determined potentiometric data are reported with reference to the ferrocene/ferrocenium ($Fc^{0/+}$) couple, which was used as an internal standard in all experiments. Authoritative voices have endorsed the universal application of $Fc^{0/+}$ as the standard reference for electrochemical measurements performed in organic solvents.[5] Potentiometric responses were generally measured using cyclic voltammetry, and so the numbers reported are usually averages ($E_{1/2}$) of the voltages at the anodic (E_{pa}) and cathodic (E_{pc}) current peaks. It is generally true that $E_{1/2}$ lies within a few millivolts of the formal potential $E^{0\prime}$.[6]

A classic convention of inorganic electrochemistry is to present potentiometric responses as reductions, stemming from the discipline's origins in polarography;[7] this is evident in the symbols still used for these potentials, $E^{-/0}$, $E^{2-/-}$, $E^{0/+}$, $E^{+/2+}$, etc. While these symbols will be used throughout this dissertation, a more modern convention is applied to the textual descriptions of potentiometric responses: when a species in its described "ground" state (usually neutral) loses an electron, an oxidation potential is mentioned, and when a species in its described "ground" state (usually neutral) gains an electron, a reduction potential is mentioned. These terms provide a sense of directionality, which may be arbitrary in some cases but is often useful to the reader.

1.3 n-Type materials

The projects included in this dissertation can all be contained under the umbrella of efforts to develop next-generation organic electron-transport media, or, to rephrase, semiconductors that feature high negative-charge mobilities or "n-type" materials. Semiconductors are distinguished as materials with conductivities between ~10^0 and ~10^{-6} S/cm; metals are more conductive and insulators less so.[8]

Semiconductors are useful because there are often ways to dynamically manipulate their conductivities, permitting their use in transistors, switches, and sensors, and many absorb and emit electromagnetic radiation. The most prevalently used semiconducting materials for commercial applications remain group IV elements such as silicon and germanium, or compounds of group III and group V elements. Nevertheless, π-conjugated organic compounds are considered to be promising alternatives to inorganic semiconductors, and while few commercial products currently exploit these materials, many major companies have organic electronics divisions.

As a broad generalization, most of the well-performing organic semiconductors currently known transport positive charges more readily than they do negative charges; they are thus more p-type than n-type. The line between p-type and n-type organics is not sharp or absolute, and electron mobilities can be measured for all of these materials. However for many n-type applications, the best known π-conjugated organic materials evince electron mobilities too low, and reduction potentials too negative, to be useful.

One prototypical p-type organic material is poly(3-hexyl)thiophene (P3HT); this polymer has an oxidation potential of 0.36 V and a reduction potential of -1.72 V (vs $Fc^{0/+}$, Chapter three). Any material to be used in the role of accepting an electron from P3HT should have a reduction potential less negative than ~-1.6 V. While there is no absolute correlation, it has been generally found that materials with high electron mobilities are also those with more modest reduction potentials.[9]

1.4 Goals of the dissertation

The subjects selected for inclusion herein tell a story about the adaptation of porphyrin-derived supermolecules as n-type materials. My reasons for pursuing this research are simple: n-type π-conjugated materials are less prevalent than their p-type counterparts, and monodisperse molecules demonstrate the potential to usurp the place of polymers in organic electronics. *Meso*-to-*meso* ethyne-bridged porphyrin oligomers, in particular, have exhibited an adaptability to solid-state applications,[10] and in fact may represent an architecture of unrivaled utility for photonic and electronic functions.

Chapter two describes vis-NIR spectroscopic and magnetic resonance measurements revealing that these porphyrin arrays possess a remarkable aptitude for the delocalization of negative charge. In fact, the miniscule electron-lattice interactions exhibited in these rigid molecules allow them to host the most vast electron-polarons ever observed in a π-conjugated material. This might be characterized as a primarily

analytical study that reveals a capacity for n-type applications that had not been heretofore expected of porphyrin derivatives.

Chapter three describes the development of an ethyne-bridged porphyrin-isoindigo hybrid chromophore that can take the place of fullerene derivatives in the conventional thin film solar cell architecture. Particularly noteworthy is the key role played by the 5,15-bis(heptafluoropropyl)porphyrin building block in the engineering of a chromophore that, gram for gram, is twice as absorptive as poly(3-hexyl)thiophene, exhibits a lower energy absorption onset than this polymer, and yet possesses a photoexcited singlet state sufficiently energetic to transfer a hole to this polymer. Thus, this chapter presents a multidisciplinary materials-science study which points to the utility of porphyrin-based compounds in an organic electronics application.

Chapter four describes synthetic efforts that expand the repertoire of readily available (*meso*-heptafluoropropyl)porphyrin building blocks. The findings suggest that the remaining challenges to the exploitation of these pigments will be overcome by a sufficiently firm grasp of their subtle electronic structures, and a willingness to eschew the customary strategies of chromophore assembly. This is, in effect, an agglomeration of synthetic results, successful and abortive. Also appearing here are some interesting computational results and proposals for the most promising routes to attain (*meso*-heptafluoropropyl)porphyrin arrays.

Historically, dissertations provided the definitive accounts of the doctoral research. They were comprehensive, containing many details and even entire projects that were not included in publications. This has not been the goal here; instead subjects were selected for this dissertation based upon their adherence to a narrow theme. Two appear in very similar form to publications, while the last clearly does not. Readers who desire further information and insights are encouraged to consult my notebooks, which might occasionally be marginally helpful, or better, to contact me directly. My mentorship skills have been endorsed by authoritative voices, including Dr. Dude (Figure 1).

Figure 1. Dr. Dude, as featured in the 1990 pinball game machine of the same name. (Warning: this image is not appropriate for the workplace. Dr. Dude is not a board-certified medical doctor.)

2. Unsurpassedly vast electron-polarons in conjugated porphyrin arrays

Jeff Rawson synthesized all compounds, designed the apparatus for and performed all reduction experiments, processed and interpreted all spectroscopic data, orchestrated the calculations, and drafted the manuscript.

Paul J. Angiolillo provided access to and instruction with the ESR instrument, supervised interpretation of ESR data, and contributed to writing the manuscript.

Michael J. Therien conceived the study, supervised the execution of all experiments, and wrote the final version of the manuscript.

2.1 Introduction

Organic π-conjugated materials are approaching commercial success in devices such as photovoltaics, field-effect transistors, and especially light-emitting diodes;[11] they are infiltrating spintronics research as well.[12] Facilitating this ascendance is the advent of structures that extensively delocalize charges over rigid sp^2 frameworks, minimizing the intramolecular electron-phonon coupling (internal reorganization energy, λ_i);[13, 14] this allows these organic materials to accommodate and transmit charges in spite of dielectric constants that are low (1 -3). Particular current interest in organic electron transport media (n-type materials)[9] fuels ongoing exploration into the fundamental properties of the electron-polaron, a negatively charged, spin ½ excitation and its associated lattice deformation.[15, 16] Here, we describe radical anion (n-doped) π -conjugated multiporphyrin arrays to reveal unsurpassedly vast electron-polarons. This

discovery signals that electron-lattice couplings are extraordinarily weak in n-doped porphyrin oligomers; because these couplings contribute to interchain hopping rates,[17] the rate and efficiency for photogeneration of charge-separated states,[18] and the strength of the hyperfine field,[19] our findings identify a conjugated material uniquely suited for a broad swath of commercial and emerging applications.

2.2 Results

The polaron is the principle charge carrier in organic electronic media, as observed by electron spin resonance (ESR) measurements on field-effect devices.[20, 21] The inverse relationship between the number of π-conjugated atoms over which a polaron is delocalized and the associated λ_i connects polaron dimension directly with thermal barriers to hopping transport.[17] One class of conjugated materials that displays exceptional transport properties as evinced by break junction single molecule conductance measurements is *meso*-to-*meso* ethyne-bridged (porphinato)zinc(II) oligomers (**PZn$_n$**, Figure 2)[22] and related butadiyne-bridged counterparts;[23] indeed, variable-temperature solution-phase X-band ESR spectroscopic studies of p-doped **PZn$_n$** showed that [**PZn$_n$**]$^{\bullet+}$ structures define the longest hole polarons yet measured for a conjugated material (~7.5 nm).[24] Furthermore, 2-probe dark conductivity measurements on undoped films of suitably engineered **PZn$_n$** revealed dark conductivities of 3.8×10^{-5} S/cm,[10] greater than those found for poly(3-hexyl)thiophene (3×10^{-7} S/cm)[25] or

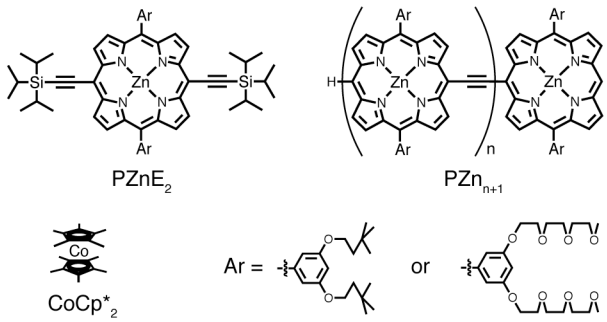

Figure 2. Structures of PZn$_n$ structures and decamethylcobaltocene (CoCp$^*_2$).

crystalline polyacetylene (1×10^{-5} S/cm).[26] Taken together, these previous findings establish exceptional hole-transport capabilities for **PZn$_n$**, but this material's potential for n-type applications has yet to be explored.

In the current study, electron-polaron states of **PZn$_n$** compounds were chemically generated using decamethylcobaltocene ($CoCp^*_2$) in a custom airfree apparatus that permitted parallel electronic absorption and ESR spectroscopic measurements. For these purposes, $CoCp^*_2$ was found to be an exemplary reagent; it has an oxidation potential of -1.86 V vs ferrocene in tetrahydrofuran, weak and featureless visible-range electronic absorptions,[27] and, like cobaltocene,[28] evinces no observable ESR spectrum at room temperature. The n-doping of **PZnE$_2$** with $CoCp^*_2$ (Figure 3) produced features in the electronic absorption spectrum that are characteristic of a porphyrin anion radical (electron-polaron), including diminution of the neutral species absorptions and the emergence of several peaks in the 600-900 nm domain.[29]

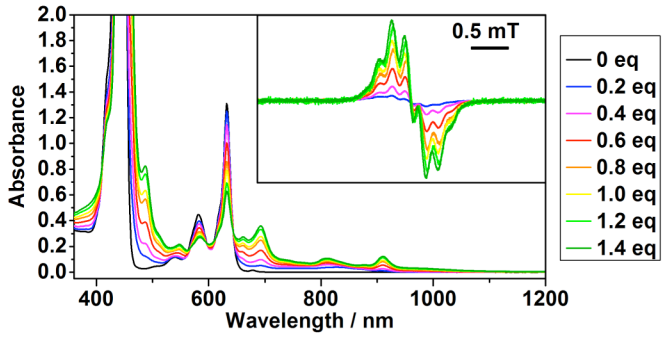

Figure 3. Electronic absorption spectra recorded during n-doping of PZnE$_2$ with $CoCp^*_2$ in THF at room temperature. (inset) ESR spectroscopic measurements for each doping step.

Concomitant with the appearance of these vis-NIR spectral features, ESR measurements revealed a paramagnetic signal at g = 2.0008±0.0002.

The ESR spectra of D_{4h} porphyrins are broadened by the Jahn-Teller effect into Gaussian envelopes with peak to peak linewidths ($\Delta B_{p\text{-}p}$) ~ 2 mT due to the degeneracy of the ^2E_g state.[30, 31] The ESR spectrum of **[PZnE$_2$]$^{\bullet-}$**, with $\Delta B_{p\text{-}p}$ of under 0.6 mT and partially resolved hyperfine features, reveals that the two ethyne substituents relieve the orbital degeneracy sufficiently to obliterate this effect;[32] microwave power saturation experiments confirm the absence of Jahn-Teller mediated spin relaxation for this species. For porphyrin anion radicals whose orbital degeneracies are lifted sufficiently to relieve

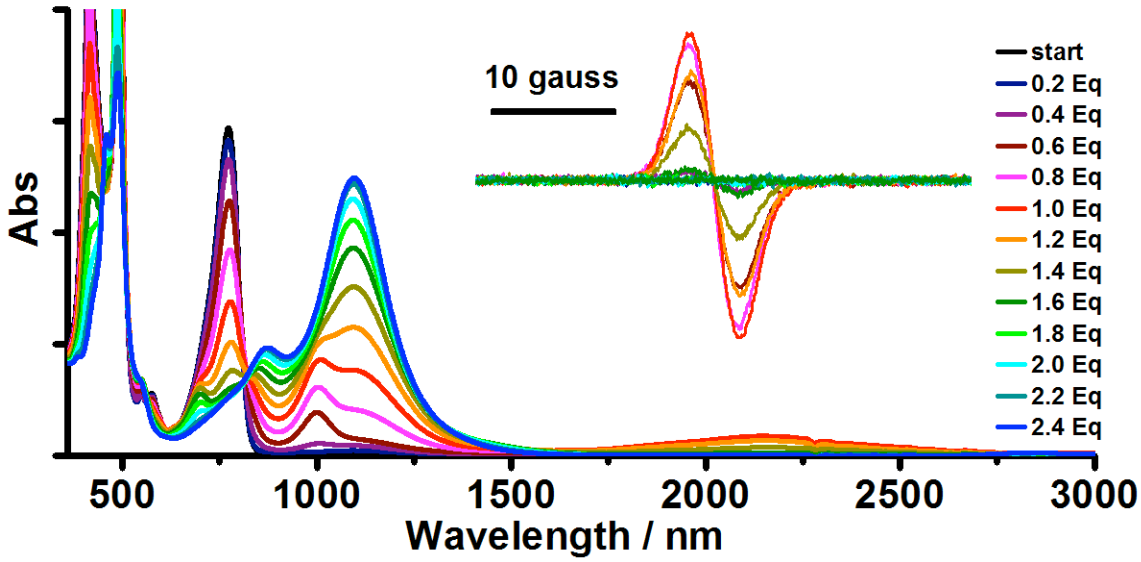

Figure 4. Spectroscopic measurements recorded during the electron doping of PZn$_3$ with permethylcobaltocene in THF solvent. The larger graph plots the electronic absorption spectra, and the inset chronicles ESR measurements. Equivalents of permethylcobaltocene added are noted on the right side.

Jahn-Teller broadening, the strongest hyperfine interactions are with peripheral protons, principally at the *meso* positions.[32] The **[PZnE$_2$]$^{\bullet-}$** spectrum displays couplings to the beta protons proximal to the ethyne and aryl groups of -0.56 and 0.23 mT, respectively, and density-functional theory (DFT) calculations suggest that significant spin density lies on the ethyne carbons.

For the **PZn$_n$** compounds, n-doping with CoCp*$_2$ evoked electronic absorptions between 800 – 3000 nm [1.55 – 0.41 eV] and ESR signals whose intensities peaked for one electron per molecule (Figure 4). For **[PZn$_2$]$^{\bullet-}$** and **[PZn$_3$]$^{\bullet-}$**, further doping produced a diamagnetic product with no absorptions below 1200 nm; for **[PZn$_5$]$^{\bullet-}$** and **[PZn$_7$]$^{\bullet-}$**, additions of CoCp*$_2$ beyond one electron per molecule led to diminution and broadening of ESR spectra and reduced NIR peaks. For all compounds studied, no further changes were observed for n-doping beyond two electrons per molecule, and bubbling air through the solutions resulted in reversible oxidation to the neutral **PZn$_n$** spectra. These observations are consistent with the formation of electron-polarons at lower doping levels, with further doping producing spinless bipolaron species on shorter oligomers and side-by-side polaron pairs on longer **PZn$_n$**, as observed previously for oligofluorenes.[15] An alternating least squares curve resolution analysis[33] deconvoluted the NIR spectral features associated with **[PZn$_n$]$^{\bullet-}$**, using the neutral spectra as constraints and starting with concentration profiles derived from the integrated ESR intensities.

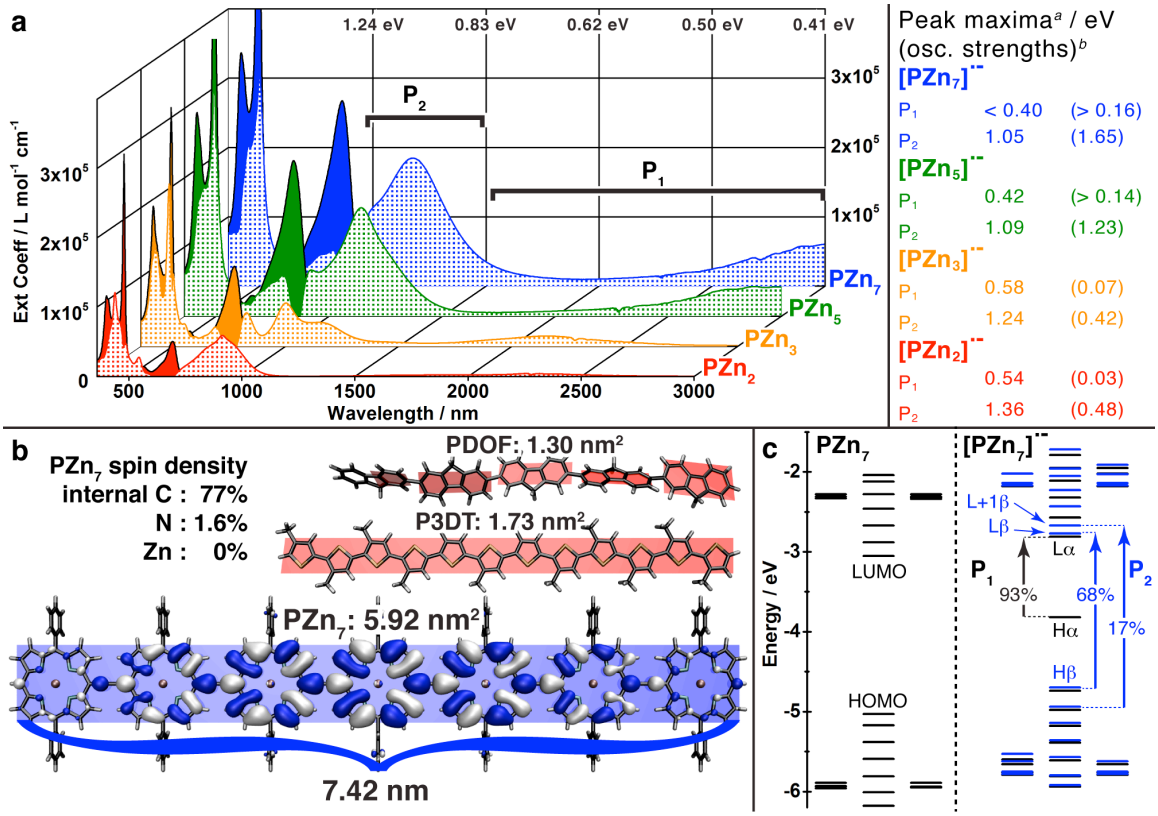

Figure 5. a. Absorption spectra of PZn_n neutral (solid fill) and anion radical states (checked fill) in THF solvent; polaron bands P_1 and P_2 are labeled. b. Comparison of electron polaron areas for PZn_7 and conjugated polymers poly(3-decyl)thiophene (P3DT) and poly(9,9′-dioctyl)fluorene (PDOF). For PZn_7 the SOMO is depicted as an 0.007 isodensity surface to illustrate the extent of the anion radical state; the spin density population is broken down into percentages that can be assigned to internal C atoms (no bonds to H), N atoms, and Zn atoms. c. Energy level diagrams for neutral and n-doped PZn_7, with vertical arrows depicting one-electron configurations that contribute to the principle NIR transitions predicted for $[PZn_7]^{\bullet-}$ by TDDFT calculations. ***a) note that peak maxima do not reflect [0,0] transition energies due to the vibronic and electronic complexity of the polaron spectra b) details of oscillator strength determination reported in the methods section.***

The species associated spectra for **$[PZn_{2\text{-}7}]^{\bullet-}$** are displayed alongside the electronic absorption data for the neutral compounds in Figure 5a. Several trends are apparent in these NIR spectroscopic data: (i) the polaron states evince two principle absorption

manifolds of lower energy than those of the neutral oligomers, labeled as P_1 and P_2 in Figure 5a, (ii) the transitions in the 1000 – 3000 nm (1.24 – 0.41 eV) spectral window show oscillator strengths that increase with the number of porphyrin repeat units, analogously to the visible-range transitions for their neutral counterparts, and (iii) the lowest energy transition P_1 for **[PZn$_{2\text{-}7}$]$^{\bullet-}$** is progressively redshifted and intensified with increasing oligomer length. In the context of Furukawa's modification[34] to the one-electron band theory attributed to Fesser, Bishop and Campbell (FBC model),[35] P_1 and P_2 may be interpreted as intragap transitions between levels whose energies are associated with the degree of polaronic structural relaxation. In this regard, points (ii) and (iii) above are especially salient: these polaron bands show dependencies of their oscillator strengths and energy maxima upon oligomer length that remain unsaturated for the range of compounds explored here, implying that the effective conjugation length is not reached, even for **[PZn$_7$]$^{\bullet-}$**.

Time-Dependent DFT (TD-DFT) calculations using several common range-corrected hybrid functionals[15] show that the absorption spectra of **[PZn$_n$]$^{\bullet-}$** are only well represented using a model that delocalizes the highest-occupied majority spin orbital (HOMOα) over the entire porphyrin oligomers. Accurate simulations of the experimental NIR spectra employed the LC-ωPBE functional,[36] with values of the range-separation parameter ω tuned to provide strong agreement between simulated and observed spectra.[15] The most intense P_1-region transitions are of HOMOα → LUMOα

character, while the principle P_2-region transitions are dominated by HOMOβ → LUMOβ configurations (Figure 5c). The complexity of the experimental spectra is reflected in the prediction of numerous minor transitions.

A direct measure of electron-polaron dimensions in conjugated materials is provided by ESR measurements through the hyperfine interactions $H_{hf} = \Sigma_i A_{oi} S \cdot I_i$ (where S and I_i refer to the electron and nuclear spins, respectively, and A_{oi} denote the isotropic hyperfine coupling constants of spin-carrying nuclei). The ESR spectra for **[PZn$_{2\text{-}7}$]$^{\bullet-}$**, displayed in Figure 6a, show unresolved couplings that manifest approximately Gaussian line shapes; $\Delta B_{p\text{-}p}$ narrows from 0.60 mT for **[PZn$_2$]$^{\bullet-}$** to 0.22 mT for **[PZn$_7$]$^{\bullet-}$**. An important mechanism resulting in line width narrowing stems from the

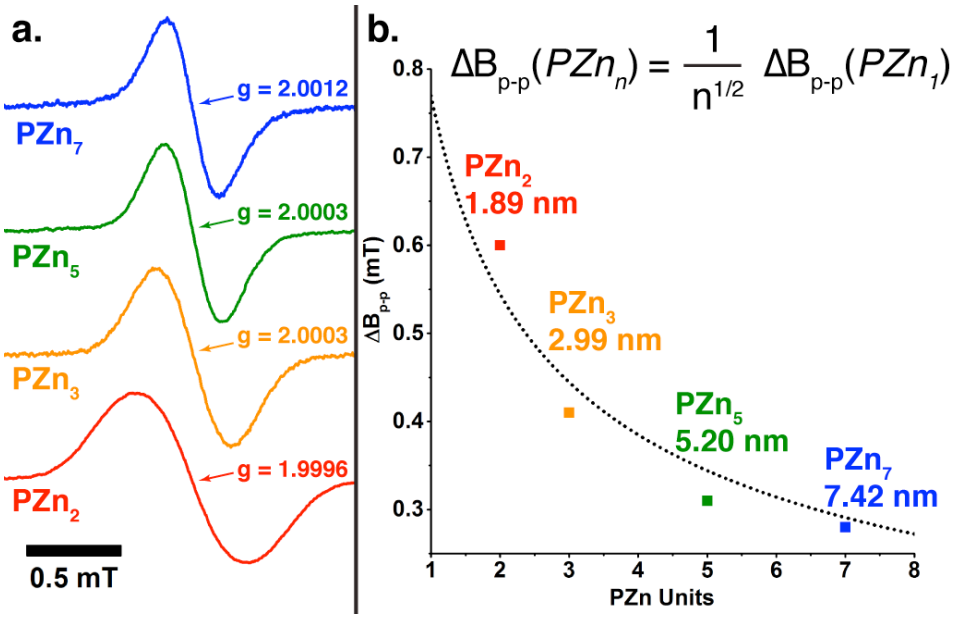

Figure 6. a. X-band ESR spectra of PZn$_n$ electron-polarons recorded at 298 K in THF solvent. b. (squares) Peak-to-peak line widths $\Delta B_{p\text{-}p}$ from ESR spectroscopic measurements on PZn$_n$ electron-polarons plotted as a function of PZn repeat units, and (dotted line) fit of $\Delta B_{p\text{-}p}$ to the Norris relationship.

averaging of the hyperfine field experienced by the spin system; this averaging originates from either coherent delocalization of the excitation, or incoherent hopping on a time scale more rapid than that associated with the hyperfine interaction (> ~1 MHz). Norris has shown that in the limit of stochastic, near-barrierless, one-dimensional charge hopping between N equivalent sites the theoretical line width is given by $\Delta B_{p\text{-}p}(N\text{-mer}) = (1/N^{1/2})\Delta B_{p\text{-}p}(\text{monomer})$.[19] The fit to this relationship for the ESR line width measurements on **[PZn$_{2\text{-}7}$]$^{\bullet-}$** directly assesses these spin systems to extend the full length of their porphyrin oligomers (Figure 6b).

Time-resolved radiolysis measurements of electron-polarons in conventional polymers have estimated spatial extents for [poly(3-decyl)thiophene]$^{\bullet-}$ (P3DT, 4.67 nm)[16] and [poly(9,9′-dioctyl)fluorene]$^{\bullet-}$ (PDOF, 3.55 nm)[15] that are about half of the 7.42 nm for **[PZn$_7$]$^{\bullet-}$**. Note that the **PZn$_n$** chain width is twice those of conventional conjugated materials; approximating each material as a two-dimensional ribbon (Figure 5b), the 5.92 nm^2 area of **[PZn$_7$]$^{\bullet-}$** dwarfs **[P3DT]$^{\bullet-}$** (1.73 nm^2) and **[PDOT]$^{\bullet-}$** (1.41 nm^2). The discovery of anomalously spacious electron-polarons in **PZn$_n$** compounds reveals that the electron-lattice coupling operating upon this system is extraordinarily weak.

The miniscule electron-lattice coupling in **[PZn$_n$]$^{\bullet-}$** has several profound, application-relevant implications. First, barriers for self-exchange reactions are low; using a four-point method,[37] we calculate λ_i = 91.4 meV for **[PZn$_2$]$^{\bullet-}$** and 79.9 meV for **[PZn$_5$]$^{\bullet-}$**, compared with λ_i = 107 meV for C_{60}. Because λ_i can impact charge mobility in

the solid state,[17] this observation is significant to all fields of organic electronics. Second, λ_i contributes to the total reorganization energy of electron transfer between donors and acceptors; minimization of this factor expedites charge separations with minimal driving forces ($-\Delta G^0 \sim 160$ meV) in the photosynthetic reaction center.[18] The engineering of photovoltaic devices to exploit low reorganization energies has been proposed as a strategy to double power conversion efficiencies by enhancing open-circuit voltages with no cost to short-circuit currents.[38] Third, the hyperfine and spin-orbit interactions become negligible, as indicated by narrow line widths, g-factors for longer **[PZn$_n$]$^{\bullet-}$** that approach the free electron value, and a spin-relaxation time for **[PZn$_5$]$^{\bullet-}$** of 3.2±0.4 μs at 298 K; given even conservative mobilities of 10^{-3} – 10^{-2} cm^2/Vs, spin diffusion length would be on the order of 100's of nm in **[PZn$_n$]$^{\bullet-}$**.[12]

2.3 Conclusion

In conclusion, we have discovered that vast electron-polarons can be generated in **PZn$_n$** compounds, as quantified by ESR measurements, NIR spectroscopic data, and computational evidence. The unusual dimensions of these charged defects reveal that the intrinsic electron-lattice coupling is extraordinarily low in this system. In light of previous work which showed that **PZn$_n$** structures can be engineered to provide spin-cast films with optimized conductivities and intermolecular order,[10] the intrinsic properties revealed herein are especially significant: *we suggest that highly-ordered ethyne-bridged chromophore arrays have the potential to usurp many of the roles of conventional,*

narrow-chain, flexible and inherently disordered conjugated polymers, ushering in a new generation of conjugated materials inherently suited to their applications.

2.4 Methods

2.4.1 Experimental methods

General materials: All manipulations were carried out under argon previously passed through an O_2 scrubbing tower (Schweitzerhall R3-11G catalyst) and a drying tower (Linde 3-Å molecular sieves) unless otherwise stated. Air sensitive materials were handled and stored in a Braun 150-M glove box. Standard Schlenk techniques were employed to manipulate air-sensitive solutions, using 10 micron vacuum. THF solvent used for these experiments was freshly distilled from sodium/benzophenone ketyl under argon onto freshly activated molecular sieves and subsequently purged with argon gas for at least two minutes per mL. The synthesis of **PZn$_n$** compounds has been reported previously,[24, 39] and all presented pristine characterization data. Permethylcobaltocene was synthesized by sonicating a THF suspension of the hexafluorophosphate salt over sodium metal for two hours and sublimed twice before use. Doping experiments were performed in a custom airfree cell that could be attached to a Schlenk line; an image of this apparatus appears in Figure 7.

Instrumentation: Electronic absorption spectra were collected using a Cary 5000 spectrometer. Deconvolution of the electronic spectral data from multistep doping experiments was performed using the MCR-ALS toolbox[33] running in Matlab™. All

deconvolutions were found to exhibit negligible rotational ambiguity as determined by MCR-BANDS analysis.[40] X-band ESR measurements were performed using a Varian E-109 spectrometer; all spectra were collected at 10 mW power and the magnetic field was referenced to dpph and weak pitch standards.

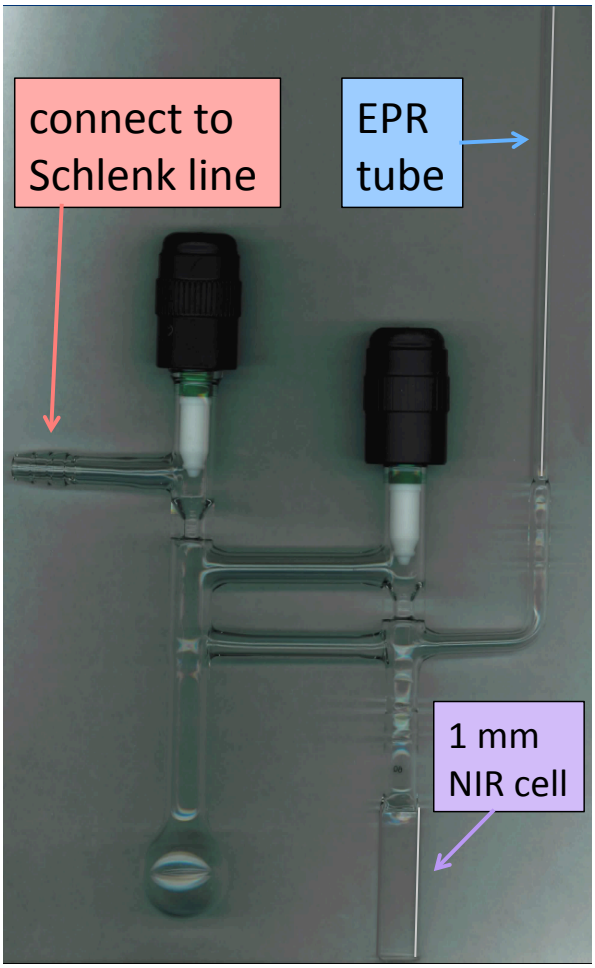

Figure 7. Airfree tandem vis-NIR and ESR cell used for doping of PZn_n molecules with $CoCp^*_2$.

2.4.2 Computational methods

The structures of **PZn$_n$** compounds were simplified by modeling the aryl groups as unsubstituted phenyl rings. For all polaron wavefunction models used in the text, as well as for TDDFT calculations, the structures were further simplified to the D_{2h} point group by restricting the individual porphyrin rings to lie in a single plane. Optimization of PZn_2 with no symmetry constraint finds an angle between the neighboring N,N,N,N consensus planes of 26.7°, and for $[PZn_2]^{\bullet-}$ this angle is calculated to be 16°. The consequences of these small deviations in interporphyrin dihedral angles on the electronic structures of the molecules is small, and the planar approximation provides a useful qualitative model. For the calculations of intramolecular electron-phonon coupling λ_i models with no symmetry and more realistic interporphyrin plane angles were used (Figure 8)

Structure optimizations and single-point energy calculations were performed with Density Functional Theory (DFT) using Gaussian09, Rev C.1.[41] The Becke three-parameter hybrid[42] and the Lee-Yang-Parr correlation functional[43, 44] (B3LYP) were employed for initial optimizations of the neutral species. All calculations employed tight convergence criteria and the 6-311g basis set[45-53] with two additional d functions (6-311G(2d)) as implemented in Gaussian09. A polarized continuum solvation model (SCRF=IEF-PCM in Gaussian09) with THF as solvent was used for all calculations.

Optimizations of the electron polaron states of PZn_n were initally performed using the M11 functional[54] with the default parameters implemented in Gaussian 09. TDDFT calculations using these structures were found to severely overestimate the energies of the major polaron transitions in the energy range below 1.55 eV (800 nm), with virtually no effect for oligomer lengthening beyond **PZn_2**. Employing the LC-ωPBE[36] functional with the range-separation parameter ω set to 0.05 dramatically improved the agreement of the calculated spectra with those observed; for all oligomers transition energies within 0.1 eV of major absorption maxima were modeled using this technique (Figure 9). A comparison of the highest occupied majority-spin orbital (HOMOα, sometimes referred to as SOMO) spatial extents determined using these two functionals, as manifested in their 0.01 isodensity surface plots, reveals that with the M11 functional the polaron wavefunction is essentially localized upon the central porphyrins; in contrast the LC-ωPBE polaron wavefunction extends to the limits of the **PZn_n** frameworks (Figure 10). Thus agreement of the TDDFT-calculated transitions with the observed spectra is correlated with structures that feature highly delocalized HOMOα wavefunctions.

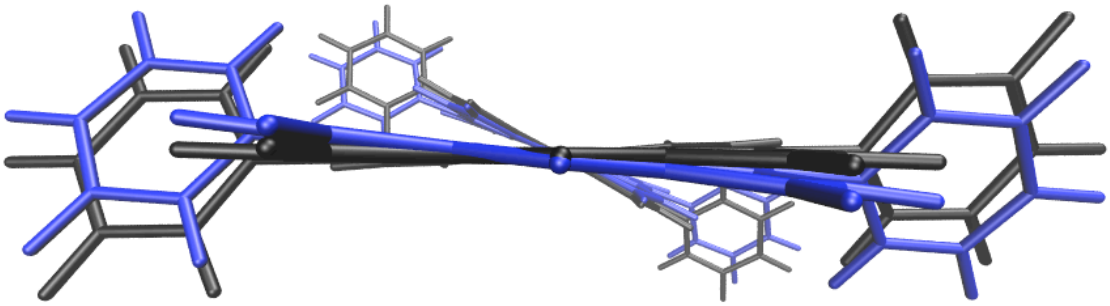

Figure 8. (black structure) PZn_2 and (blue structure) $[PZn_2]^{\bullet -}$ modeled using the LC-ωPBE functional with range-correction parameter ω = 0.05 and no symmetry constraints. This view is down the ethyne axis to provide a sense of the degree of deviation from coplanarity in this system, and to illustrate the principle displacements required in the relaxation from the neutral species to the electron polaron state.

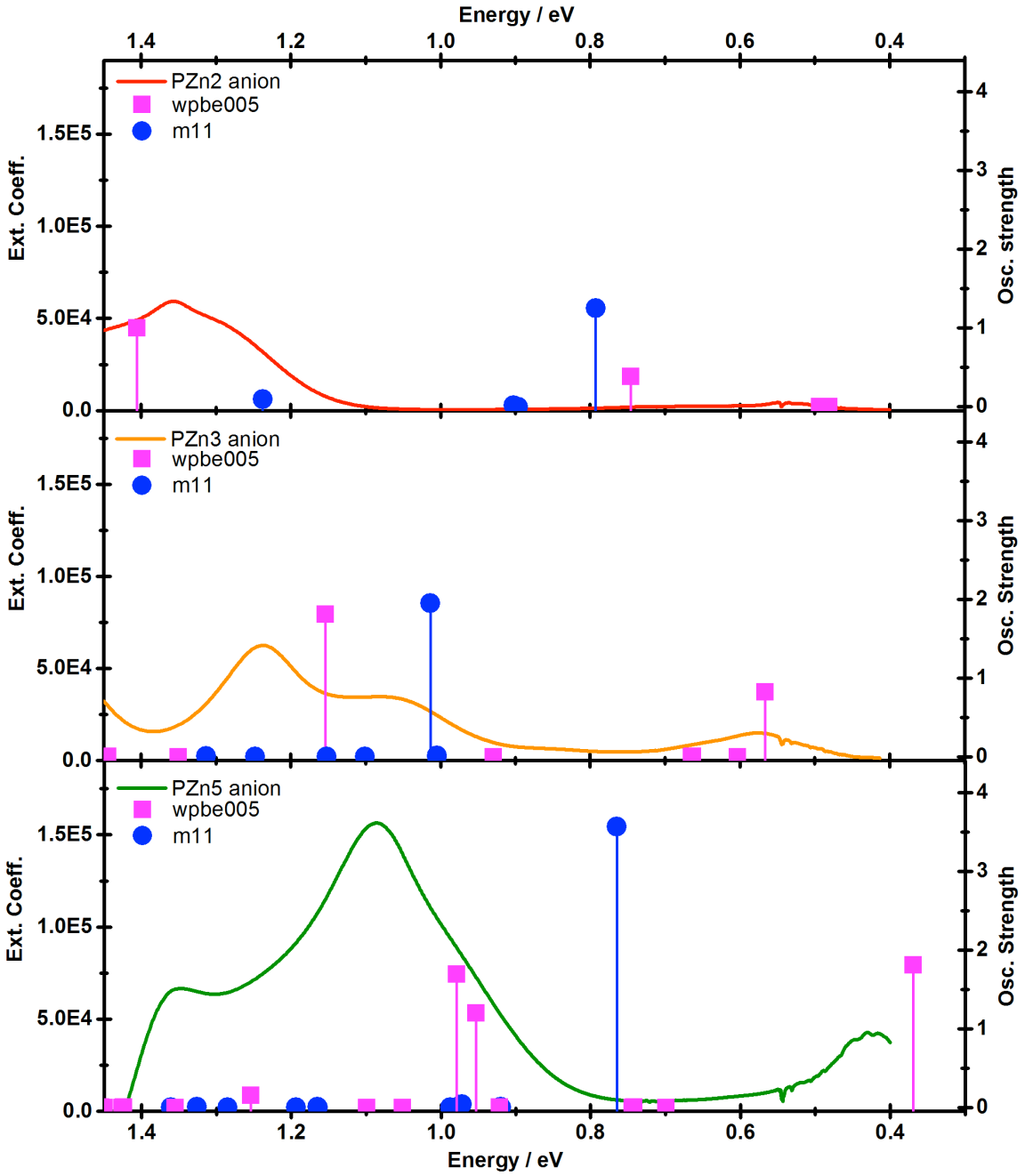

Figure 9. Comparison of deconvoluted electron-polaron spectra recorded for $[PZn_n]^{\bullet-}$ in THF solvent with TDDFT-calculated transitions determined using either the (blue circles) M11 or (magenta squares) LC-ωPBE functionals.

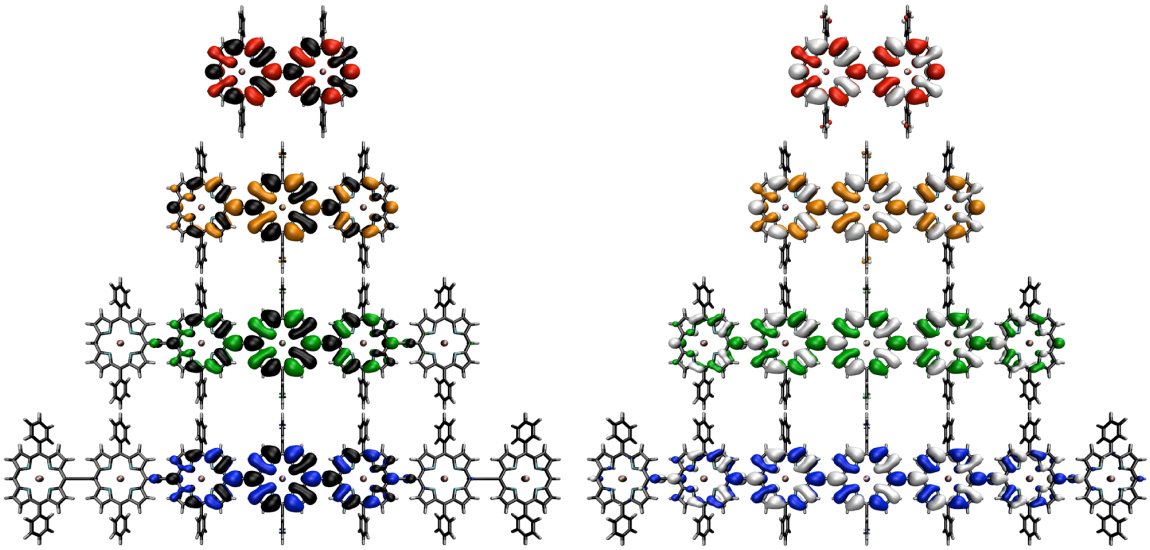

Figure 10. Comparison of α-HOMO wavefunctions calculated for $PZn_n]^{\bullet-}$ using (left) M11 functional and (right) ω-PBE functional with ω set to 0.05. All orbitals plotted as 0.01 isodensity surfaces.

3. Tailoring Porphyrin-based Electron Accepting Materials for Organic Photovoltaics

Jeff Rawson designed and synthesized all novel compounds, performed all potentiometric and spectroscopic measurements, orchestrated and interpreted all calculations, and drafted the manuscript.

Andrew C. Stuart fabricated and analyzed photovoltaic devices, and contributed to writing the manuscript.

Wei You proposed the collaboration, supervised device fabrication and analysis, and contributed to writing the manuscript.

Michael J. Therien supervised the project and wrote the final version of the manuscript.

3.1 Introduction

The syntheses, potentiometric responses, optical spectra, electronic structural properties, and integration into photovoltaic devices are described for ethyne-bridged isoindigo-(porphinato)zinc(II)-isoindigo chromophores built upon either electron-rich 10,20-diaryl porphyrin (**Ar-Iso**) or electron-deficient 10,20-bis(perfluoroalkyl)porphyrin (**Rf-Iso**) frameworks. These supermolecules evince electrochemical responses that trace their geneses to their respective porphyrinic and isoindigoid subunits, revealing the roles of these constituent pigment motifs in defining the potentiometrically determined HOMO and LUMO energies of **Ar-Iso** and **Rf-Iso**. The ethyne linkage motif effectively

mixes the comparatively weak isoindigo-derived visible excitations with porphrinic π-π* states; **Ar-Iso** and **Rf-Iso** possess high extinction coefficient ($\varepsilon \sim 10^5$ $M^{-1}cm^{-1}$) long-axis polarized absorptions and total visible spectral domain integrated oscillator strengths that exceed 2; time-dependent density functional theory calculations highlight the delocalized nature of the low energy singlet excited states of these chromophores, and reveal that the enhancement of S_1 state charge-resonance character for **Ar-Iso** correlates with its augmented degree of HOMO level destabilization relative to that determined for **Rf-Iso**. These exceptional electronic characteristics endow **Ar-Iso** and **Rf-Iso** with total absorptivities per unit mass that greatly exceed that for poly(3-hexyl)thiophene (**P3HT**) over the 375-900 nm wavelength range where solar flux is maximal, highlighting how coupled oscillator photophysics can yield OPV materials having absorptive properties that supersede those of conventional semiconducting polymers. While both these supermolecules manifest LUMO levels poised for exergonic electron transfer (ET) from photoexcited poly(3-hexyl)thiophene (^{1}P3HT*), the [(perfluoroalkyl)porphinato]zinc unit of **Rf-Iso** engenders the electronically excited state of this chromophore (^{1}Rf-Iso*) with an excited state oxidation potential ($E^{-/*}$) sufficient to drive hole transfer (HT) from ground-state **P3HT**. Prototype organic photovoltaic devices (OPVs) crafted from the **P3HT** donor and these new materials (i) confirm that solar power conversion depends critically upon the driving force for photoinduced HT from these low-bandgap acceptors, and (ii) underscore the importance of the $E^{-/*}$

parameter as a general design criterion for low-bandgap acceptors for OPVs. Because **Rf-Iso** possesses *both* a ground-state reduction potential appropriate for photoinduced ET with ^{1}P3HT*, and an excited-state reduction potential appropriate for photoinduced HT with ground-state **P3HT**, OPVs constructed from **Rf-Iso** and poly(3-hexyl)thiophene define rare examples whereby the acceptor material extends the device operating spectral range into the NIR. This work demonstrates for the first time that high oscillator strength porphyrinic chromophores, conventionally utilized as electron donors in OPVs, can also be exploited as electron acceptors.

A principal challenge in the design of next generation organic photovoltaics (OPVs) lies in engineering materials that provide high absorptivity (extinction coefficient $\varepsilon > 10^4$ $M^{-1}cm^{-1}$) over the spectral range corresponding to the solar irradiance spectrum at the earth's surface. The Air Mass 1.5 (AM1.5) solar irradiance spectrum provides a measure of the sun's energy to reach earth's surface in units of $W \bullet m^{-2} \bullet nm^{-1}$; it is most intense (> 0.75 $W \bullet m^{-2} \bullet nm^{-1}$) between 375 nm and 900 nm, and 66% of the total flux lies within this range.[55] Because of the inverse proportionality between film thickness and charge collection efficiency, there is a motivation to craft OPV films that are thinner than 100 nm, yet capable of capturing most of the incident 375-900 nm light.[56-58] Optimizing the absorptive oscillator strength of electron donor (D) and acceptor (A) materials over the 375-900 nm spectral domain is thus critical to next-generation OPV design.

Poly(3-hexylthiophene) (**P3HT**) and phenyl-C_{61}-butyric acid methyl ester (**PCBM**) are the best studied OPV materials and continue to stand as benchmarks in this field.[59-61] The development of new polymers with lower optical bandgaps and larger per mass absorptivities than those of **P3HT** has advanced rapidly,[62-68] and devices that blend these polymers with fullerene electron acceptors have achieved power conversion efficiencies (η) as high as 9.2% for single junction,[65] and 10.6% for tandem devices.[69] Great strides have been made using monodisperse alternatives to polymeric materials,[70-77] culminating in the recent disclosure of an 8.9% efficient solar cell that employed a silolodithiophene-derived donor and phenyl-C_{71}-butyric acid methyl ester acceptor.[77]

Considerably less progress has been made toward designing new organic acceptor materials that might replace fullerenes, and summaries of the state of the art in OPV development sometimes ignore this category altogether.[78, 79] The immaturity of efforts in this area contrasts the potential impact of molecular electron acceptors that absorb broadly over the vis-NIR spectral domain at high oscillator strength, as fullerenes such as **PCBM** are characterized by faint visible-range electronic transitions that are known to contribute negligibly to photocurrent.[58] Electron-deficient pigments such as perylene diimide,[80] boron perfluorosubphthalocyanine,[81] isoindigo, or perfluoralkylporphyrins[82-84] are characterized by $S_0 \rightarrow S_1$ transitions in the range of 500-600 nm with ε on the order of 10^4 $L \bullet mol^{-1} \bullet cm^{-1}$. When these easily reduced pigments are coupled to electron-rich moieties such as thiophene derivatives[85-87] or amine groups[88, 89],

push-pull chromophores result that can have NIR intramolecular charge transfer (ICT) absorption bands with onsets as low as 800 nm and maxima as large as ~5×10^4 $L\bullet mol^{-1}\bullet cm^{-1}$. The spectral characteristics of these push-pull chromophores are impressive; however, when they are employed as acceptor materials in OPVs, it is often found that a negligible portion of the devices' photocurrent can be attributed to acceptor excitation.[86]

A potent alternative method for crafting high oscillator strength, broad spectral domain absorbers involves coupling multiple pigment motifs via ethyne bridges in a manner that aligns their component transition dipoles.[1, 3, 10, 22, 24, 39, 90-99,2, 100-105] Such coupled-oscillator architectures, composed of building-block pigments capable of significant charge-resonance interactions, provide supermolecular chromophores that exhibit large polarizabilities and hyperpolarizabilities, and electronically excited states that manifest extensive spatial delocalization. With respect to designing a supermolecular electron acceptor (A) for OPV applications, additional considerations include: (i) an acceptor LUMO level (an $A^{-/0}$ potential) appropriate for electron transfer (ET) from the photoexcited donor ($^1D^*$), (ii) a corresponding electronic excited state ($^1A^*$) having sufficient thermodynamic driving force (an $A^{-/*}$ potential) to facilitate $^1A^*$-to-D hole transfer (HT), and (iii) high oscillator strength absorptivity across a broad range of vis-NIR wavelengths.

Porphyrin derivatives are well known for their strong coloration, and the prevalence of this motif in biological light-harvesting structures has inspired

incorporation of this conjugated unit into a wealth of functional materials.[106, 107] One strategy for augmenting the distribution, breadth, and intensities of the porphyrin-derived absorption bands is to extend the conjugated framework by attaching various aromatic groups using ethyne bridges at the macrocycle *meso* positions.[108-110,111-118] Some such ethyne-extended porphyrins have been employed as donor materials in OPVs,[119-123] as well as dye sensitized solar cells.[124-128] The porphyrin motif has been heretofore unrepresented as an OPV molecular acceptor due to its inherently electron-rich nature; congruent with this fact, the few reported attempts to achieve charge separation in porphyrin/**P3HT** blends did not meet with success (for example, such exemplary OPVs showed power conversion efficiencies < 0.01%).[129, 130] Electron-deficient meso-(perfluoroalkyl)porphyrins, characterized by energy levels suitable for application to the molecular acceptor problem have been devised;[82-84, 131-133] while such structures have been incorporated into supermolecular chromophores,[39] they have yet to be conjugated to complementary electron-poor pigment motifs.

N,N′-dialkyl isoindigo and related structures define an emergent class of technologically important electron-deficient chromophores;[134-136] for example, isoindigo has served as a building block for n-type and ambipolar polymers that possess electron mobilities as high as 0.6 $cm^2\ V^{-1}\ s^{-1}$.[137-140] While this structural motif has become quite common in donor polymers[141-158] and small molecules[87, 159-166] for OPVs, there is only one report of isoindigo polymers being used as OPV acceptor materials.[167] Isoindigo, while a

classic dye motif, possesses modest vis-spectral domain oscillator strength;[168] incorporation of the isoindigo motif into electron accepting materials for OPVs is further discouraged by the rapid depopulation of its excited state due to fast nonradiative decay.[168]

We report herein supermolecular chromophores based on ethyne-linked (porphinato)zinc (PZn) and isoindigo (Iso) units that exhibit intense panchromatic absorptions, long-lived S_1 states, and LUMO energy levels suitably poised for photoinduced electron transfer from **P3HT**. Because these materials feature higher absorptivities per unit mass than **P3HT** in the critical 375-900 nm window, they have the potential to contribute significantly to light harvesting in OPVs. The availability of both electron rich *meso*-diarylporphyrin and electron deficient *meso*-bis(perfluoralkyl)porphyrin building blocks allows the ready syntheses of two archetypal PZn-Iso chromophores, [5,15-bis(N,N'-bis(2-ethylhexyl)-6-isoindigoyl)ethynyl-10,20-bis(2,6-(3,3-dimethyl-1-butyloxy)phenyl)porphinato]zinc(II) (**Ar-Iso**) and [5,15-bis(N,N'-bis(2-ethylhexyl)-6-isoindigoyl)ethynyl-10,20-bis(heptafluoropropyl)porphinato]zinc(II) (**Rf-Iso**). The isoindigo moiety in these chromophores determines the $A^{-/0}$ potential; because the [5,15-bis(perfluoralkyl)porphinato]zinc(II) unit possesses a HOMO level ~0.3 eV stabilized with respect to that of [5,15-diphenylporphinato]zinc(II),[39, 83] **Ar-Iso** and **Rf-Iso** permit direct evaluation of the significance of the chromophore excited state reduction potential

($A^{-/*}$) as a design parameter in OPVs where the acceptor's absorptive properties strongly contribute to the photocurrent. This study illustrates how manipulation of coupled oscillator photophysics can yield conjugated acceptor materials that feature visible-light absorptivities that supersede those of conventional semiconducting polymers and electronically excited states that possess large driving forces for photoinduced hole transfer; furthermore, this work demonstrates for the first time that high oscillator strength porphyrinic chromophores, conventionally used as electron donors, can also be exploited as electron acceptors in OPVs.

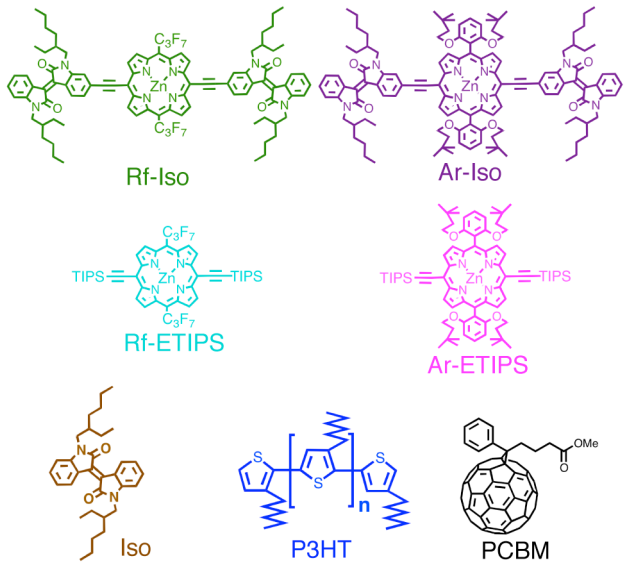

Figure 11. Structures of chromophores Rf-Iso and Ar-Iso, key precursor molecules, and benchmark OPV materials.

3.2 Results and Discussion

3.2.1 Supermolecular Chromophores Ar-Iso and Rf-Iso

The molecular structures of **Ar-Iso** and **Rf-Iso** are shown in Figure 11. Figure 12 displays the electronic absorption spectra acquired over the 375-850 nm spectral domain for supermolecular acceptors **Ar-Iso** and **Rf-Iso**, and the classic OPV benchmark materials, **P3HT** and **PCBM**. Electronic absorption spectra recorded for the **Ar-Iso** and **Rf-Iso** chromophoric building blocks are displayed in the Supporting Information. To facilitate quantitative absorptivity comparisons between these molecular and benchmark polymeric materials, the Figure 12 spectra are reported in units of (absorbance • L)/(g • cm); this expresses the intrinsic light harvesting capacity of these materials on a basis of direct relevance to device applications, where compositions are typically reported as

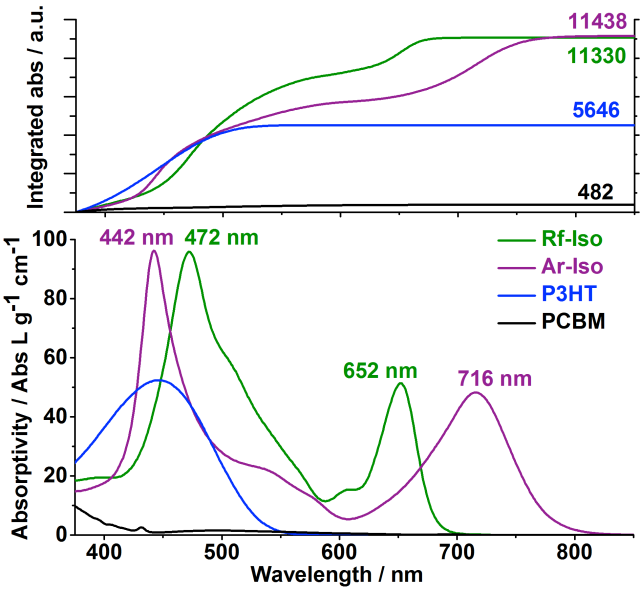

Figure 12. (bottom) Electronic absorption spectra of Rf-Iso, Ar-Iso, P3HT, **and** PCBM **in THF solvent normalized by mass. (top) Integrated, mass-normalized**

absorption spectra of these chromophores determined over the 375 - 850 nm spectral range.

weight ratios.[169] To permit comparisons of the total visible range absorptivity per unit mass, integrations of these spectra from 375 – 850 nm are depicted in the upper panel of Figure 12. Note that **Ar-Iso** and **Rf-Iso** provide high intrinsic absorptivity over the 375 – 850 nm window relative classic OPV donor and acceptor chromophores: as evident in the Figure 12 data, **Ar-Iso** and **Rf-Iso** feature mass-normalized absorbances approximately twice that of **P3HT**, and over 23 times that manifest by **PCBM** (Figure 12).

Rf-Iso and **Ar-Iso** evince Q-state derived transitions centered at 652 and 716 nm, respectively; note that the extinction coefficients for these absorptive maxima exceed 10^5 $M^{-1}•cm^{-1}$ (Table 1). The high oscillator strengths of these absorptions (f > 0.3; Table 1) derive from frontier orbital degeneracies for these supermolecules which are greatly

Table 1. Absorption Band Maxima, Energies, Extinction Coefficients, Full Widths at Half Maximum (FWHM), and Oscillator Strengths of PZn-Isoindigo Compounds and Chromophoric Benchmarks in THF Solvent.

	B-band region					Q-band region					total
compound	λ / nm	ν / cm^{-1}	log(ε)	FWHM/ cm^{-1}	oscillator strength	λ / nm	ν/ cm^{-1}	log(ε)	FWHM/ cm^{-1}	oscillator strength	oscillator strength
Iso	368 391	27174 25575	4.10 4.08	--	0.105 [b]	494	20243	3.55	--	0.048 [c]	0.153 [a]
Ar-ETIPS	439	22779	5.66	792	1.345 [d]	540 582 635	18519 17182 15748	3.52 4.12 4.69	367	0.126 [e]	1.471 [a]

Rf-ETIPS	444	22523	5.70	547	1.256 [d]	568 590 635	17606 16949 15748	4.03 4.16 3.31	--	0.078 [e]	1.334 [a]
Ar-Iso	442	22624	5.27	2143	1.994 [f]	716	13966	4.97	1547	0.514 [g]	2.508 [a]
Rf-Iso	472	21186	5.22	3278	2.077 [h]	652	15337	4.95	903	0.318 [i]	2.395 [a]

a Oscillator strengths calculated over the 375-850 wavelength domain. b Oscillator strength calculated over the 375-445 wavelength domain. c Oscillator strength calculated over the 445- 850 wavelength domain. d Oscillator strengths calculated over the 375-485 wavelength domain. e Oscillator strengths calculated over the 485-850 wavelength domain. f Oscillator strength calculated over the 375-608 wavelength domain. g Oscillator strength calculated over the 608-850 wavelength domain. h Oscillator strength calculated over the 375-587 wavelength domain. i Oscillator strength calculated over the 587-850 wavelength domain.

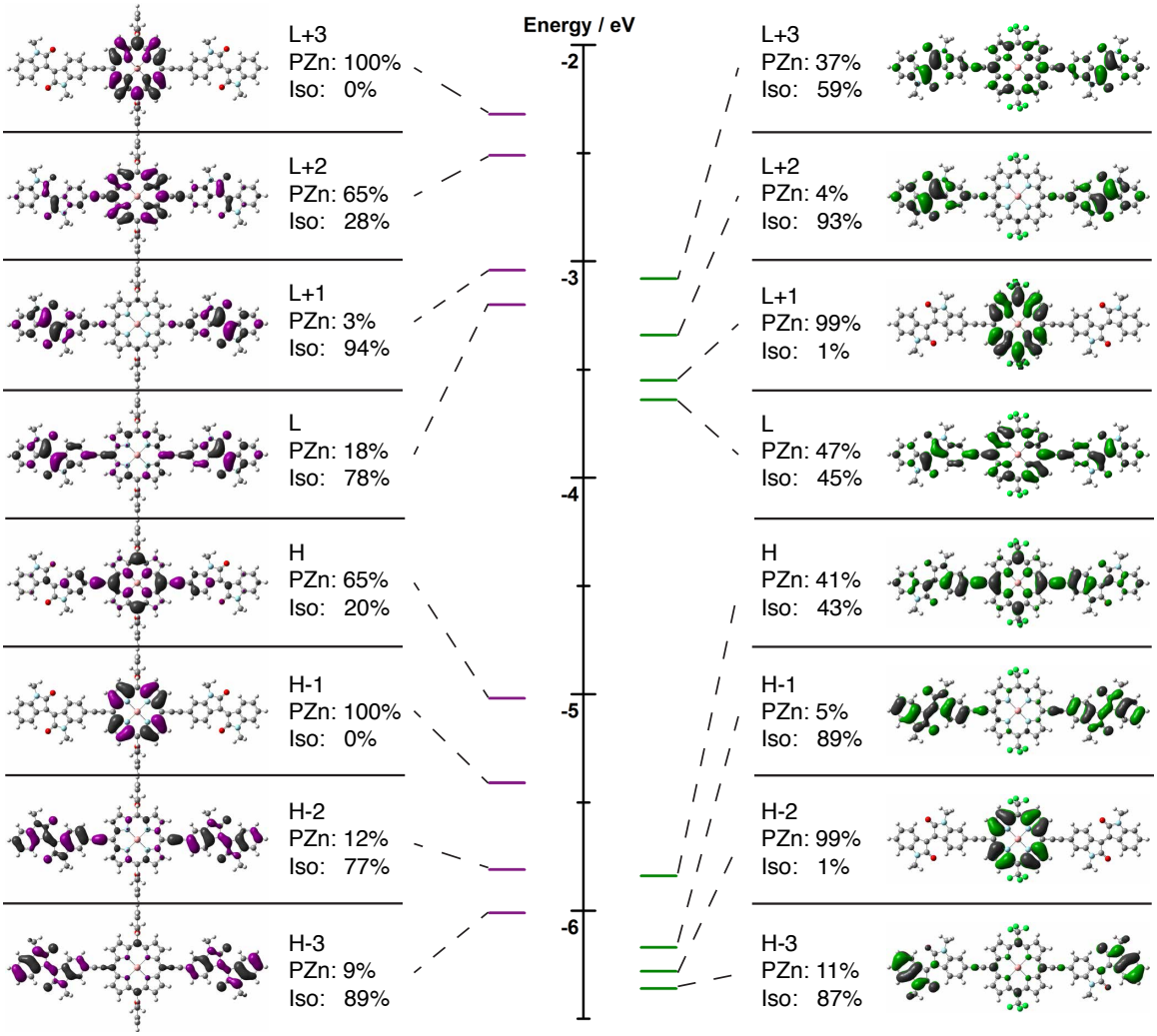

Figure 13. Frontier orbitals plotted as 0.02 isodensity surfaces for (left) Ar-Iso and (right) Rf-Iso, along with a diagram comparing their calculated energies. Percentages are the coefficients of each molecular orbital contributed by porphyrin (PZn) and isoindigo (Iso) atoms, excluding ethyne carbons, determined by population analysis.

diminished (Figure 13) compared with their respective parent (porphinato)zinc (PZn) building blocks, **Ar-ETIPS** and **Rf-ETIPS** (Figure 14), leading to modest degrees of configuration interaction for their lowest energy electronic transitions. Time-dependent DFT calculations confirm the long-axis polarizations of these supermolecular Q-state

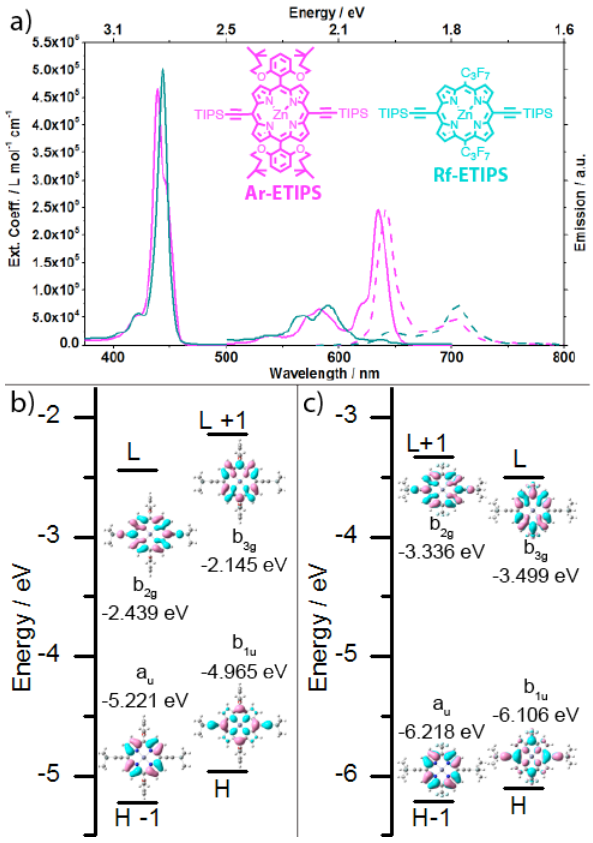

Figure 14. a) Absorption spectra (solid lines) and emission spectra scaled to the S_1 absorption peak (dashed lines) for monomeric porphyrins Ar-ETIPS (magenta) and Rf-ETIPS (cyan); b) energy level diagram depicting the four frontier orbitals of Ar-ETIPS; c) energy level diagram depicting the four frontier orbitals of Rf-ETIPS. (wavefunctions plotted as isodensity 0.02 surfaces). Symmetry labels for the D_{2h} point group have been applied.

derived transitions. This reduction in configuration interaction relative to that evident for the parent PZn framework is particularly dramatic for **Rf-Iso**: note all major vis-spectral domain transitions for this chromophore lie parallel to its long axis, whereas for **Rf-ETIPS**, x- and y-polarized excitations contribute approximately equally to the transitions that lie in this spectal region (Figure 15). Commensurate with this reorientation of the principal optical axis in **Rf-Iso**, a dramatic increase of Q-domain

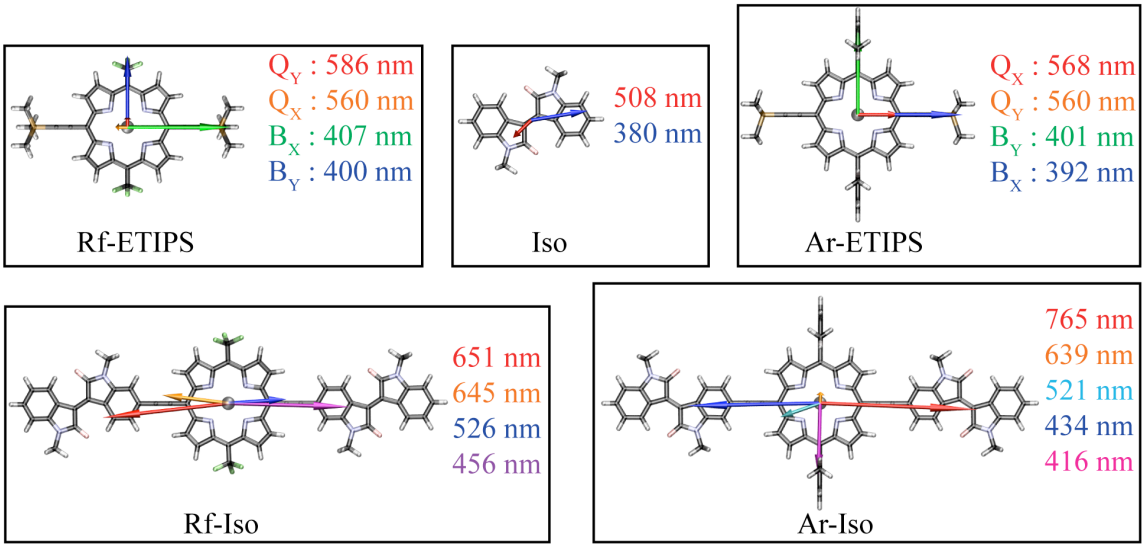

Figure 15. Transition dipole moments of major excitations for Rf-ETIPS, Iso, Ar-ETIPS, Rf-Iso, and Ar-Iso plotted over their molecular structures to illustrate the oscillator polarizations. Vectors were taken from TDDFT calculations using B3LYP functional and 6-311+G basis set; they were scaled for visibility on a consistent basis for all molecules and plotted using the molecule centers as the origins. Note that the lengths of these vectors are proportional to the predicted oscillator strengths, and the wavelengths of these transitions are given to the right of each structure. Throughout the text, the X-axis is defined as the horizontal direction, the Y-axis as the vertical, and the Z-axis as normal to the plane of the page as these structures are oriented.

absorptive oscillator strength relative to the **Rf-ETIPS** benchmark is also evident (Table 1). In these **Rf-Iso** and **Ar-Iso** supermolecules, the Iso units direct significant redistributions of PZn-derived oscillator strength due to the head-to-tail alignment of the PZn and Iso low energy transition dipoles and the substantial interactions between the Iso and 5,15-diethynyl(porphinato)zinc fragment frontier orbitals (Figure 13).[2, 98, 100-105, 170]

The spatial distributions of the frontier orbital wavefunctions, and the first excited state electron density difference maps for the **Rf-Iso** and **Ar-Iso** supermolecules, reveal that **Ar-Iso** features significantly more charge resonance character in its low-lying

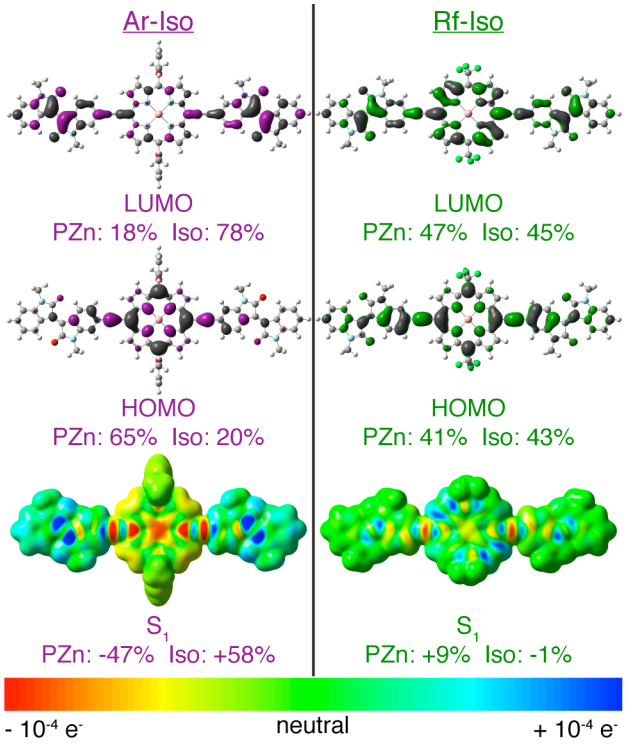

Figure 16. Frontier molecular orbitals and first excited state density differences for Ar-Iso and Rf-Iso plotted as 0.02 (orbitals) and 0.002 (densities) isodensity surfaces. Percentages reflect the ratio of orbital coefficients contributed from either the PZn or Iso fragments, excluding ethyne carbons, as determined by population analysis.

singlet excited state relative to **Rf-Iso** (Figure 16). In spite of the strong coupling provided by the ethyne bridges, the energetic mismatch between the PZn and Iso fragment energy levels restricts the extent of electronic delocalization within the frontier orbitals; note that Iso atom-derived electron density contributes only 20% to the **Ar-Iso** HOMO amplitude, but 78% to the corresponding **Ar-Iso** LUMO amplitude.

Photoexcitation of **Ar-Iso** thus redistributes electron density from the PZn to the Iso unit, giving rise to a delocalized S_1 state having substantial charge resonance character. Due to the σ-electron withdrawing character of the *meso*-perfluoroalkyl substituents, the HOMO and LUMO of the [5,15-bis(perfluoralkyl)porphinato]zinc(II) unit are equivalently stabilized by ~0.3 eV relative to the corresponding orbitals of [5,15-diphenylporphinato]zinc(II);[39, 82, 83, 133] as a result, the **Rf-Iso** frontier orbitals feature similar wavefunction amplitude contributions from the PZn and Iso building blocks. Likewise, the first excited state electron density difference map for **Rf-Iso** resembles that of a classic, delocalized π- π^* electronic transition. While the S_1 state electron density distributions differ for **Rf-Iso** and **Ar-Iso**, these chromophores possess significant and similar Q-state derived transition oscillator strengths (Table 1), congruent with large dispersions of their frontier orbital energy levels (Figure 13).[110, 171]

Figure 17 displays electronic absorption spectra of films of **Ar-Iso** and **Rf-Iso** drop-casted from THF solutions. The low-energy absorption band maxima observed for the **Ar-Iso** (739 nm) and **Rf-Iso** (685 nm) films lie, respectively, 1292 and 1732 cm^{-1} to the

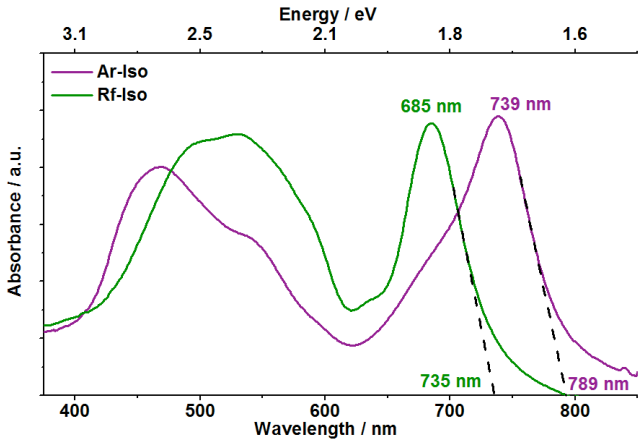

Figure 17. Electronic spectra of Ar-Iso and Rf-Iso thin films drop casted from THF solution onto quartz slides; peak absorption wavelengths are labeled; dashed lines mark absorption onset wavelengths.

red of their corresponding Q-state-derived transitions in solution, consistent with significant π-cofacial intermolecular interactions in the solid state.[87, 172] The greater thin film transition red-shift observed for **Rf-Iso** is congruent with its sterically unencumbering *meso*-perfluoroalkyl substituents: the 2′,6′-disubstituted meso-aryl substituents of **Ar-Iso** partially shroud the porphyrin plane and attenuate the extent of intermolecular interactions in the thin film.[10] Importantly, the solid-state absorption spectral onset (E_g) for **Ar-Iso** and **Rf-Iso** are 1.571 eV and 1.687 eV, respectively, significantly below the ~1.9 eV onset for **P3HT**.

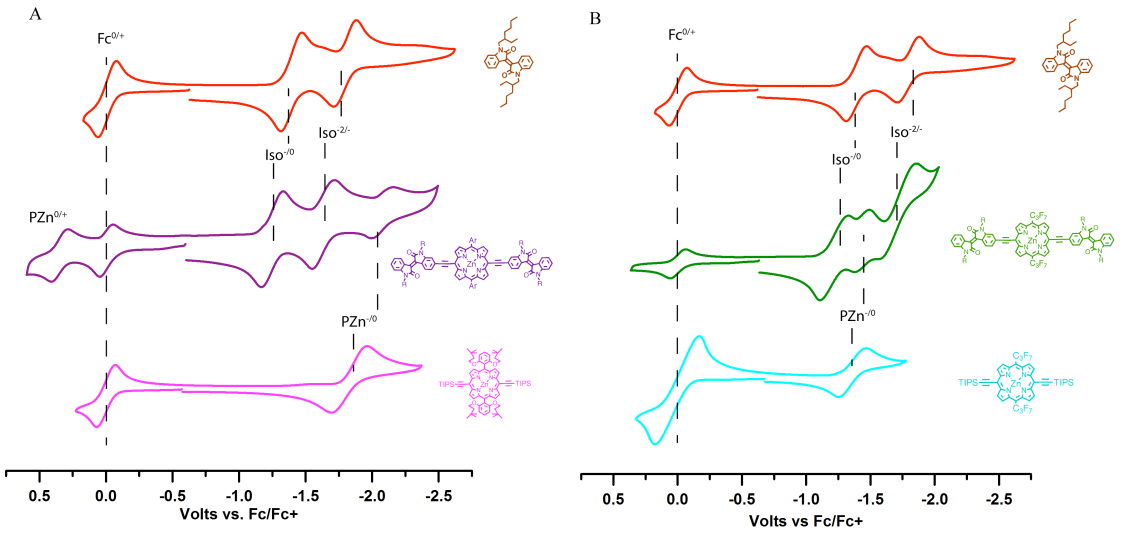

Figure 18. Cyclic voltammograms in THF solvent for (A) Ar-Iso and (B) Rf-Iso compared with those of their Iso and PZn subunits. [analyte] ~ 1mM; [Bu_4NPF_6] = 0.1 M; scan rate = 100-200 mV/s; pseudoreference electrode = Ag/AgCl•3.5 M NaCl; Fc/Fc+ used as internal standard.

Table 2. Electrochemically determined potentiometric data in THF solvent or thin films referenced to Fc/Fc^+ internal standard.

compound	$Iso^{-/0}$	$Iso^{-/2-}$	$PZn^{-/0}$	$PZn^{0/+}$
Iso	-1.389	-1.792	n/a	n/a
Ar-ETIPS	n/a	n/a	-1.830	--b
Rf-ETIPS	n/a	n/a	-1.361	--c
Ar-Iso (THF)	-1.248	-1.633	-2.078	0.353
Ar-Iso (film)	-1.234	-- *d*	-- *d*	0.300
Rf-Iso (THF)	-1.218	-1.711	-1.435	-- *c*
Rf-Iso (film)	-1.204	-- *d*	-- *d*	0.757

a. Experimental conditions: [chromophore] = 1 – 3 mM; scan rate = 200 mV/s; pseudoreference electrode = Ag/AgCl; solvent = THF / 0.1 M NBu4PF6 b. Oxidation not measured. c. Oxidation lay outside the solvent's electrochemical window. d Only first reduction is reported.

The potentiometric data acquired for these compounds determined in THF solvent reveal responses that trace their genesis to the redox processes of their respective chromophoric subunits (Table 2; Figure 18). The cathodic electrochemistry for **Ar-Iso** and **Rf-Iso** display two isoindigo-centered 1-electron reduction events; cyclic voltammetric data show that for **Ar-Iso**, these $Iso^{-/0}$ and $Iso^{2-/-}$ redox processes occur at higher potential than that for the (porphinato)zinc(II)-centered 1-electron reduction [$E_{1/2}(PZn^{-/0})$ = -2.078 V]; in contrast, for **Rf-Iso**, the potentials of these two Iso-centered reductions bracket $E_{1/2}(PZn^{-/0})$ [($E_{1/2}(Iso^{-/0})$ = -1.218 V; $E_{1/2}(PZn^{-/0})$ = -1.435 V; $E_{1/2}(Iso^{2-/-})$ = -1.711 V; Figure 18]. These data evince the closer energetic matching of the low-lying

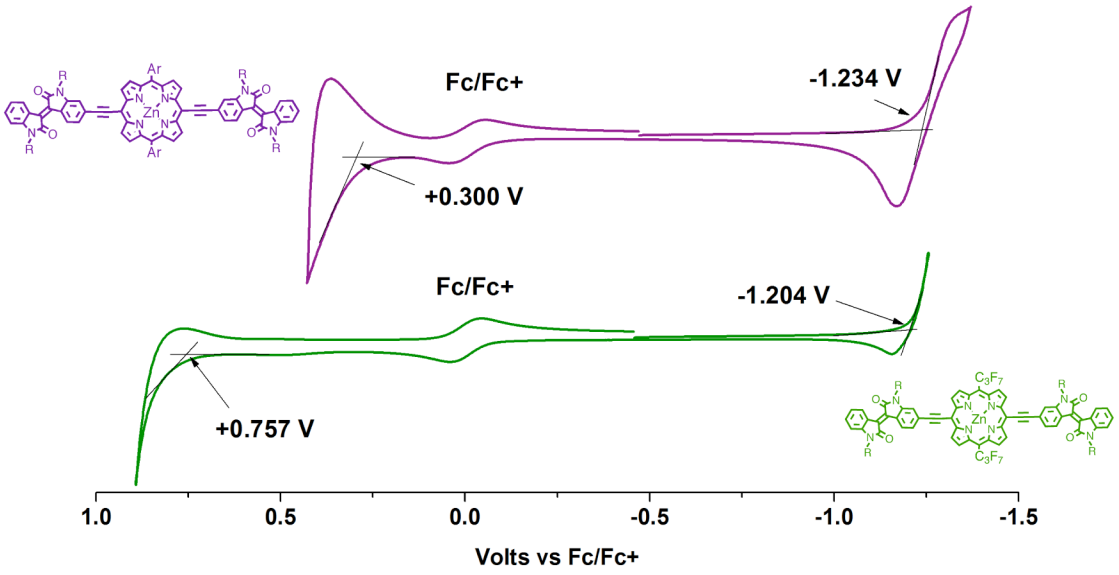

Figure 19. Cyclic voltammograms from thin films of (purple) Ar-Iso and (green) Rf-Iso drop casted onto a platinum electrode. Arrows denote the points taken as onset potentials. Solvent = CH_3CN; [Bu_4NPF_6] = 0.1 M; scan rate = 100 mV/s; pseudoreference electrode = Ag/AgCl•3.5 M NaCl; Fc/Fc+ used as internal standard.

empty Iso and PZn fragment molecular orbitals in **Rf-Iso** relative to **Ar-Iso**, congruent with electronic structure calculations. Cyclic voltammetric measurements carried out on thin film samples of these compositions found onset potentials of similar magnitude to the solution $E_{1/2}$ values determined for the initial oxidative and reductive processes of **Rf-Iso** and **Ar-Iso** (Table 2; Figure 19).

The energy of formation for free charges from excitons ($-\Delta G_{CS}$) quantifies the thermodynamic driving force for electron or hole transfer between a given D/A pair at organic semiconductor junctions; this can be evaluated using formalism developed by Weller.[173-177] The donor and acceptor excited state oxidation ($D^{*/+}$) and reduction ($A^{-/*}$) potentials can be estimated from $D^{0/+}$ and $A^{-/0}$ determined potentiometrically and E_g

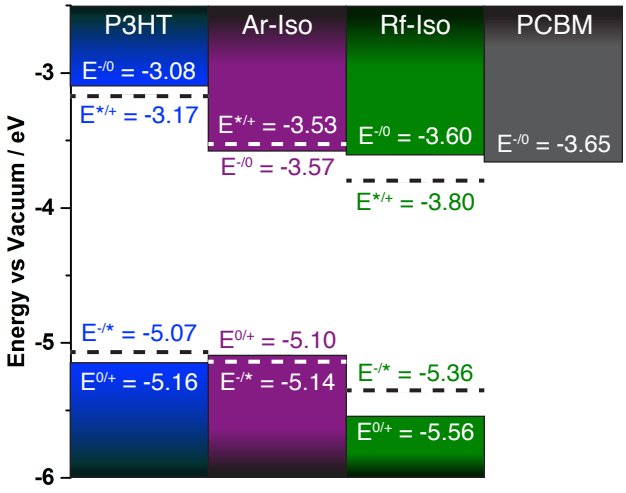

Figure 20. (solid rectangles) Potentiometrically determined frontier energy levels for P3HT, Ar-Iso, and Rf-Iso in thin films compared with PCBM for reference; all energy levels are versus the vacuum energy by the relation $E_{vac} = -e(4.8 + E_{ox/red})$. (dashed lines) Excited state redox potentials for P3HT, Ar-Iso, and Rf-Iso determined by adding the singlet excitation energy E_g to the ground state frontier levels.

determined by absorption onset.[175] The effective work function for the ferrocene/ferrocenium ($Fc^{0/+}$) couple of – 4.8 eV relates the potentiometric data acquired for thin films of these materials to an absolute scale by $E_{vac} = -e(4.8 + E_{po})$,[178] where E_{vac} is the vacuum energy level and E_{po} are the electrochemically measured potentials. For values of E_g, $D^{0/+}$, and $A^{-/0}$ determined from measurements in the solid state, where excitonic effects can enhance the mismatch between optical and potentiometric bandgaps, a correction factor $\Delta = (E^{-/0} - E^{0/+}) - E_g$ can be used to provide a more accurate estimate of the singlet exciton energy.[175, 176] The excited state reduction potential is then

$$E^{-/*} = E^{-/0} - (\tfrac{1}{2}\,\Delta + E_g)$$

and the excited state oxidation potential is

$$E^{*/+} = E^{0/+} + (\tfrac{1}{2}\,\Delta + E_g).$$

These values for **Ar-Iso**, **Rf-Iso**, and **P3HT** are displayed as dashed lines in Figure 20. The free energies of charge separation ΔG_{CS} between two materials X and Y are then

$$\Delta G_{CS} = X^{-/*} - Y^{0/+}$$

for hole transfer (HT) and

$$\Delta G_{CS} = X^{-/0} - Y^{*/+}$$

for electron transfer (ET), respectively.

These considerations indicate that electronically excited **P3HT** (^{1}P3HT*) should undergo photoinduced ET reactions with both **Ar-Iso** and **Rf-Iso**: ^{1}P3HT* + Ar-Iso → P3HT$^{+\bullet}$ + Ar-Iso$^{-\bullet}$, $-\Delta G_{CS}^{o} \sim 400$ mV; ^{1}P3HT* + Rf-Iso → P3HT$^{+\bullet}$ + Rf-Iso$^{-\bullet}$, $-\Delta G_{CS}^{o} \sim 430$ mV. If the role of the electron accepting material in an OPV includes augmenting the light harvesting capability of the donor polymer, factors other than the acceptor reduction potential and electronic absorptive properties need to be considered. In such an OPV, as electronically excited acceptors may be produced via direct light absorption or via an energy transfer reaction with an electronically excited donor polymer (e.g., ^{1}P3HT* + Ar-Iso → P3HT + ^{1}Ar-Iso*), engineering acceptor energy levels to facilitate exergonic photoinduced HT is critical. In this regard, it is important to appreciate that **Ar-Iso** and **Rf-Iso** possess significantly different driving forces for photoinduced HT reactions with **P3HT**: P3HT + ^{1}Ar-Iso* → P3HT$^{+\bullet}$ + Ar-Iso$^{-\bullet}$, $-\Delta G_{CS}^{o} \sim -20$ mV; P3HT + ^{1}Rf-Iso* → P3HT$^{+\bullet}$ + Rf-Iso$^{-\bullet}$, $-\Delta G_{CS}^{o} \sim 200$ mV. Thus, while both **Ar-Iso** and **Rf-Iso** may undergo phototoinduced ET reactions with electronically excited **P3HT**, only ^{1}Rf-Iso* is

predicted to possess sufficient driving force to photo-oxidize ground-state **P3HT**, as these thermodynamic driving force considerations indicate that such a HT reaction involving ^{1}Ar-Iso* and **P3HT** would be endergonic.

3.2.2 Photovoltaic devices exhibiting acceptor-derived photocurrent

OPV devices were produced for **P3HT**/**Ar-Iso** and **P3HT**/**Rf-Iso** in bilayer architectures; reference devices with **P3HT**/**PCBM** compositions were also studied. A conventional bilayer device configuration was employed consisting of ITO glass/PEDOT:PSS/P3HT/acceptor material/evaporated metal cathode; further fabrication details are available in the Supporting Information. As anticipated from the driving force considerations discussed above, no significant photocurrent [≥ 0.01% power conversion efficiency (PCE)] could be obtained from films of **P3HT**/**Ar-Iso**, while **P3HT**/**Rf-Iso** devices reliably gave efficiencies of 0.3-0.5%. These prototypical devices were not optimized, although several different film thicknesses were explored by variation of the revolution rate from 400-800 rpm in the **Rf-Iso** spin coating cycle. The best film, with an active layer of ~ 90 nm thickness, gave PCEs that averaged at a modest 0.57%.

PCEs in P3HT solar cells that exploit molecular acceptors now approach 4%.[179-185] The best of these compositions, which featured a zinc(azadipyrromethene) complex as acceptor, exhibited a fill factor (FF) of 0.57, an open-circuit voltage (V_{OC}) of 0.76 V, and a short-circuit current (J_{SC}) of 8.8 mA/cm^2. The open-circuit voltage (V_{OC}) of 0.79 V

determined for these **P3HT/Rf-Iso** devices is thus comparable to those reported for high-efficiency OPV compositions that feature molecular acceptors. In contrast, the best **P3HT/Rf-Iso** devices gave a J_{SC} of 2.43 mA/cm^2 and a fill factor of 0.29, values below the aforementioned benchmarks; these results suggest that suboptimal film morphologies played a role in the low efficiencies of **Rf-Iso/P3HT** devices by limiting the efficiency of charge carrier generation and collection.[58] In this regard it is noteworthy that **Rf-Iso** displayed negligible solubility in the absence of coordinating solvents, thus these films were deposited from solutions of 2:8 THF:*o*-dichlorobenzene. Optimization of the deposition conditions for [(*meso*-perfluoroalkyl)porphinato]zinc(II) – based materials is likely to be a fruitful area of research but falls beyond the scope of the present work. A relationship between J_{SC} and $-\Delta G_{CS}$ has been established,[175, 177] and it is possible that the thermodynamic driving force of 200 mV for Rf-Iso/P3HT is insufficient to drive charge dissociation yields that approach unity in this system, which might also contribute to a low current density.

External quantum efficiency (EQE) spectra normalized to the peak efficiency of each composition for a **P3HT/Rf-Iso** film and a benchmark **P3HT/PCBM** OPV are depicted in Figure 21. In compositions with **P3HT**, **PCBM** is known to provide a negligible contribution to light harvesting at wavelengths beyond 375 nm; thus the **P3HT/PCBM** spectrum provides a benchmark for **P3HT**-derived photocurrent.[186-188] The device using **Rf-Iso** as an acceptor shows an unmistakable contribution to its activity

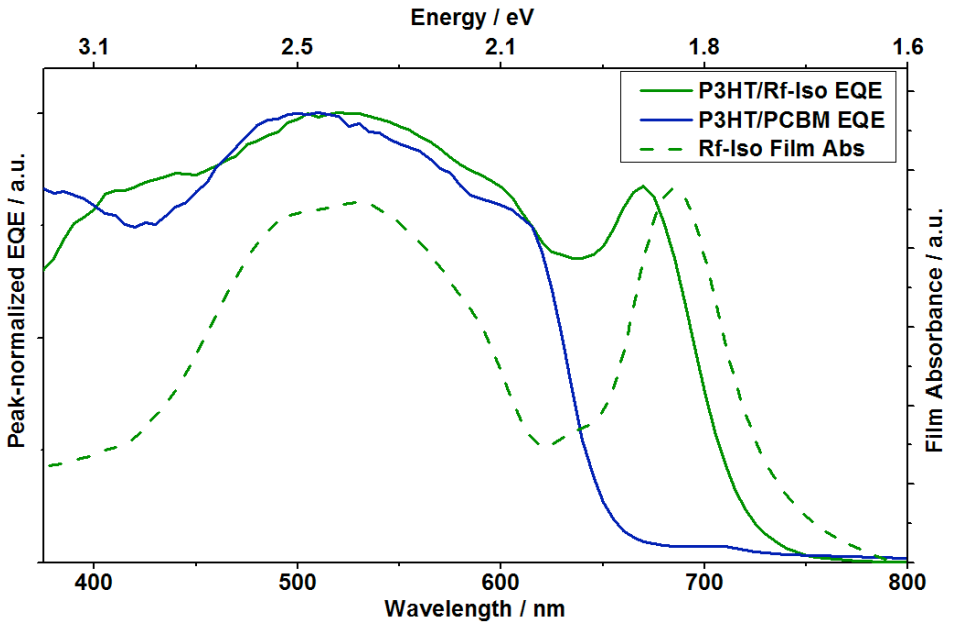

Figure 21. Peak-normalized EQE spectra from thin film OPV devices made from P3HT/Rf-Iso and P3HT/PCBM compositions, with the absorption spectrum of an Rf-Iso thin film for comparison.

from the porphyrin derivative in the form of an EQE peak at 670 nm, with ~15% of this film's integrated photocurrent produced beyond the long-wavelength onset for the **P3HT/PCBM** device at 650 nm. This NIR photocurrent is generated by photoinduced HT resulting from direct excitation of the **Rf-Iso** acceptor, sometimes called the channel-II path;[186-188] this observation highlights the importance of designing low-bandgap, strongly absorbing electron accepting materials that feature excited state reduction potentials ($E^{-/*}$ values) having sufficient driving force to undergo photoinduced HT with the ground-state donor polymer.

A prevalent first approximation for $-\Delta G_{CS}$ is the energetic offset between the frontier orbitals of D and A;[189, 190] it is common practice to compare LUMO levels

between D/A pairs to determine whether charge separation should be observable within a given system, with ~ 0.3 eV typically assumed to be the threshold energetic offset below which electron transfer will not occur.[177, 191, 192] Because the **Ar-Iso** and **Rf-Iso** LUMO levels are determined predominantly by the Iso unit, both Ar-Iso$^{-/0}$ and Rf-Iso$^{-/0}$ lie at ~ – 3.6 eV vs. vacuum; note that these both lie more than 0.3 eV below P3HT$^{-/0}$ (Figure 20). It has long been postulated that, for systems in which the acceptor significantly contributes to light absorption, a similar comparison of D/A HOMO levels assesses the propensity for hole transfer from A to D;[190] this finds that Rf-Iso$^{0/+}$ lies ~ 0.4 eV below P3HT$^{0/+}$, while Ar-Iso$^{0/+}$ is 0.06 eV *above* this level. As the significance of channel II photocurrent has become appreciated, the importance of molecular acceptor HOMO levels has recently garnered increased attention;[184, 185, 187, 188] our findings underscore this significance by identifying at least one system (**P3HT**/**Ar-Iso**) where the lack of sufficient – ΔG_{CS} for hole transfer leads to PCEs ~ 0% at all wavelengths. Because the magnitudes of the Rf-Iso$^{0/+}$ and Ar-Iso$^{0/+}$ potentials are essentially determined by the nature of their respective PZn units, these data highlight the utility of the [5,15-(perfluoroalkyl)porphinato]zinc(II) building block, with an A$^{0/+}$ potential stabilized by ~ 300 meV relative to common meso-arylporphyrin ligand frameworks, for the design of electron accepting chromophores for OPVs.

3.3 Conclusion

In summary, a supermolecular design strategy has afforded ethyne-conjugated isoindigo-(porphinato)zinc(II)-isoindigo chromophores built upon either electron-rich 10,20-diarylporphyrin (**Ar-Iso**) or electron-deficient 10,20-bis(perfluoroalkyl)porphyrin (**Rf-Iso**) frameworks. **Rf-Iso** and **Ar-Iso** exhibit intense, porphyrin Q-state derived $S_0 \rightarrow S_1$ NIR transitions, and total visible spectral domain integrated oscillator strengths that exceed 2; both **Rf-Iso** and **Ar-Iso** exhibit greater total absorptivities per unit mass than poly(3-hexyl)thiophene in the 375 – 900 nm wavelength range where solar flux is maximal. Time-dependent density functional theory calculations highlight the delocalized nature of the low energy singlet excited states of these chromophores and reveal that the extent of S_1 state charge-resonance character tracks with the extent of HOMO level destabilization. Prototype organic photovoltaic devices (OPVs) crafted from the donor poly(3-hexyl)thiophene and these new materials confirm that solar power conversion depends critically upon the thermodynamic driving force for photoinduced hole transfer (HT) reactions involving these electronically excited low-bandgap acceptors and the ground-state poly(3-hexyl)thiophene (**P3HT)** polymer. While both the **Rf-Iso** and **Ar-Iso** supermolecules manifest LUMO levels poised for exergonic electron transfer (ET) from photoexcited **P3HT** (^{1}P3HT*), the [(perfluoroalkyl)porphinato]zinc unit of **Rf-Iso** engenders the electronically excited state

of this chromophore (^{1}Rf-Iso*) with an excited state reduction potential ($E^{-/*}$) sufficient to drive hole transfer (HT) from ground-state **P3HT**.

This work highlights the effectiveness of coupled oscillator photophysics and the *meso*-perfluoroalkylporphyrin ligand framework for the design of an acceptor chromophore for OPVs that: (i) possesses an excited-state reduction potential appropriate for photoinduced HT with the ground-state of the classic donor polymer **P3HT**, (ii) features a ground-state reduction potential appropriate for photoinduced ET with the electronically excited donor polymer (^{1}P3HT*), (iii) supersedes the total visible-range absorptivity of **P3HT** and (iv) extends the device operating spectral range into the NIR. This work demonstrates for the first time that high oscillator strength porphyrinic chromophores, conventionally utilized as electron donors in OPVs, can also be exploited as electron acceptors.

3.4 Methods

3.4.1 Experimental Methods

Materials: All manipulations were carried out under argon previously passed through an O_2 scrubbing tower (Schweitzerhall R3-11G catalyst) and a drying tower (Linde 3-Å molecular sieves) unless otherwise stated. Air sensitive materials were handled in a Braun 150-M glove box. Standard Schlenk techniques were employed to manipulate air-sensitive solutions. All solvents utilized for chromatography in this work were obtained from Fisher Scientific (ACS grade except for THF, which was

Optima HPLC grade). Dry, deoxygenated solvents were obtained from a solvent purification system (Puresolv™, Innovative Technologies, inc.). Triethylamine (TEA) was dried over KOH pellets and distilled from CaH under argon. N-bromosuccinamide was recrystallized from water and dried under high vacuum for at least 24 hours before use. All NMR solvents were used as received. Tris(dibenzylideneacetone)-dipalladium(0) (Pd_2dba_3) and triphenylarsine ($AsPh_3$) were purchased from Strem Chemicals and stored in the glovebox. Air-sensitive reactions were performed by charging a Schlenk tube with the catalysts in the glovebox, then cannulating solvents degassed by at least three freeze-pump-thaw cycles in the hood. Silica gel and preparative size exclusion column chromatography were performed on the bench top, using respectively silica gel (Silicycle, 230–400 mesh) and Bio-Rad Bio-Beads SX-1 as media.

Instrumentation: NMR spectra were recorded on a 400 MHz
Varian spectrometer and processed using MestReNova LITE version 5.2.5-4119 software. Chemical shifts for ^{1}H NMR spectra are reported relative to the internal standard tetramethylsilane (TMS) in deuterated solvent (TMS =0.00 ppm). All *J* values are reported in Hertz. MALDI-TOF mass spectroscopic data were obtained with an Applied Biosystems Voyager DE pro instrument under the supervision of Dr. George Dubay at Duke University. Samples were prepared as micromolar solutions in THF, and α-cyano-4-hydroxycinnamic acid (CHCA) or 2-(4-hydroxyphenylazo)benzoic acid (HABA) were

utilized as matrices. Absorption spectra were collected on a Shimadzu Pharmaspec UV-1700 or a Cary 5000 spectrometer. Emission and excitation spectra were collected on an Ediburgh FLSP 920. Potentiometric measurements were performed using a Bioanalytical Systems BASi Epsilon EC Electrochemical Workstation.

The synthesis of **Ar-Iso** and **Rf-Iso** was accomplished as outlined in Scheme S1. No efforts were made to optimize these reaction conditions. N,N′-bis(2-ethylhexyl)-6-bromoisoindigo **Br-iso**,[87] [5,15-diethynyl-10,20-bis(2,6-(3,3-dimethyl-1-butyloxy)phenyl)porphinato]zinc(II) **Ar-E**,[2] and [5,15-diethynyl-10,20-bis(heptafluoropropyl)porphinato]zinc(II)[39] were synthesized according to established procedures.

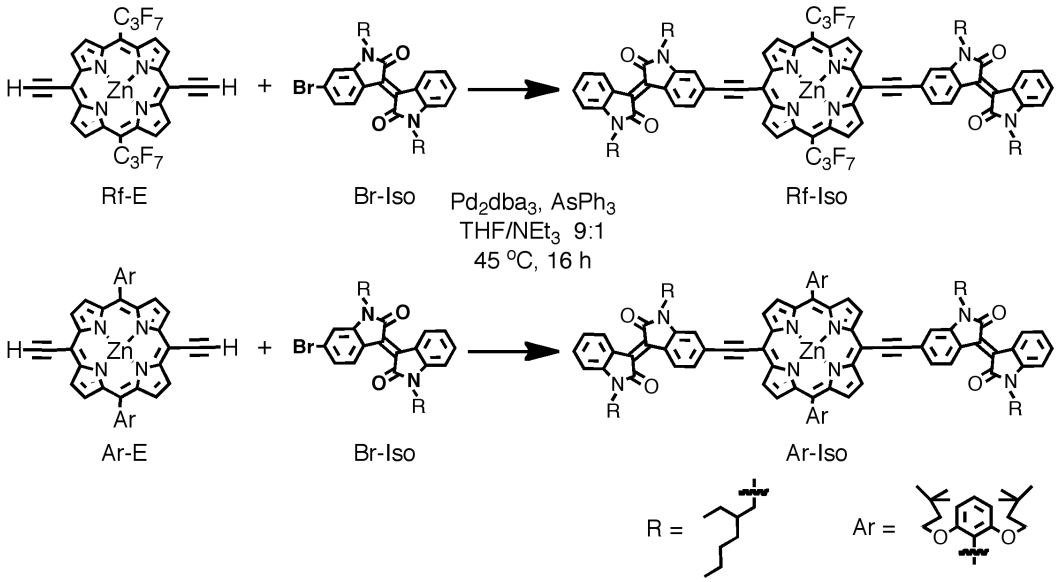

Figure 22. Structures of precursors and outline of the synthetic approach to Rf-Iso and Ar-Iso.

[5,15-Bis(N,N′-bis(2-ethylhexyl)-6-isoindigoyl)ethynyl-10,20-bis(2,6-(3,3-dimethyl-1-butyloxy)phenyl)porphinato]zinc(II) (**Ar-Iso**)

A 50 ml Schlenk reaction tube was charged with a stir bar, diethynyl porphyrin **Ar-E** (143 mg, 1.47 x 10^{-4} mol) and bromoisoindigo (208 mg, 3.68 x 10^{-4} mol). This tube was introduced into a glove box where Pd_2dba_3 (54 mg, 5.88 x 10^{-5} mol) and $AsPh_3$ (180 mg, 5.88 x 10^{-4} mol) were added. The sealed reaction vessel was removed from the glove box and purged with argon, then charged with 20 ml of 9:1 THF/triethylamine. The stirred solution was shielded from light and heated at 45 C for 16 hours. The solvent was removed under a stream of nitrogen and the residue was chromatographed over silica eluted with CH_2Cl_2. The first dark brown band was collected, evaporated at reduced pressure, and rechromatographed over silica eluting with 1:4 THF:hexanes. The first brown band was again collected and evaporated, and the residue was chromatographed using Biobeads SX-1 media eluted with THF. The product was then purified by one final silica column with 1:4 THF:hexanes to give Ar-Iso (114 mg, 5.86x10^{-5} mol, 40 % yield).

^{1}H NMR (400 MHz, $CDCl_3$, ppm vs. Me_4Si = 0) δ 9.70-9.65 (m, 4H), 9.380 (d, 2H, *J* = 8.3 Hz), 9.208 (d, 2H, *J* = 8.0 Hz), 8.901 (d, 4H, *J* = 4.5 Hz), 7.758 (t, 2H, *J* = 8.5 Hz), 7.716 (d, 2H, *J* ~ 8 Hz), 7.394 (t, 2H, *J* = 7.5 Hz), 7.375 (s, 2H), 7.101 (t, 2H, *J* = 7.4 Hz), 7.034 (d, 4H, *J* = 8.5 Hz), 6.826 (d, 2H, *J* = 7.7 Hz), 3.955 (t, 8H, *J* = 7.2 Hz), 3.90-3.80 (m, 4H), 3.75-3.65 (m,

4H), 2.12-2.02 (m, 2H), 1.95-1.85 (m, 2H), 1.52-1.26 (m, 32H), 1.072 (t, 6H, *J* = 7.3 Hz), 0.99-0.85 (m, 26H), 0.280 (s, 36H).

Ar-Iso: $C_{124}H_{148}N_8O_8Zn$; MW = 1943.93 g/mol; M/z = 1944.98 : H^+[Ar-Iso].

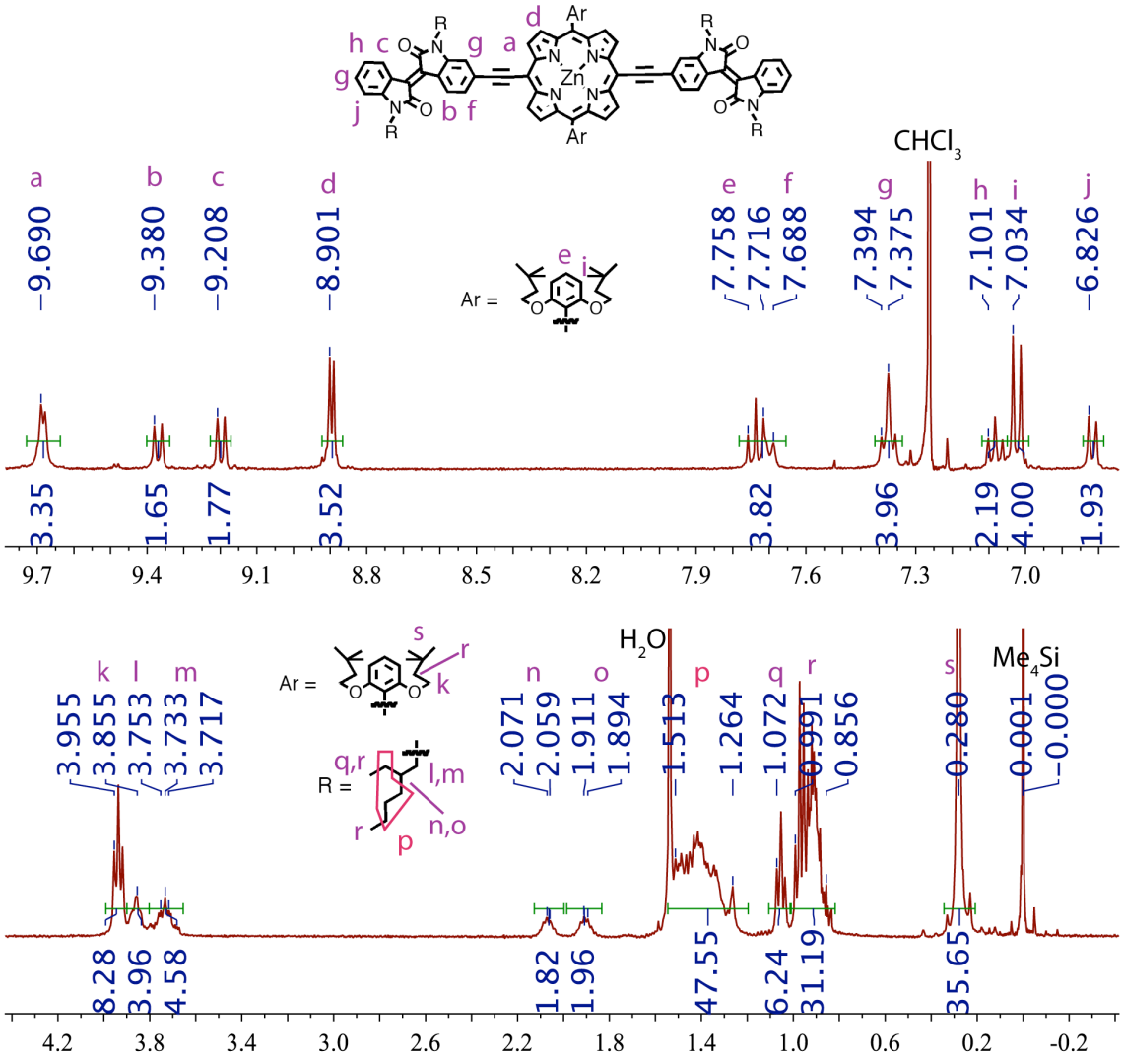

Figure 23. Proton NMR spectrum of Ar-Iso, with compound structure and peak assignments.

[5,15-Bis(N,N′-bis(2-ethylhexyl)-6-isoindigoyl)ethynyl-10,20-bis(heptafluoropropyl)porphinato]zinc(II) (Rf-Iso)

A 50 ml Schlenk reaction tube was charged with a stir bar, diethynyl porphyrin (209 mg, 2.76 x 10^{-4} mol) and bromoisoindigo (390 mg, 6.90 x 10^{-4} mol). This tube was introduced into a glove box where Pd_2dba_3 (101 mg, 1.10 x 10^{-4} mol) and $AsPh_3$ (338 mg, 1.10 x 10^{-3} mol) were added. The sealed reaction vessel was removed from the glove box and purged with argon, then charged with 20 ml of 9:1 THF/triethylamine. The stirred solution was shielded from light and heated at 45 °C for 16 hours. The solvent was removed under a stream of nitrogen and the residue was chromatographed over silica eluted with 4:6 THF:hexanes. The first purplish-brown band was collected, evaporated at reduced pressure, and loaded onto a silica column in pure THF, then eluted with 1:4 THF:hexanes. The first purplish-brown band was again collected and evaporated, and the residue was chromatographed using Biobeads SX-1 media eluted with THF. The product was then chromatographed over a silica column with 1:2:2 THF:hexanes:CH_2Cl_2. After stripping off the solvent, the residue was taken up in a minimal volume of THF (~5 ml) and added to 100 ml of rapidly stirring hexanes. The precipitate was collected by filtration to give Rf-Iso (85 mg, 4.92 x 10^{-5} mol, 18% yield).

^{1}H NMR (400 MHz, THF-d_8, ppm vs. THF H_α = 3.580) δ 9.506 (s, 4H), 9.349 (d, 4H, *J* = 8.1 Hz), 8.794 (s, 4H), 7.257 (t, 2H, *J* = 7.6 Hz), 7.001 (t, 2H, *J* = 7.6 Hz), 6.821 (d, 2H, *J* = 7.8

Hz), 6.631 (d, 2H, *J* = 7.2 Hz), 6.332 (s, 2H), 3.97-3.82 (m, 8H), 2.03-1.95 (m, 4H), 1.61-1.45 (m, 32H), 1.16-1.00 (m, 24H).

^{19}F NMR (376.3 MHz, THF, ppm vs. $CFCl_3$ = 0.0) δ -78.822 (s, 4F), -80.079 (t, 6F, *J* = 10.5 Hz), -119.605 (s, 4F).

Rf-Iso: $C_{94}H_{90}F_{14}N_8O_4Zn$; MW = 1727.13 g/mol; M/z = 1727.48 : H^+[Rf-Iso]; M/z = 1749.82 : Na^+[Rf-Iso].

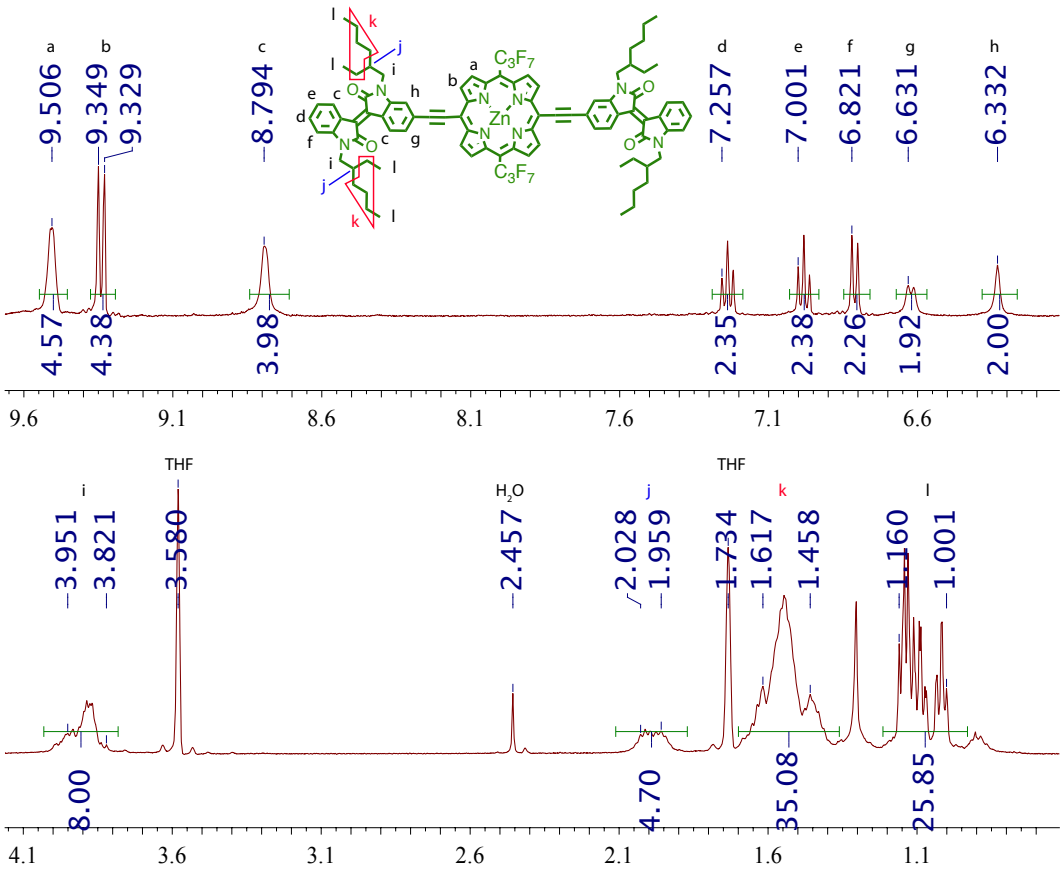

Figure 24. Proton NMR spectrum of Rf-Iso, with molecular structure and peak assignments.

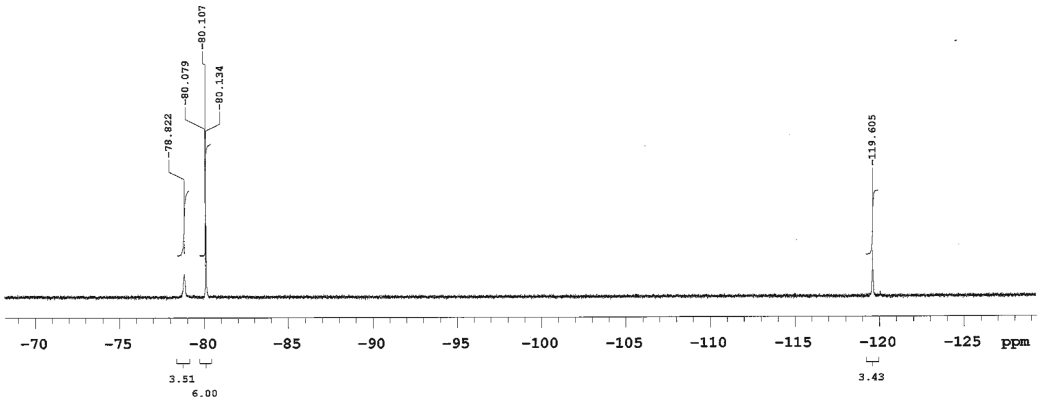

Figure 25. Fluorine NMR spectrum of Rf-Iso.

Potentiometric methods: Cyclic voltammetric experiments carried out in solution were performed in THF solvent containing 0.1 M Bu_4NPF_6 as supporting electrolyte. For measurements in the solid state, films were drop casted onto a platinum electrode from THF solutions and dried under vacuum; the cyclic voltammetric responses of these thin films were acquired in acetonitrile solvent containing 0.1 M Bu_4NPF_6. All electrochemical measurements utilized scan rates that ranged between 100-200 mV/s, and ferrocene as an internal potentiometric standard.

Photovoltaic device fabrication and testing: Glass substrates coated with patterned indium-doped tin oxide (ITO) were purchased from Thin Film Devices, Inc. (Anaheim, CA). The 150 nm thick sputtered ITO pattern had a sheet resistance of 15Ω/□. Prior to use, the substrates were ultrasonicated for 20 min in 2-propanol. The substrates were then dried under a stream of nitrogen and placed in a UV-Ozone cleaner (42 UVO Cleaner, Jelight Company Inc.) for 20 min. A 0.45 μm PVDF (Polyvinyl difluoride)

filtered dispersion of Poly(3,4-ethylenedioxythiophene):Polystyrene sulfonate (PEDOT:PSS) in water (Baytron PH500) was then spin-cast onto clean ITO substrates at 4000 rpm for 60 s and baked at 140 °C for 20 minutes yielding a thin film with a thickness of 40 nm. Beyond this point all fabrication and testing steps were performed inside an inert atmosphere glove box. Bilayer devices were made by dissolving P3HT at 15 mg/mL in DCB and Ar-Iso or Rf-Iso at 10 mg/mL in 4:1 DCB:THF. The P3HT layer was spin-cast first between 400 – 800 rpm for 30 – 60 s onto the PEDOT:PSS layer and left to dry at room temperature under N_2 for 12 h. Once dry, the Ar-Iso or Rf-Iso solution was spin-cast onto the P3HT film between 400 – 800 rpm for 30 – 60 s. The substrates were then left to dry at room temperature under N_2 for 12 h. The cathode was deposited by thermal evaporation of 100 nm of aluminum with a shadow mask at a pressure of ~ 1×10^{-6} mbar. There are 8 devices per substrate, with an active area of 12 mm^2 per device. The thicknesses of films were recorded by a profilometer (Alpha-Step 200, Tencor Instruments). Device characterization was carried out under AM 1.5G irradiation with an intensity of 100 mW/cm^2 (Oriel 91160, 300 W), which was calibrated by a NREL certified standard silicon cell. I-V curves were recorded with a Keithley 2400 digital source meter. All fabrication steps after adding the PEDOT:PSS layer onto ITO substrate, and all I-V characterizations were performed in a glovebox under nitrogen atmosphere.

3.4.2. Theory and computational methods

Energy levels and driving forces

$A^{-/0}$, $D^{0/+}$, etc. are energies wrt vacuum determined from potentiometric measurements using Fc/Fc^{+} work function:

$E_{VAC} = -e(4.8 + E_{PO})$

Several values for this are prevalent in the literature; what is important for comparative purposes is that all of our redox potentials were determined in identical fashion from solid films and referenced to ferrocene internal standard.

$P3HT^{0/+}$: -5.16 eV	$P3HT^{-/0}$: -3.08 eV
$Ar\text{-}Iso^{0/+}$: -5.100 eV	$Ar\text{-}Iso^{-/0}$: -3.566 eV
$Rf\text{-}Iso^{0/+}$: -5.557 eV	$Rf\text{-}Iso^{-/0}$: -3.596 eV

Excited state reduction/oxidation potentials are determined using potentiometric orbital levels defined above, bandgap (E_g) determined from absorption onset, and ½ exciton binding energy (E_B), defined as $E_B = (E^{-/0} - E^{0/+}) - E_g$

P3HT E_B = 0.180 eV; E_g = 1.90 eV

Ar-Iso E_B = 0.0 eV; E_g = 1.571 eV

Rf-Iso E_B = -0.143 eV; E_g = 1.687 eV

excited state reduction potential $E^{-/*} = E^{-/0} - (½ E_B + E_g)$

excited state oxidation potential $E^{*/+} = E^{0/+} + (½ E_B + E_g)$

$P3HT^{*/+}$: -3.17 eV $P3HT^{-/*}$: -5.07 eV

$Ar\text{-}Iso^{*/+}$: -3.529 eV $Ar\text{-}Iso^{-/*}$: -5.137 eV

$Rf\text{-}Iso^{*/+}$: -3.799 eV $Rf\text{-}Iso^{-/*}$: -5.355 eV

driving forces for hole transfer and electron transfer (ΔG_{hT} and ΔG_{eT})

$\Delta G_{hT} = A^{-/*} - D^{0/+}$

$\Delta G_{eT} = A^{-/0} - D^{*/+}$

^{1}Rf-Iso*/P3HT ΔG_{hT} = -5.355 + 5.16 = -0.20 eV

^{1}Ar-Iso*/P3HT ΔG_{hT} = -5.137 + 5.16 = +0.023 eV

^{1}P3HT*/Rf-Iso ΔG_{eT} = -3.596 + 3.17 = -0.43 eV

^{1}P3HT*/Ar-Iso ΔG_{eT} = -3.566 + 3.17 = -0.40 eV

Quantum chemical calculations: All calculations were performed upon structures with aliphatic chains truncated to methyl groups (Figure 26). For Ar-Iso and Rf-Iso, both C_{2v} and C_{2h} conformeric minima could be formulated; because the total

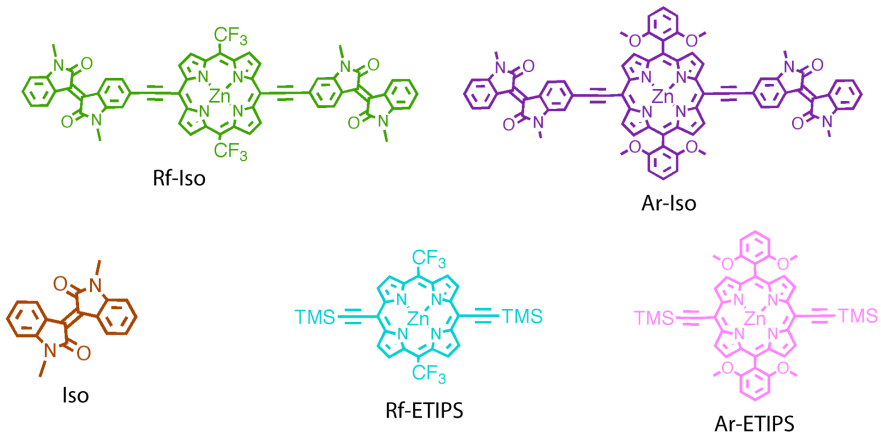

Figure 26. Structural abbreviations utilized for quantum chemical calculations.

energies and properties of these were nearly indistinguishable the results for the C_{2h} structures are reported here. The (perfluoroalkyl)porphyrin derivative Rf-ETIPS lacks a strict plane of symmetry due to the tetrahedral fluoromethyl groups on the 10- and 20-*meso* positions, but symmetry elements from the D_{2h} point groups are approximated for this molecule in Figure 14 and Figure 30. Structure optimizations and linear response calculations were performed with Density Functional Theory (DFT) using Gaussian 09, Rev C.1.[41] The Becke three-parameter hybrid[42] and the Lee-Yang-Parr correlation functional[43, 44] were employed for all calculations (B3LYP). Optimizations were performed with minimal symmetry constraints using tight optimization criteria; initial optimizations used smaller basis sets but the final optimizations and TDDFT calculations employed the 6-311+g basis set[45-53] as implemented in Gaussian 09.

Selected frontier orbital wavefunctions were plotted as isosurfaces (iso=0.02) using Gaussview 5.[193] This software was also used to produce S_1 state electron density difference plots for **Ar-Iso** and **Rf-Iso** by subtracting the ground state density from the excited state electron density distribution; this electron density difference was displayed as a mapped isosurface onto the ground state density (isosurface value = 0.002). TDDFT result files were post-processed using the Gausssum package;[194] this software partitions the wavefunction amplitudes onto atomic components using Mulliken population analysis,[195] and parses the electronic configurations contributing to each excitation. Transition dipole moment vectors were plotted using VMD.[196]

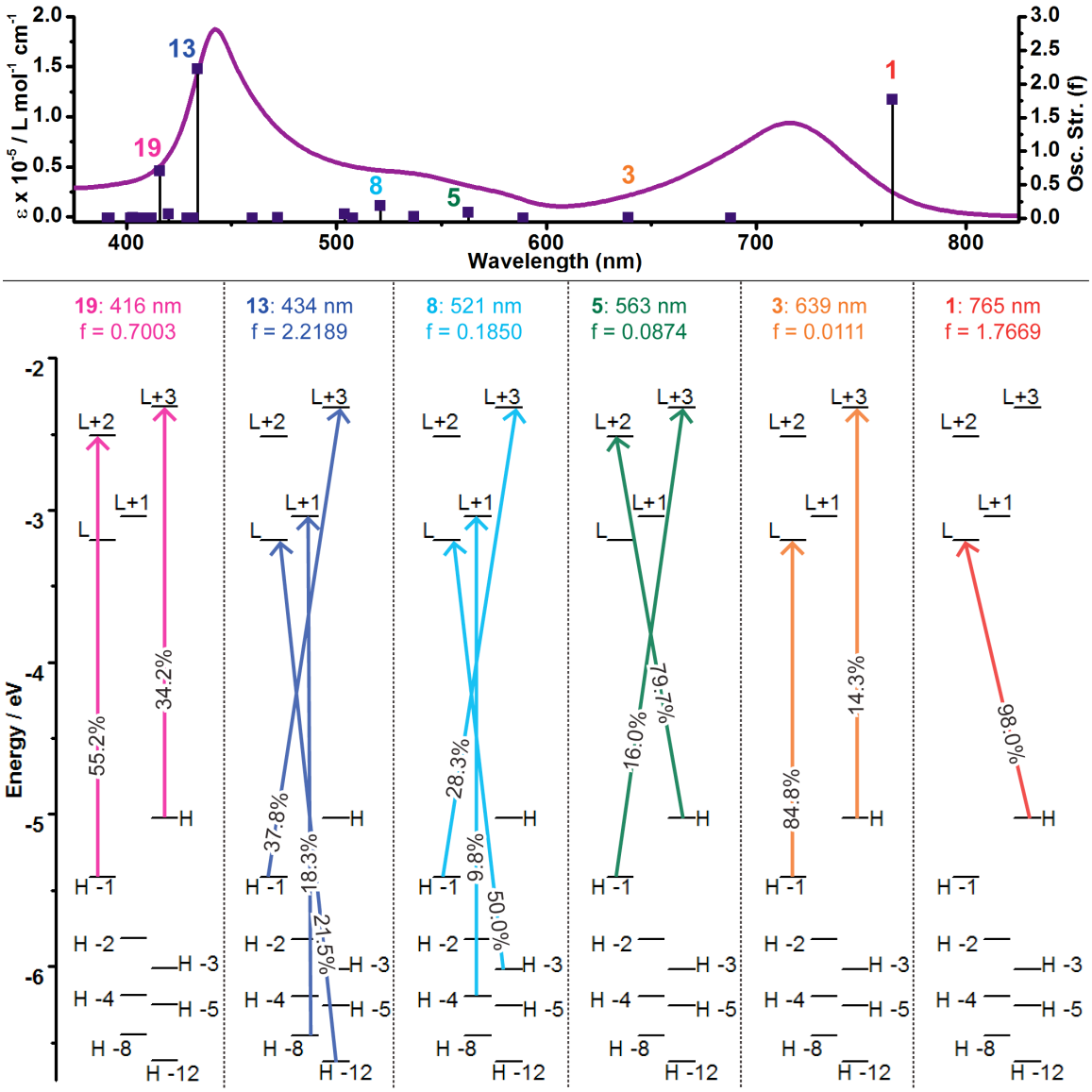

Figure 27. (top) TDDFT-determined transtions for a model of Ar-Iso overlayed with an experimentally determined absorption spectrum in THF solution; (bottom) TDDFT-determined transitions, their polarizations, computed oscillator strengths, and major one-electron configurations depicted as arrows with percentages representing each excitation's contribution to the transition for Ar-Iso.

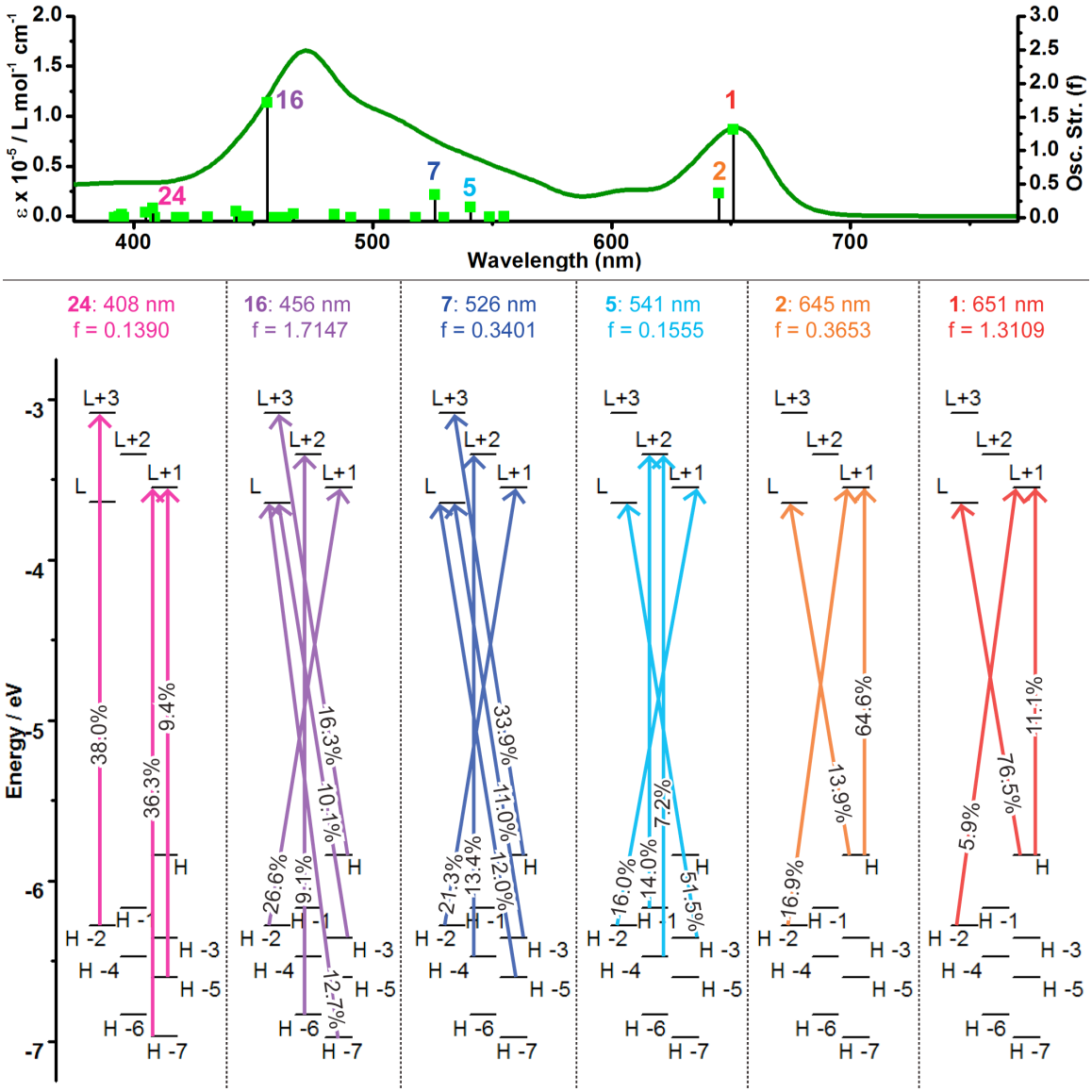

Figure 28. (top) TDDFT-determined transtions for a model of Rf-Iso overlayed with an experimentally determined absorption spectrum in THF solution; (bottom) TDDFT-determined transitions, their polarizations, computed oscillator strengths, and major one-electron configurations depicted as arrows with percentages representing each excitation's contribution to the transition for Rf-Iso.

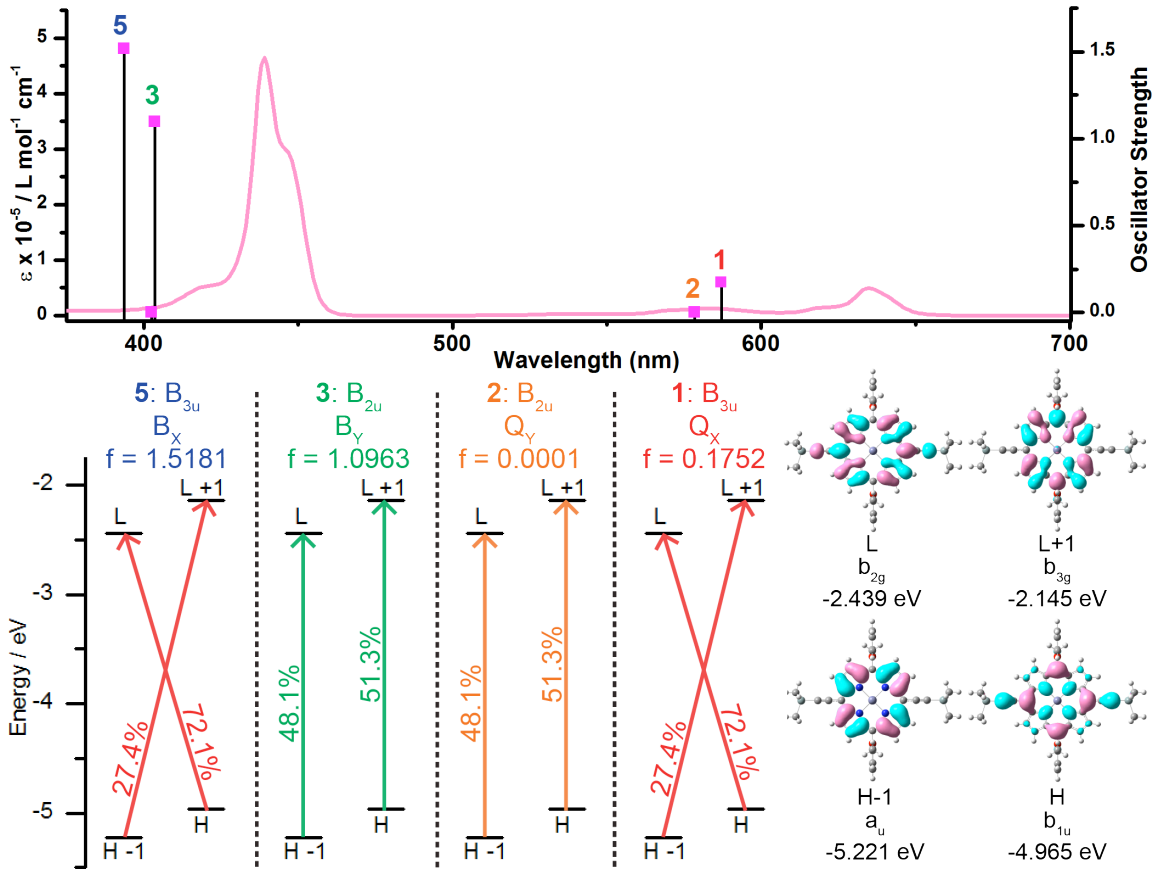

Figure 29. (top) TDDFT-determined transtions for a model of Ar-ETIPS overlayed with an experimentally determined absorption spectrum in THF solution; (bottom left) TDDFT-determined transitions, their polarizations, computed oscillator strengths, and major one-electron configurations depicted as arrows with percentages representing each excitation's contribution to the transition for Ar-ETIPS; (bottom right) frontier wavefunctions calculated for Ar-ETIPS plotted as 0.2 isodensity surfaces.

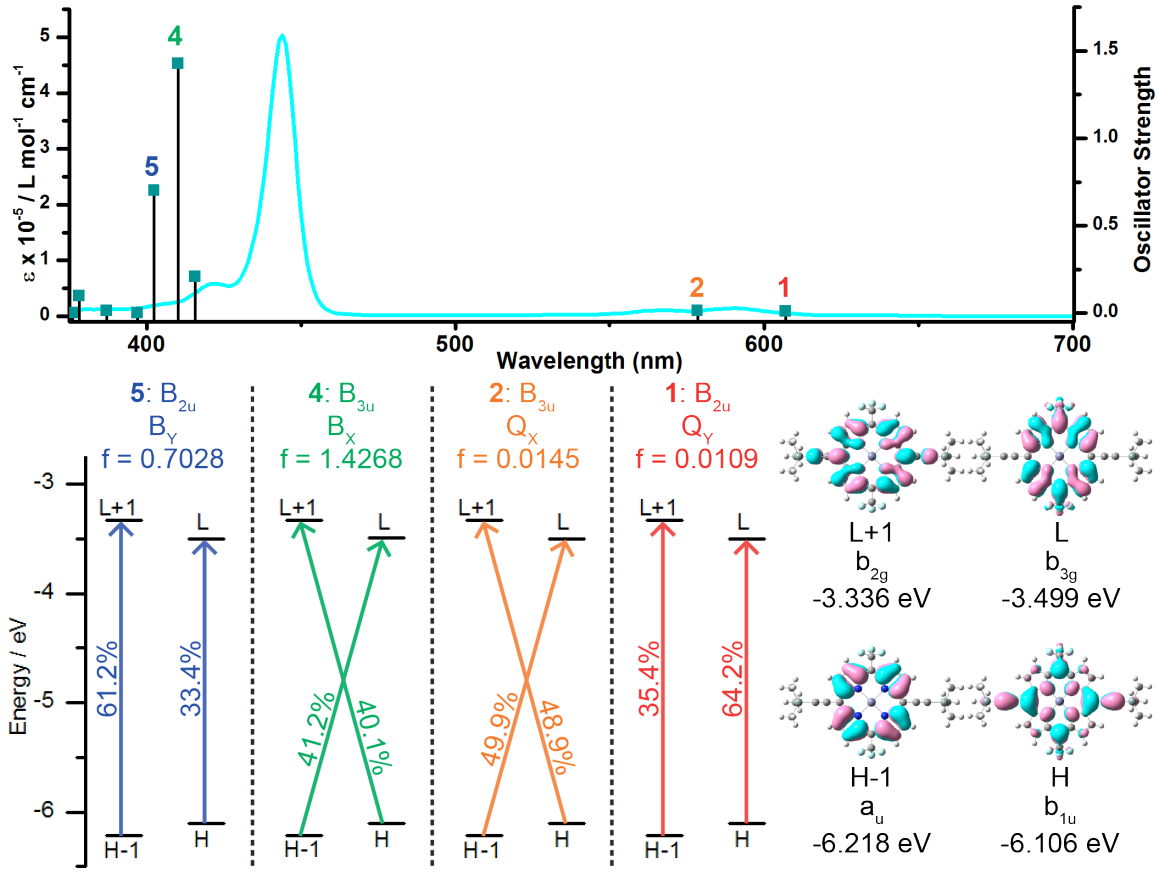

Figure 30. (top) TDDFT-determined transtions for a model of Rf-ETIPS overlayed with an experimentally determined absorption spectrum in THF solution; (bottom left) TDDFT-determined transitions, their polarizations, computed oscillator strengths, and major one-electron configurations depicted as arrows with percentages representing each excitation's contribution to the transition for Rf-ETIPS; (bottom right) frontier wavefunctions calculated for Rf-ETIPS plotted as 0.2 isodensity surfaces.

4. Synthesis of *meso*-(heptafluoropropyl)porphyrins

Jeff Rawson conceived and performed all of this research.

Michael J. Therien supervised this work.

4.1 Introduction

A class of conjugated materials relevant to photovoltaics, nonlinear optics, imaging, and other opto-electronic applications is comprised of strongly-coupled supermolecular chromophore arrays that feature porphyrin macrocycles linked together, or to auxiliary pigments, by ethyne bridges.[1-3, 90] The cylindrically π-symmetric alkyne provides strong interchromophore electronic communication, resulting in globally delocalized ground and excited states. However, there are specific requirements

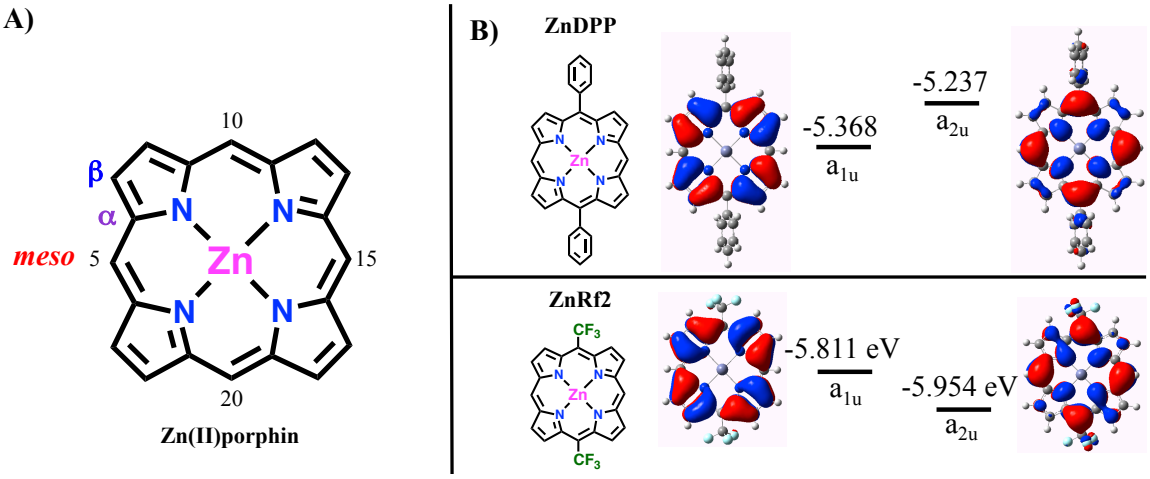

Figure 31. A. Structure of (porphinato)zinc(II) with site labels used in the text. B. (5,15-diphenylporphinato)zinc(II) (ZnDPP, top) and (5,15-bis[heptafluoropropyl]porphinato)zinc(II) (ZnRf2, bottom), pictured with 0.02 isodensity surface plots and calculated energy levels of their two highest occupied molecular orbitals. Symmetry labels from the higher D_{4h} point group have been applied.

regarding the topology of this linkage in order for maximum coupling to be achieved; spectroscopic measurements and potentiometric methods have thoroughly demonstrated that ethyne bridges provide stronger coupling than the longer butadiyne bridges, and that connection to the porphyrin *meso* positions maximizes interpigment communication.[90]

One of the most extreme modulations of the fundamental porphyrin electronic structure occurs when several of the *meso* positions are appended with perfluorinated alkyl groups.[82, 83] These strongly σ-electron-withdrawing substituents dramatically stabilize all of the frontier energy levels, especially those having large wavefunction amplitude at the *meso*-positions (Figure 31). As a result, the spectroscopy and reactivity of these electron-deficient (**A**) porphyrins differ substantially from those of their aryl-substituted (**D**) counterparts. These fascinating pigments have only seen limited incorporation into conjugated arrays,[39] however, due largely to synthetic challenges. The successful application of techniques to construct and derivatize porphyrins is intimately tied with the fundamental electronic structures of these macrocycles. Extreme electronic modulation of porphyrins in multipigment arrays thus intrinsically demands the development of new synthetic methods.

This chapter differs from the others in this dissertation; it serves as a personal memoire, and possibly as a pedagogical tool. Some elements are likely to eventually appear in journal publications, but most will not, and so this is the definitive chronicle of

the work I pursued most passionately during my graduate studies. Section 2 describes a series of efforts that culminated in the synthesis of 5-triisopropylethynyl-10,15,20-tris(heptafluoropropyl)porphyrin **MCQ**. Section 3 describes a computationally-guided exploration of strategies to achieve *meso*-halogenation of *meso*-perfluoroalkyl porphyrins. Section 4 describes experimental results and strategic analysis cogent to the synthesis of *meso*-ethyne-bridged arrays of perfluoroalkyl porphyrins.

4.2 Synthesis of 5-triisopropylsilylethynyl-10,15,20-tris(heptafluoropropyl)porphyrin MCQ

Two *meso*-perfluoroalkylporphyrin precursors suitable for the construction of more complicated arrays are known. Conjugated multipigment chromophores have been constructed starting from 5,15-diethynyl-10,20-bis(heptafluoropropyl)porphyrin **RfE**$_2$ (Figure 32A).[39] The tetrakis(trifluoromethyl) porphyrin can be brominated at one or multiple β-positions following zinc metallation (Figure 32B); this provides a reactive handle for Sonogashira[197] or Suzuki[198] couplings to permit the construction of multipigment systems. The first target for investigation of new synthetic approaches to perfluoroalkyl porphyrins was 5-triisopropylsilylethynyl-10,15,20-tris(heptafluoropropyl)porphyrin **MCQ**. This structure could be readily exploited in the construction of **A**-porphyrin analogues to existing **D**-porphyrin-pigment chromophores, so it would have immediate significance. Furthermore, the pursuit of this compound served as an opportunity to develop methodologies that might eventually yield further advanced structures.

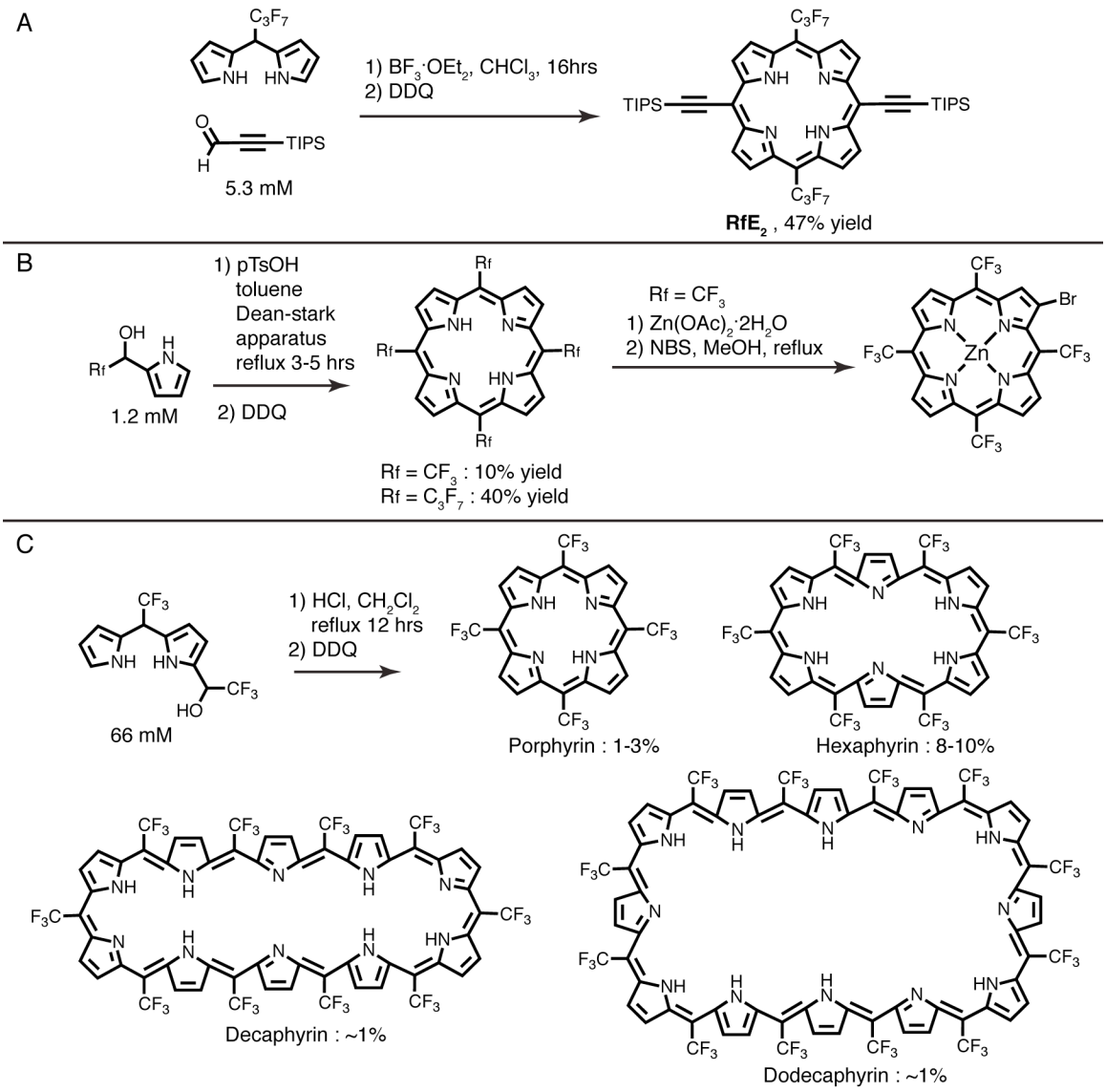

Figure 32. A sampling of precedented approaches to the synthesis of *meso*-perfluoroalkyl porphyrins and porphyrinoids. A) Relatively mild, room-temperature reaction conditions promote the condensation of 5-heptafluoropropyl dipyrromethane with triisopropylsilyl propyne.[39] B) High temperature, high dilution, and water scavenging provide access to tetrakis(perfluoroalkyl)porphyrins.[82, 83] C) Elevated temperature, strong acid, and high concentration favor condensations to form ring-expanded porphyrinoids.[199]

A summary of the known strategies that provide access to *meso*-perfluoroalkyl porphyrins is presented in Figure 32. **RfE$_2$** may be obtained in high yield, using conditions that are mild when compared to those providing other perfluoroalkyl porphyrins; this synthetic accessibility is a consequence of the reactivity of the propargyl aldehydes used in the condensation. The most successful strategies for obtaining *tetrakis*-perfluoroalkyl porphyrins have recognized that a prohibitive reaction step in these condensations is dehydration of an α-fluoro alcohol to form a cationic intermediate.[82, 83] In these cases (Figure 32B), high temperature and water scavenging have been combined to overcome this limitation, and these conditions have also been successfully exploited in condensations of α-perfluoroalkoxy-dipyrromethanes to give bis- and tris(heptafluoropropyl) porphyrins, albeit in yields of only 4-5%.[84] Higher concentrations and a variety of acids have been employed in the pursuit of trifluoromethyl-substituted expanded porphyrinoids (Figure 32C). These conditions appear to reflect the common approach to 5-perfluoroalkyl dipyrromethanes,[200] and while they have not generally been optimized for high yields they offer insights into the fundamental reactivity of fluoroalkylated pyrroles.

The initial efforts to synthesize **MCQ** involved condensations of dipyrromethane intermediates, sometimes referred to as 2+2 approaches (Figure 33). 5-heptafluoropropyl dipyrromethane **1** is available in moderate yield using a literature protocol.[200] Acylation of dipyrromethane **1** with heptafluorobutyric anhydride to give

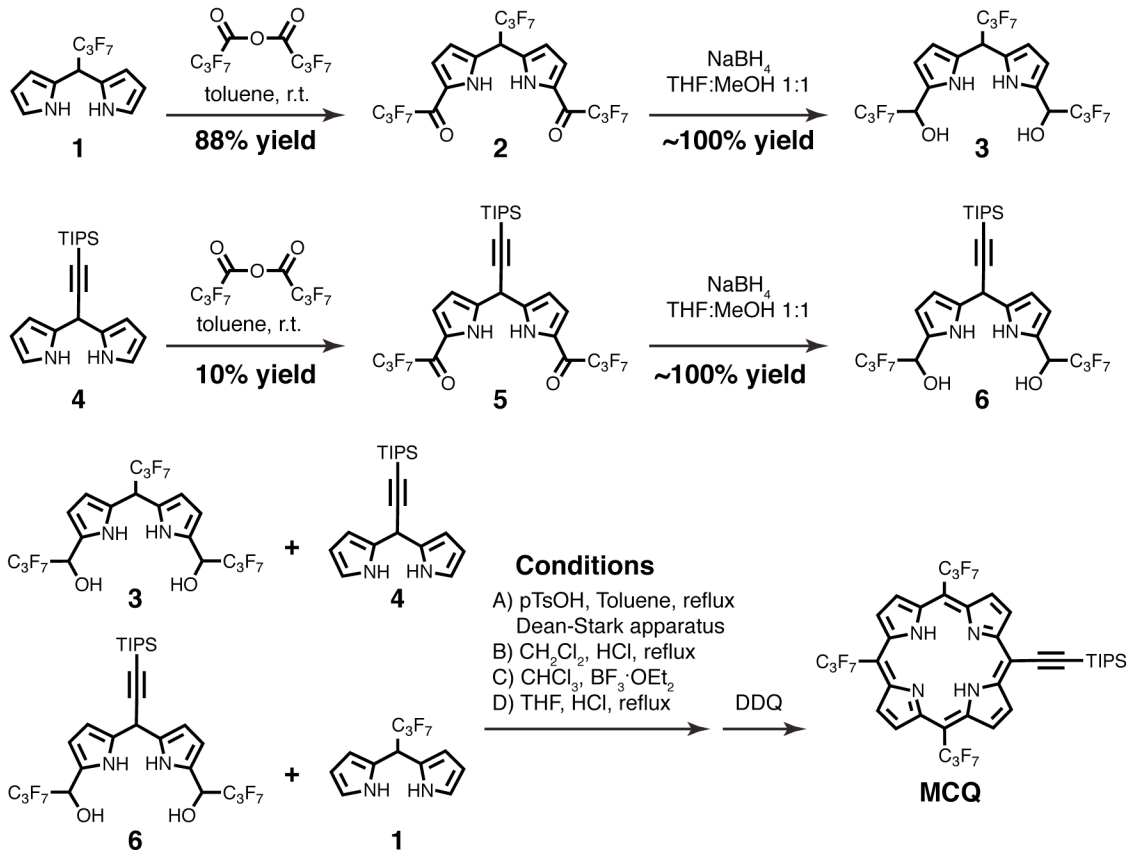

Figure 33. Approaches to dipyrromethane functionalization with heptafluoropropyl and triisopropylsilylethynyl groups, culminating in 2+2 cross-condensations that afforded at best traces of porphyrin MCQ.

diketone **2** was facile, and this extremely stable intermediate could be produced on a 50 gram scale. In our hands, an acylation procedure using heptafluorobutyric chloride[84] provided intractable mixtures of products.

Ethynyl dipyrromethane **4** was obtained reproducibly in greater than 60% yield by modification of an established procedure for synthesis of such structures.[201] Acylation of this using heptafluorobutyric chloride led to recovery only of black tar and starting material, while efforts that employed the acid anhydride gave low yields of ketone **5**.

Reductions of either ketone **2** or **5** by sodium borohydride proceeded in less than one hour to provide diols **3** and **6** in quantitative yields, as reported previously for similar dipyrromethane ketones.[199] However, the alcohols did not readily crystallize and proved to be less stable intermediates than the ketones, and so were prepared upon demand and used immediately.

Because of the bottleneck in preparing ethynyl ketone **5**, efforts to synthesize porphyrin **MCQ** primarily involved condensations between tris(heptafluoropropyl)diol **3** and ethynyl dipyrromethane **4**. Numerous variations of literature conditions were explored, as outlined in Figure 5.2. Reflux in the presence of hydrochloric acid using either THF or methylene chloride solvents (conditions B and D) gave no traces of product that could be detected by matrix-assisted laser desorption ion time-of-flight mass spectrometry (MALDI). Room-temperature treatment with catalytic boron trifluoride diethyl etherate (condition C) gave a complex mixture that provided MALDI results consistent with the presence of **MCQ**, but purification gave an insufficient quantity of material for NMR analysis, even when using several hundred milligrams of precursors **3** and **4**. Treatment with *p*-toluenesulfonic acid in refluxing toluene with water scavenging (condition A) gave the most promising results; with a reflux time of two hours, a quantity of **MCQ** sufficient for NMR analysis could be obtained.

However, optimization of this reaction proved impossible. With shorter reaction times, the primary product recovered was 5-triisopropylsilylethynyl dipyrromethene,

resulting from DDQ oxidation of dipyrromethane **4**. As reaction times were extended, the quantity of this product lessened without any commensurate increase in the yield of **MCQ**; with a reaction time of 16 hours only tar was recovered with no traces of desired product whatsoever. Several efforts that explored condition A using diol **6** and dipyrromethane **1** did not give appreciably increased yields of **MCQ**.

At this point, a reexamination of the reactions of fluoroalkylated pyrroles which proceed most readily was profitable. For 2+2 condensations that produce *meso*(heptafluoropropyl)porphyrins, yields of around 5% have been reported.[84] Furthermore, these reactions must be performed at high dilution (1.2 mM concentration of each reactant) to minimize the probability of successive intermolecular condensation steps, and as concentrations are increased the formation of ring-expanded porphyrins is favored.[199, 202, 203] In contrast, these same sources report yields of 50% or higher for condensations of pyrrole with 1-(2-pyrrolyl)alcohols. The greater success of this latter reaction can be attributed to i) the greater nucleophilicity of pyrrole as compared to fluorinated pyrrole derivatives ii) the greater concentrations and excess equivalents of pyrrole that may be employed in these reactions since only intermolecular condensations are required. Highly scalable syntheses of compounds such as **MCQ** should ideally exploit this facility of condensations with pyrrole nucleophiles, as well as the aforementioned unusual competency of the triisopropylsilylpropynal electrophile (Figure 32A) in condensations with fluorinated pyrrole derivatives.

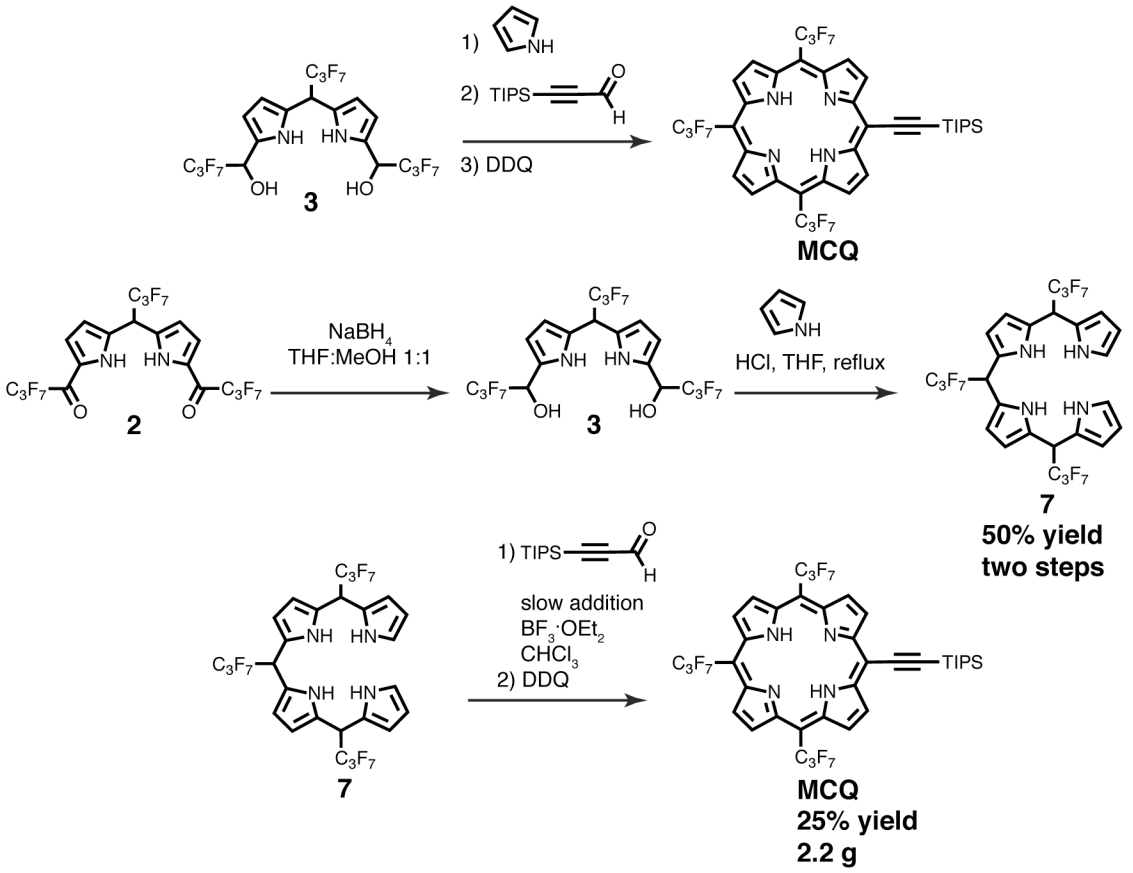

Figure 34. Synthetic approach to the key tris(heptafluoropropyl)bilane and its cyclization to give MCQ in quantities on the order of several grams.

Several attempts were made to achieve a one-pot synthesis of **MCQ** based upon these principles (Figure 34), but yields were still poor and the number of parameters for optimization was a deterrent. Instead, it was recognized that the bilane **7** could be isolated in a respectable 50% yield; substantial decomposition into intractable darkly-colored side products during chromatography could be avoided by employing 1-2% triethylamine in the eluent. For the optimization of the final condensation between bilane **7** and triisopropylsilylpropynal, treatment with hydrochloric acid in refluxing

THF was compared alongside milder conditions employing BF_3•OEt_2 in room temperature chloroform. While the latter provided isolated yields of **MCQ** that neared 5%, it was found that a significant quantity of an acyclic side product was also produced. While this side product was not fully characterized, its presence indicated that the final intramolecular ring closure was a rate-limiting step in the formation of the porphyrinogen whose DDQ oxidation leads to **MCQ**. Furthermore, it suggests that intermolecular attack of the reactive propargyl aldehyde by the bilane might outpace this closure, risking a significant loss of material to sideproducts if this attack were to occur at both ends of the same bilane molecule.

To minimize the effective concentration of aldehyde with respect to bilane, a syringe pump was employed to effect addition of the propynal over ~5 hours. The result was a dramatic increase of the yield, and the complete elimination of the previously observed side product. Thin-layer chromatography analysis of the reaction progress supported our hypotheses regarding the relative rates of the individual condensation steps. Using this slow addition approach, accumulation of the propargyl aldehyde in the reaction mixture was never observed, and two closely eluting product spots could be seen during the first two hours of addition. One of these nascent products was presumably the porphyrinogen, and it is reasonable to assume that the other was the acyclic adduct of bilane **7** with the propynal. Several hours after the addition of

aldehyde was completed, the lower-R_f product spot was no longer observable; at this point oxidation with DDQ gave porphyrin **MCQ** as the sole isolable product.

Optimized yields of 25% with respect to bilane **7** could be achieved, and most gratifyingly, this method was amenable to multigram throughput. The acquisition of **MCQ** in these quantities has made accessible a variety of new multipigment chromophores.

4.3 Experimental study of porphyrin bromination regiochemistry guided by conceptual DFT calculations

4.3.1 Fukui functions for electron loss calculated for a series of (porphinato)zinc(II) complexes

A pivotal reaction for the functionalization of porphyrins and their incorporation into chromophore arrays is halogenation, especially bromination. The bromide serves as a reactive handle that can be targeted by palladium-catalyzed C-C bond forming reactions such as Sonogashira and Suzuki cross-couplings. The original explorations of the bromination reaction of free-base porphin, primarily using N-bromosuccinimide (NBS) as a bromine source, revealed exclusive selectivity for substitution at the *meso* carbons.[204] No comprehensive mechanistic study has explored this reaction, and a recent review asserts no mechanism;[205] nevertheless it is generally accepted that the bromination of porphyrins with NBS, in the absence of radical initiators, proceeds by an electrophilic aromatic substitution[204, 206] and therefore its regioselectivity is governed by the nucleophilicity of the respective porphyrin postitions. Some evidence for this

mechanism in brominations of β-octaalkyl porphyrins using NBS is provided by the observation of side products that derived from bromodealkylation of the bromonium intermediates.[207, 208]

Studies in our lab have found that the treatment of *meso*-fluoroalkyl porphyrins with NBS leads exclusively to products resulting from β substitution. This difference in bromination regioselectivity for electron-rich *meso*-aryl porphyrins versus electron-deficient *meso*-fluoroalkyl porphyrins may be rationalized by frontier orbital analysis (for example, in Figure 31). Methods have been developed that permit the construction of electron-deficient porphyrins possessing one or two *meso*-ethyne groups, granting access to a wealth of conjugated materials based upon this motif. However, the incorporation of these pigments into ethyne-bridged arrays is impeded by the inaccessibility of building blocks that have both bromide and perfluoroalkyl *meso* substituents.

One computational tool that successfully extends beyond simple frontier orbital analysis is the Fukui function, *f*. In its most fundamental conception, it is defined as the change in the density as the electronic population of the system varies under constant external potential:

$$f(\mathbf{r}) = (\delta\rho(\mathbf{r})/\delta N)_{\nu}$$

where ρ is the density, N is the number of electrons in the system, and ν is the potential of the surroundings.[209] The application of this function to computational

problems is usually made tractable by considering a difference between two integer numbers of electrons rather than a partial derivative in what is known as the finite-difference approximation:[210]

$$f^{-}(\mathbf{r},N) \approx \rho(\mathbf{r},N) - \rho(\mathbf{r},N-1)$$

and

$$f^{+}(\mathbf{r},N) \approx \rho(\mathbf{r},N+1) - \rho(\mathbf{r},N)$$

providing two expressions: f^{-}, which describes the change in density upon removal of an electron, and f^{+}, describing the change in density upon gaining an electron. Conceptually, these functions relate the regions of a molecule that most readily lose an electron (f^{-}) or gain an electron (f^{+}); these functions will have large positive values in regions that favor these respective reactions, describing the most likely approach for nucleophiles (f^{+}) or electrophiles (f^{-}).[209] There are two advantages of these functions over qualitative frontier orbital analysis: 1) the possibility to include electron correlation and orbital relaxation effects, and 2) the consideration of the entire system rather than only one molecular orbital might be beneficial in systems, such as porphyrin, where two or more orbitals are very close in energy.

The global Fukui function as defined above is three-dimensional and can be expressed as contours, surfaces, or clouds about the molecule. It is also possible and often desirable to express it in a numerical form on a per-atom basis, in order to

quantitatively predict the regioselectivity of a given reaction. This can be accomplished without, in principle, any loss of theoretical rigor, by substituting atomic populations such as those generated by Mulliken analysis[195] for the densities in the equations above.[211] The resulting condensed-to-atom Fukui functions f_a^- and f_a^+, and their global counterparts, have been found to rationalize the product ratios for electrophilic aromatic substitution reactions such as bromination more successfully than frontier orbital analysis or electrostatic potential mapping.[212] Further elaborations consider the Fukui functions in conjunction with electrostatic potentials; while these have offered improvements for a few cases where the Fukui function failed, these are considered to be unnecessary for reactions with a high degree of electron-transfer character, where outcomes aren't dictated by electrostatic preorganization.[213, 214]

One potential shortcoming of the condensed-to-atom approach is the need to assign electron density to the constituent atoms of a molecule; Mulliken analysis has fallen into disfavor for this purpose and some other approaches are viewed with skepticism.[210] The Natural Bonding Orbital analysis offers a generally accepted approach to partitioning a molecule's electron density among its atoms.[215-218]

The Fukui function has enjoyed only limited application to porphyrin derivatives, in spite of its suitability for describing the reactions of this electronically complex structure. Several efforts have explored metal-centered reactivity in metalloporphyrins using Fukui functions.[219-221] Limited examples of ligand-centered

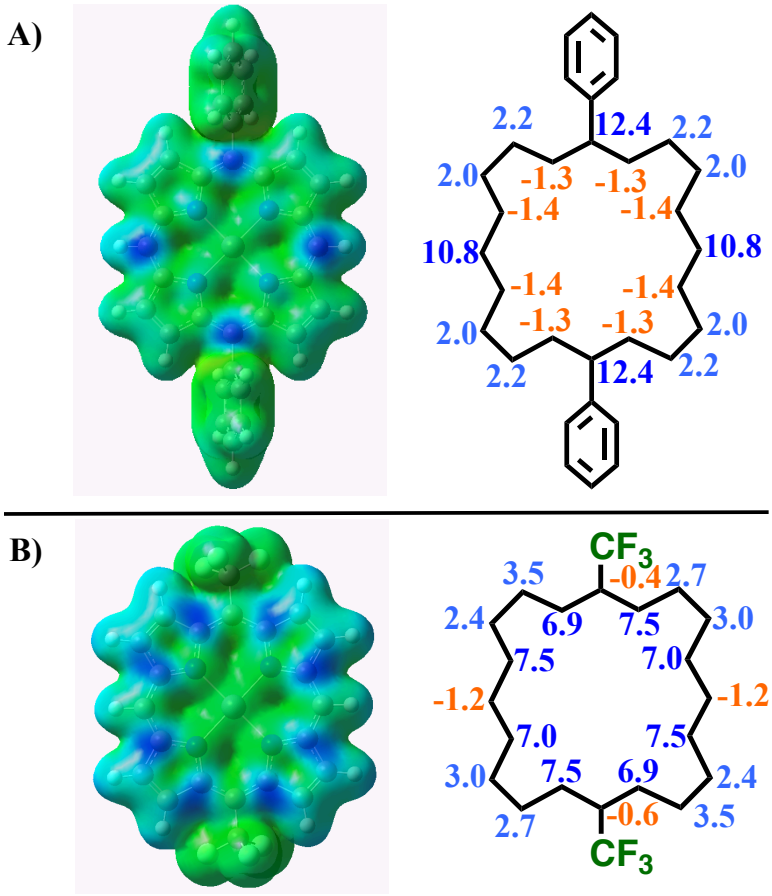

Figure 35. Global f^- functions mapped to isodensity surfaces (blue for positive values, green for values near zero, red for negative) and their condensed-to-atom analogues (f_a^- x100) for A) ZnDPP and B) ZnRf2

Fukui function plots have been reported,[221, 222] but none that explored the regiochemistry of substitutions upon the porphyrin macrocycle.

Error! Reference source not found. compares the Fukui functions for electron loss from **ZnDPP** and **ZnRf2**. These computational results are confirmed by the known experimental selectivities in the reactions of these porphyrins with NBS, and they do not differ from what would be predicted by frontier orbital analysis. Several points are

noteworthy: 1) in both cases, the global f^- maps resemble the HOMO isosurfaces 2) the largest f_a^- values are found at carbons that lack hydrogen atoms and therefore cannot undergo substitution 3) the relative magnitudes of these f_a^- values appear to reflect the relative reactivities of these two porphyrins, where the electron-deficient **ZnRf$_2$** should be less susceptible to electrophilic substitution. This third point should be examined with some caution; the absolute values of condensed-to-atom Fukui functions are known to depend upon system size. For each porphyrin the substitutionally available carbon with largest f_a^- is that which has been experimentally shown to undergo bromination.

One strategy for influencing the site of perfluoroalkyl porphyrin bromination without requiring covalent modification of the porphyrin skeleton is axial ligation. The porphin ligand provides Zn(II) with a square-planar environment in which the ion is coordinatively satisfied, but it is capable of accepting a fifth and even sometimes a sixth ligand. The binding of these ligands results in 1) moderation of the first oxidation potential 2) a red shift of the low-energy absorption maximum 3) a change in the relative intensities of the Q bands lying in the visible region of the spectrum.[223-225] These effects result from electron density transferring to the porphyrin ring, particularly to the a_{2u}-derived occupied orbital with large amplitude at the nitrogen atoms and *meso* positions.[224] A previous study that presented Fukui functions for Zn(II) metalated protoporphyrin IX featuring zero, one, and two axial ligands found little difference between these three;[221] however here we find for electron-deficient porphyrins that the

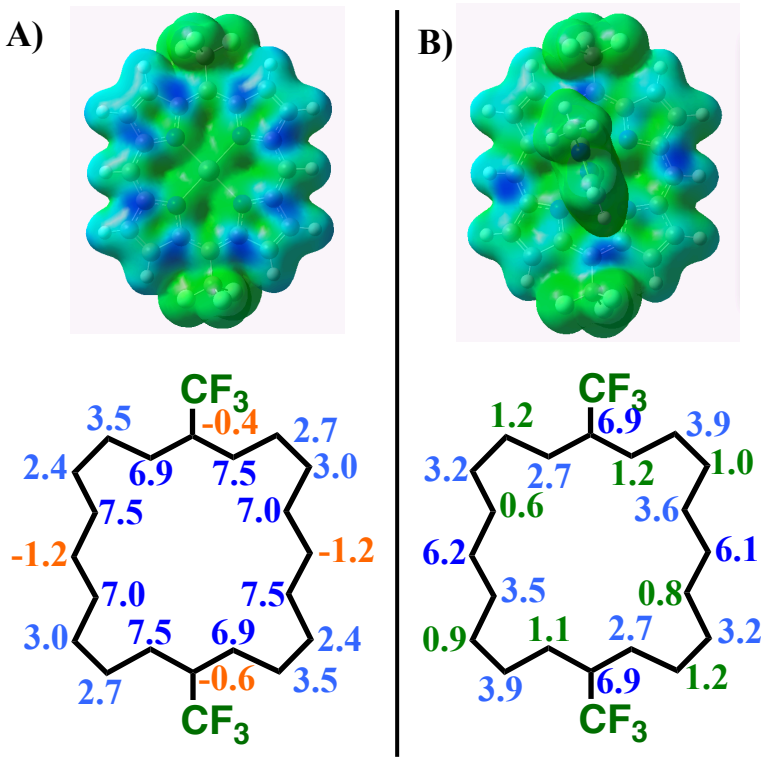

Figure 36. (top) Global maps of f^- onto isodensity surfaces (blue for positive values, green for values near zero, red for negative) and (bottom) the corresponding condensed-to-atom functions determined from NBO populations for A) $ZnRf_2$ and B) Im-$ZnRf_2$.

presence or absence of the methyl imidazole (**MeIm**) axial ligand leads to differing predictions by this metric.

Addition of an axial ligand to **$ZnRf_2$** produces a dramatic change in the Fukui functions, as can be seen in Figure 36. The f^- maps exhibit a shift from maximum polarizability at α and β carbons of **$ZnRf_2$** to maximum polarizability at the *meso* and α carbons of **Im-$ZnRf_2$**. While **MeIm** ligation reduces the energetic split between the a_{1u} and a_{2u} derived orbitals, the HOMO calculated for each is the a_{1u}-derived, pyrrolic orbital. The respective f_a^- values correspond with this trend, with the values at the free

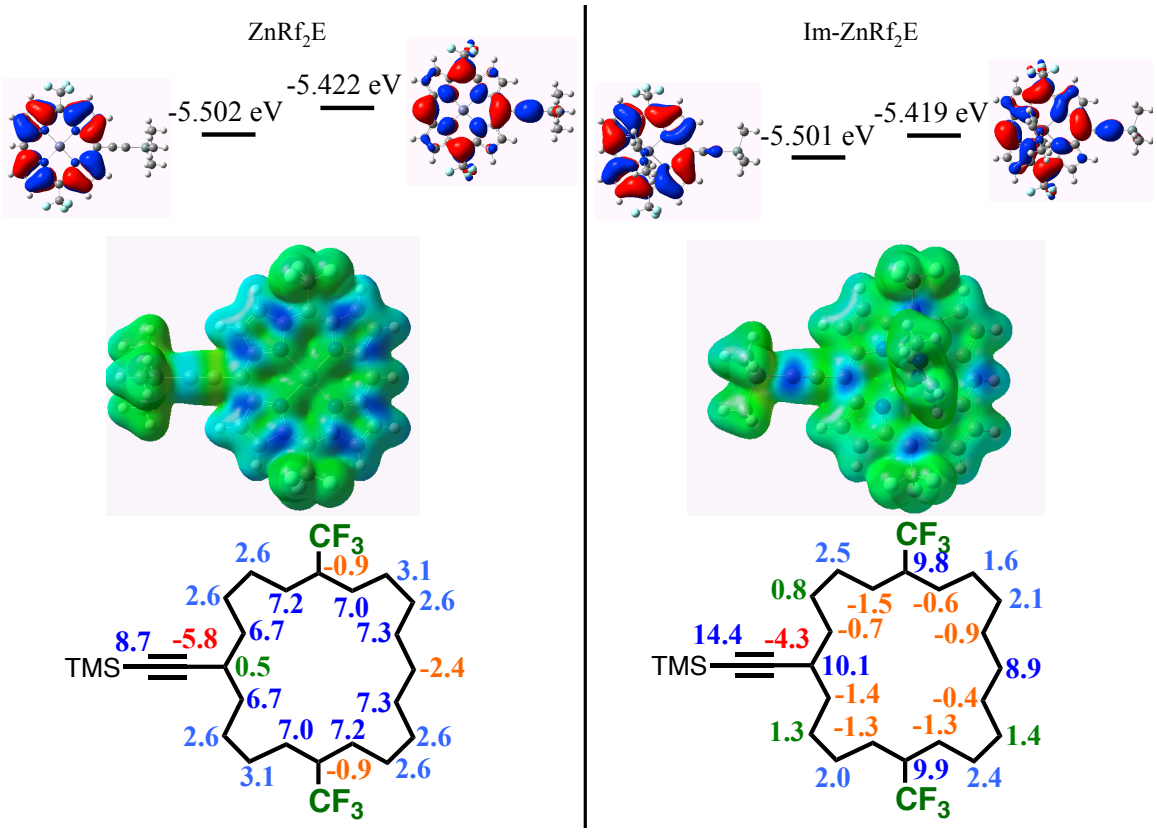

Figure 37. Chemical structures, global f^- surfaces, (blue for positive values, green for values near zero, red for negative) and condensed-to-atom (f_a^- x100) functions for (left) ZnRf$_2$E and (right) Im-ZnRf$_2$E.

meso carbons swinging from -1.2 for **ZnRf$_2$** to 6.1 and 6.2 for **Im-ZnRf$_2$**. These calculations predict that bromination **ZnRf$_2$** in the presence of a strong axial ligand such as **MeIm** may lead to *meso* bromination products.

A similar analysis was also performed for ethyne-substituted **ZnRf$_2$E**, with and without MeIm ligation (Figure 37). For this molecule, the splitting between HOMO and HOMO-1 is very small, with the a_{2u}-derived orbital higher in energy. In spite of this, both the global and the condensed-to-atom Fukui functions for **ZnRf$_2$E** compare very closely with those for **ZnRf$_2$** above; the f_a^- value is -2.4 at the **ZnRf$_2$E** free *meso* carbon,

and the α and β carbons have similar magnitudes to those of **ZnRf$_2$**. It is also noteworthy that the largest f_a^- value is found for the alkyne carbon α to the silyl group, though this is less apparent in the global map.

Axial **MeIm** ligation to **ZnRf$_2$E** reverses the Fukui functions in a fashion similar to that observed for **ZnRf$_2$**. The f_a^- values are commensurate with a favoring of the *meso* over the β position for electrophilic substitution of the ligated complex. With or without the axial ligand, the largest values of f_a^- for the ethynyl porphyrin are found at the alkyne carbon α to the silane. The two significant aspects of these results are that i) Fukui analysis for this system could not be trivialized down to frontier orbital analysis, because the two give different results ii) Fukui analysis suggests that, for **ZnRf$_2$E**, axial ligation by imidizole may play a crucial role in determining the regiochemistry of bromination.

4.3.2 Synthesis and bromination experiments for (5-triisopropylsilylethynyl-10,20-bis[heptafluoropropyl]porphinato)zinc(II)

The synthesis of porphyrin **Rf$_2$E** could be accomplished in close analogy to the approach that yielded **MCQ**, as outlined in Figure 38. The condensation of pyrrole with dipyrromethane **8** gave bis(heptafluoropropyl)bilane **9** in 51% yield, comparable to the yield for bilane **7**. However, porphyrin **Rf$_2$E** was obtained in only 6.4% yield from the subsequent reaction with triisopropylsilyl propynal, and a small amount of diethynyl porphyrin **RfE$_2$** was also recovered. Such a result suggests that individual condensation

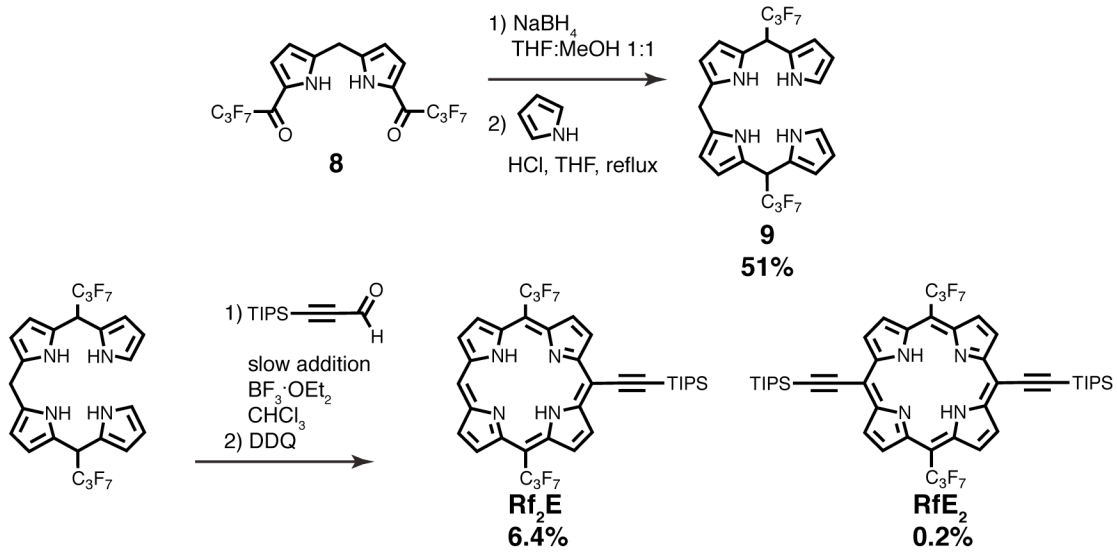

Figure 38. Synthetic scheme leading to porphyrin Rf$_2$E and unexpected side-product RfE$_2$.

steps are reversible under the reaction conditions, which may also explain the low yield of **Rf$_2$E** as compared with the 25% yield for **MCQ**.

The bromination of **Rf$_2$E** was explored by treatment with NBS in either refluxing methanol or room temperature dichloromethane. In refluxing methanol, rapid (10 minute) conversion was observed, giving a product that was more polar than the starting material. NMR and UV/vis spectral analysis demonstrated that, rather than resulting from bromination at either a *meso* or β position, a reaction at the triple bond had occurred (figure 3.9). Evidence for this includes a downfield shift of 1 ppm in the ^{1}H NMR peak corresponding to the triisopropylsilyl group, and a change in the relative intensities of the [0,0] and [0,1] subbands of the visible Q transition. Major and minor isomers in a ratio of ~ 1:4 were evidenced by NMR spectroscopy, but these initially formed products appeared to undergo further transformation during subsequent

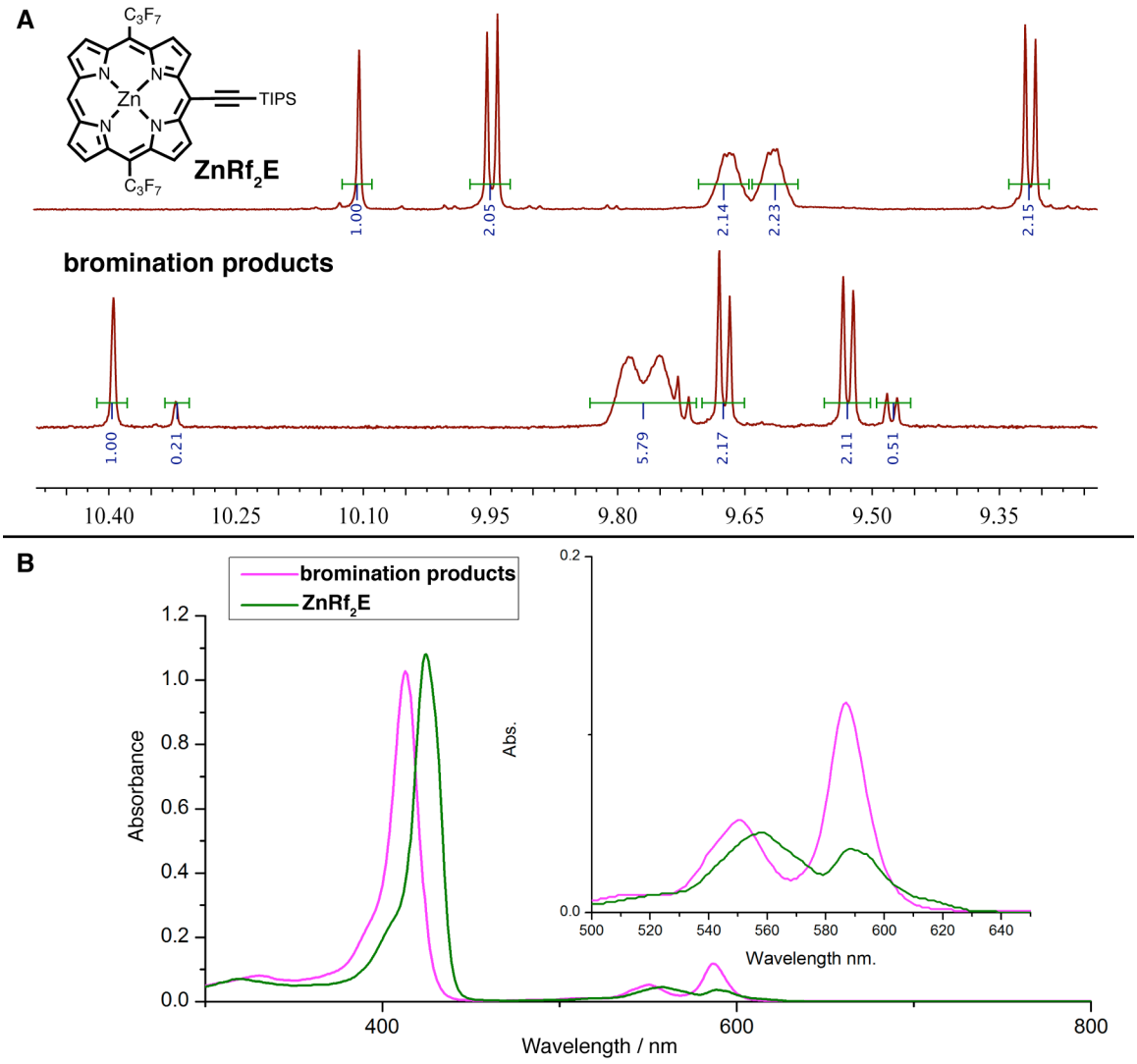

Figure 39. A. Proton NMR spectra in chloroform solvent of $ZnRf_2E$ and the products of its reaction with NBS in refluxing methanol. The presence of two products in ratio of ~1:4 is evidenced by the two signals from *meso* protons at 10.3 ppm and 10.4 ppm, and somewhat resolved beta proton signals at ~9.5 ppm and ~9.7 ppm. B. Electronic spectra in THF solvent of (green) $ZnRf_2E$ and (magenta) the products of its treatment with NBS in refluxing methanol.

purification and so more extensive analysis was not performed. In room temperature dichloromethane, only traces of products too small to be identified were observed.

Inclusion of MeIm ligand in either reaction condition led to a similar result; starting

material was recovered almost quantitatively and any other products were too small in quantity for analysis.

4.3.3 Conclusions from bromination experiments guided by conceptual DFT calculations

The Fukui function for electron loss f^- was calculated for a series of (porphinato)zinc(II) complexes in the presence and absence of methylimidazole axial ligand. For molecules where DFT-calculated HOMO and HOMO-1 were separated by ~0.1 eV or greater, qualitative frontier orbital analysis readily anticipated the f^- prediction. In cases where the split between HOMO and HOMO-1 was smaller than 0.1 eV, frontier orbital analysis and f^- often disagreed. This finding suggests that, for systems endowed with nearly degenerate frontier orbitals such as porphyrin macrocycles, the Fukui function may offer a substantial improvement over traditional frontier orbital analysis for the prediction of reactivity.

For all examples which could be compared with experiment, the Fukui functions provided accurate predictions of the regiochemistry for electrophilic attack. The investigation of NBS-mediated bromination reactions for **ZnRf$_2$E** encountered two main problems. First, the possibility that these reactions might occur at the alkyne was ignored, although f^- was highest at an alkyne carbon. Second, the potential for Lewis basic additives to interfere with the brominating reagents was not considered. Further exploration of conditions, such as the employment of other halogenating reagents or the use of smaller quantities of axial ligand, may yet achieve this important reaction.

4.4 Progress toward ethyne-bridged oligomers of meso-perfluoroalkyl porpyrins

It can be readily envisioned that the development of a successful *meso*-bromination strategy for perfluoroalkyl porphyrins would permit the assembly of an ethyne-bridged dimer **AA** and an ethyne-bridged trimer **AAA**. Even if the challenges outlined in section 3.3 were overcome, however, this strategy might not be optimal if the ultimate goal is to exploit the extraordinary properties of these materials. Note that the synthesis of 5,10,15-tris(heptafluoropropyl)porphyrin has been reported in only 4.5% yield.[84] To attain 73 mg of this material required a reaction in 1.6 L of refluxing benzene; at this rate the acquisition of one gram would require a 21.9 L scale. 5,15-bis(heptafluoropropyl)porphyrin presents a similar challenge; we have shown that while **Rf_2E** can be produced using less demanding conditions it is also obtained in low yield. These results suggest that low yields may be endemic to the synthesis of perfluoroalkyl porphyrins with free *meso* postions. Without a resolution to this challenge, any victory over the bromination problem would be hollow because of the bottleneck at the porphyrin synthesis step.

These observations motivate the consideration of electron-deficient porphyrin oligomer synthesis as a wholistic problem. One possible solution is the simultaneous condensation of bilane **7** onto both ends of acetylene dicarbaldehyde (**ADCA**) as illustrated in figure 3.10. **ADCA** can be synthesized by acidolysis of its tetraethoxy diacetal;[226] in the pure state it spontaneously explodes, even under inert atmosphere, but

methods have been reported for obtaining high-purity chloroform solutions of this reagent. Reactivity as a Diels-Alder dienophile and Michael acceptor have been most frequently observed for **ADCA**, but condensations of nucleophiles directly with the aldehydes catalyzed by trifluoroacetic acid have been reported.[227] The success of this approach is thus not assured, but its realization could afford multigram quantities of **AA**.

Another possible route to *meso*-heptafluoropropyl ethyne-bridged porphyrin oligomers would exploit formylethynyl porphyrin **10** as outlined in figure 3.11. No example of a formylethynyl porphyrin has been reported, but one can envision several possible approaches to its synthesis. Most straightforward is the direct formylation of the 5-ethynyl-10,15,20-tris(heptafluoropropyl)porphyrin acetylide with dimethylformamide, but unfortunately this was found to lead to decomposition. A formal formylation, via treatment of the acetylide with diethyl phenyl orthoformate, might provide better results, as has been observed in the synthesis of phenylpropargylaldehyde diethylacetal.[228] The diethylacetal of **10** might also be produced by a condensation of bilane **7** with the **ADCA** monoacetal, which is commercially available, albeit at a high price.

A final strategy with the potential to manifest a wealth of new multipigment chromophores would be the synthesis of a heptafluoropropyl porphyrin that incorporates a halogen surrogate, such as a triflate group. Such a structure might

putatively be derived from an oxyporphyrin as outlined in figure 3.12. One common approach to oxyporphyrins is the oxidation of a β-octaalkylporphyrin,[229-231] but some have also been constructed using 5-oxodipyrromethanes (2,2'-dipyrrylketones). Ketones such as **12** are unusual in that their carbonyl stretches lie at unusually low energies (1580 – 1610 cm^{-1}),[232] giving evidence of mesomeric resonance contributions to their structures, and their reductions with sodium borohydride give dipyrromethanes.[233] Dipyrrylketones are produced in high yield by alkaline hydrogen peroxide treatment of dipyrrylthiones, which in turn can be obtained from a mild reaction of pyrrole and thiophosgene.[232, 233]

The carbonyl group of **12** sufficiently deactivates the α-positions of the pyrroles that acylation with heptafluorobutyric anhydride, as was done to make dipyrromethanes **2** and **8**, might not be possible; meanwhile the thiocarbonyl of **11** is unlikely to be stable to the successive electrophilic and nucleophilic steps required to build up a bilane. It seems likely that treatment of bilane **7** by slow addition of thiophosgene may give the porphyrinogen **13**, and this approach is desirable because it leverages the known accessibility and stability of **7** and the high reactivity of thiophosgene. From porphyrinogen **13** it is possible to envision oxidation with hydrogen peroxide to the ketone, in analogy to the conversion of **11** to **12**, and then the final oxidation to oxyporphyrin **14** using DDQ; other sequences may also lead to **14**. Oxyporphyrins typically exist as a mixture that favors a keto form with a minor enol

component; they can often be acetylated by treatment with acetic anhydride.[234, 235] The case of **14**, which is significantly less electron-rich than typical oxyporphyrins, would be expected to favor the enol tautomer even more than these other examples, and so its treatment with triflic anhydride can be expected to readily afford the triflate **Rf$_3$OTf**.

4.5 Methods

4.5.1 Experimental Methods

Materials: All manipulations were carried out under argon previously passed through an O_2 scrubbing tower (Schweitzerhall R3-11G catalyst) and a drying tower (Linde 3-Å molecular sieves) unless otherwise stated. Air sensitive materials were handled in a Braun 150-M glove box. Standard Schlenk techniques were employed to manipulate air-sensitive solutions. All solvents utilized for chromatography in this work were obtained from Fisher Scientific (ACS grade except for THF, which was Optima HPLC grade). Dry, deoxygenated solvents were obtained from a solvent purification system (Puresolv™, Innovative Technologies, inc.). All NMR solvents were used as received. Silica gel and preparative size exclusion column chromatography were performed on the bench top, using respectively silica gel (Silicycle, 230–400 mesh) and Bio-Rad Bio-Beads SX-1 as media.

Instrumentation: NMR spectra were recorded on a 400 MHz Varian spectrometer and processed using MestReNova LITE version 5.2.5-4119 software. Chemical shifts for ^{1}H NMR spectra are reported relative to the internal standard tetramethylsilane (TMS) in

deuterated solvent (TMS =0.00 ppm). All *J* values are reported in Hertz. MALDI-TOF mass spectroscopic data were obtained with an Applied Biosystems Voyager DE pro instrument under the supervision of Dr George Dubay at Duke University. Samples were prepared as micromolar solutions in THF, and α-cyano-4-hydroxycinnamic acid (CHCA) or 2-(4-hydroxyphenylazo)benzoic acid (HABA) were utilized as matrices. Absorption spectra were collected on a Shimadzu Pharmaspec UV-1700 or a Cary 5000 spectrometer. Emission and excitation spectra were collected on an Ediburgh FLSP 920.

Pyrrole was purchased from Fisher Scientific and either distilled from CaH_2 or passed through a short plug of basic alumina before use. Triisopropylsilyl acetylene, heptafluorobutyryl anhydride, and methylimidazole were purchased from Fisher Scientific and used as received. Heptafluorobutyryl aldehyde was purchased from Matrix Scientific in technical grade (>90% pure); proton and fluorine NMR analyses determined that the principle impurity was the aldehyde hydrate, and this material was used as received. N-bromosuccinimide was purchased from Fisher scientific and recrystallized from water, then dried thoroughly under vacuum before used. Dipyrromethane was synthesized by the method reported by Lindsay *et al.*.[201] 1,1-Bis(2-pyrrolyl)-2,2,3,3,4,4,4-heptafluorobutane was synthesized as reported by Wijesekera.[200] 3-triisopropylsilylpropynal was synthesized as reported by Bourhill *et al.*.[236]

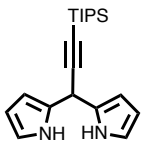

5-Triisopropylsilylethynyl-dipyrromethane (4)

3-Triisopropylsilylpropyne (8 mL, 7.58 g, 36 mmol) and pyrrole (250 mL,

3.6 mole) were combined in a 500 mL round-bottomed flask with a stir bar. Argon was bubbled through this solution for 20 minutes, then $InCl_3$ (0.796 g, 3.6 mmol) was added and the flask quickly resealed, this addition prompted an immediate darkening of the reaction mixture. After 2 hours of stirring at 65° C under argon, $NaHCO_3$ (3 g) was added to the green-brown suspension. A 20 cm Vigreux column, stillhead, condenser, and vacuum adapter were added, and the pyrrole distilled from the reaction under reduced pressure. The remaining residue was extracted three times with boiling hexanes, giving a dark yellow solution; from this the solvent was stripped by rotary evaporation. The remaining residue was chromatographed over silica eluting with CH_2Cl_2, and the product was then crystallized from a mixture of hexanes and CH_2Cl_2 to give the title compound as colorless cubes (7.4 g, 22.7 mmol, 63% yield)

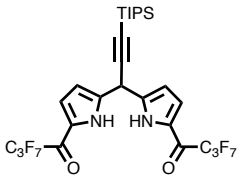

1,9-Bis(2,2,3,3,4,4,4-heptafluorobutanoyl)-5-triisopropylsilylethynyl-dipyrromethane (5)

5-Triisopropylsilylethynyl-dipyrromethane (1.384 g, 4.24 mmol), toluene (60 mL) and a stir bar were combined in a 100 mL round-bottomed flask which was shielded from light using aluminum foil. The solution was purged with argon for 15 minutes before adding heptafluorobutyric anhydride (5.26 mL, 8.69 g, 21.2 mmol) by syringe. The mixture was stirred for 5 hours under argon in the dark, then poured into 100 mL of saturated $NaHCO_3$. This mixture was extracted with several portions of CH_2Cl_2 and the combined organic layers were washed with water and brine, then dried

over Na_2SO_4. After stripping the solvent by rotary evaporation, the residue was chromatographed over silica once eluting with CH_2Cl_2, and once with CH_2Cl_2:hexanes 1:1 to give the title compound as a brown-green residue (300 mg, 0.42 mmol, 10% yield)

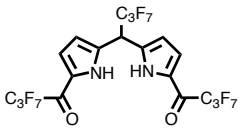

1,9-Bis(2,2,3,3,4,4,4-heptafluorobutanoyl)-5-(heptafluoropropyl)dipyrromethane (2)

5-(heptafluoropropyl)dipyrromethane (0.786 g, 2.5 mmol), 30 mL of toluene, and a stir bar were combined in a 100 mL round-bottomed flask which was shielded from light using aluminum foil. The solution was purged with argon for 15 minutes before adding heptafluorobutyric anhydride (3.10 mL, 5.126 g, 12.5 mmol) by syringe. The mixture was stirred for 5 hours under argon in the dark, then poured into 100 mL of saturated $NaHCO_3$. This mixture was extracted with several portions of CH_2Cl_2, with some ether added to enhance the solubility of the product, and the combined organic layers were washed with water and brine, then dried over Na_2SO_4. After stripping the solvent by rotary evaporation, the residue was recrystallized from CH_2Cl_2 to give the title compound as an off-white powder (1.484 g, 2.10 mmol, 84% yield).

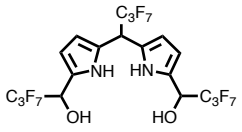

1,9-Bis(2,2,3,3,4,4,4-heptafluoro-1-butanolyl)-5-(1,1,2,2,3,3,3-heptafluoropropyl)dipyrromethane (3)

1,9-Bis(2,2,3,3,4,4,4-heptafluorobutanoyl)-5-(1,1,2,2,3,3,3-

heptafluoropropyl)dipyrromethane (500 mg, 0.708 mmol) was dissolved in 100 mL of a 1:1 mixture of THF and methanol in a 250 mL Erlenmeyer flask containing a stir bar. This was shielded from light using aluminum foil, and then $NaBH_4$ (268 mg, 7.08 mmol, 10 eq) was added in portions over ~1 minute while stirring rapidly. Some evolution of gas and warming was observed. The mixture was stirred for 2 hours, at which time TLC indicated that the starting material was exhausted. The remaining borohydride was quenched by adding ~10 mL of saturated aqueous sodium bicarbonate, producing bubbles and a white precipitate. Addition of 50 mL of saturated aqueous NH_4Cl dissolved the precipitate, and the reaction mixture was then reduced to 2/3 volume by rotary evaporation. This was extracted three times with ether, washed with brine, and dried over Na_2SO_4 before removal of solvent by rotary evaporation left a yellow oil that was found to be pure title compound in essentially quantitative yield. This material was used immediately for subsequent steps; it was found to discolor during storage, even at -40 °C.

5,10,15-Tris(heptafluoropropyl)bilane (7)

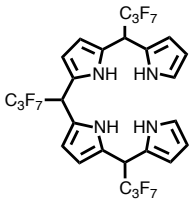

1,9-Bis(2,2,3,3,4,4,4-heptafluorobutanoyl)-5-(1,1,2,2,3,3,3-heptafluoropropyl)dipyrromethane (1g, 1.42 mmol) and 100 mL of methanol:THF 1:1 were stirred in a 250 mL Erlenmeyer flask shielded from light. To this was added $NaBH_4$ (0.536 g, 14.2 mmol, 10 eq) in portions over ~1 minute. After one hour, ~5 mL of saturated aqueous $NaHCO_3$ solution was added and

stirring continued for 30 min. The mixture was then diluted with ether, washed with $NaHCO_3$, water, brine, and dried over Na_2SO_4. The solvent was stripped by rotary evaporation; during this procedure the flask was shielded from light with a sheet of aluminum foil covering the bath. The resulting yellow residue was held under high vacuum in a 200 mL round-bottomed flask wrapped in foil for two hours. The flask was then refilled with Ar, and a stir bar, THF (100 mL), and pyrrole (0.229 mL, 3.3 mmol) were added. A condenser was then attached, the flask wrapped in foil, and the mixture heated at reflux for ½ hour using a mantle heater under a stream of argon. Concentrated HCl (0.5 mL) was then added by syringe and reflux continued for three hours. The mixture was then cooled to room temperature, diluted with water (~50 mL) and saturated aqueous $NaHCO_3$ (~40 mL), and stirred for 20 minutes. The mixture was then extracted with ether, washed with brine, dried with Na_2CO_3, and evaporated. The residue was chromatographed over silica eluting with 1% triethylamine in CH_2Cl_2 to give the title compound as a grey solid (581 mg, 0.719 mmol, 50.6% yield). This material was used immediately in subsequent steps, as it was found to convert to an insoluble black material during storage.

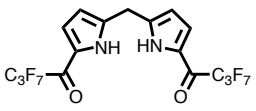

1,9-Bis(2,2,3,3,4,4,4-heptafluorobutanoyl)dipyrromethane (8)

Dipyrromethane (2.32 g, 15.9 mmol) and a stir bar were placed in an aluminum-foil shielded 500 mL round-bottomed flask, which was subsequently

purged with argon for 10 minutes. Toluene (150 mL) was added to this by cannula, and the solution bubbled with argon for 45 minutes. Heptafluorobutyric anhydride was added by syringe, and the solution stirred for 16 hours under argon atmosphere. The mixture was then added to ~200 mL of saturated aqueous $NaHCO_3$ while stirring rapidly, diluted with diethyl ether, and maintained this way shielded from light for two hours. The mixture was then diluted with more water and extracted twice with ether. The combined organic solutions were washed with $NaHCO_3$ solution, brine, and dried over Na_2CO_3 before removal of solvent by rotary evaporation. The residue was held under high vacuum for 16 hours, then stirred in 250 mL of boiling CH_2Cl_2 for one hour. Hexanes (50 mL) was added to this, and the suspension chilled at 5 °C for 36 hours. Recovery by suction filtration and washing with hexanes gave the product as an off-white solid (7.504 g, 13.9 mmol, 87.7% yield).

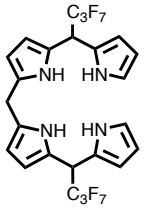

5,15-Bis(heptafluoropropyl)bilane (9)

1,9-Bis(2,2,3,3,4,4,4-heptafluorobutanoyl)dipyrromethane (7.523 g, 14.0 mmol) and 300 mL of methanol:THF 1:1 were stirred in a 500 mL Erlenmeyer flask shielded from light. $NaBH_4$ (5.30 g, 140 mmol, 10 eq) was added in portions over the course of ~1 minute while stirring rapidly. The solution was maintained this way for one hour, at which point TLC showed exhaustion of starting material. Saturated aqueous NH_4Cl (50 mL) was added and the mixture stirred for 10

minutes before concentrating by rotary evaporation. The resulting suspension was extracted twice with ether, and the combined organic solutions washed with brine, dried over Na_2SO_4, and evaporated. After the resulting residue had been held under high vacuum for 0.5 hour, it was transferred to a 2-neck, 100 mL flask equipped with a reflux condenser, aluminum foil wrapping, and stir bar. THF (50 mL) and pyrrole (3.89 mL, 3.757 g, 56.0 mmol, 4 eq) were added, and the solution was purged with argon for 1 hour. Concentrated HCl (1 mL) was added by syringe, and the solution was heated at reflux for 1.5 hours using a heating mantle. The solution was then cooled to room temperature and added to a saturated aqueous solution of $NaHCO_3$ (200 mL) while stirring rapidly. When evolution of gas had ceased, the mixture was extracted with CH_2Cl_2 (200 mL), and the organic phase was washed with $NaHCO_3$, brine, and then dried over $CaCl_2$. After stripping off the the solvent by rotary evaporation, the residue was chromatographed twice over silica eluting with CH_2Cl_2 containing 1% triethylamine to give the title compound as a grey residue (4.589 g, 7.17 mmol, 51% yield). This was used immediately to synthesize 5-Triisopropylsilylethynyl-10,20-bis(heptafluoropropyl)porphyrin.

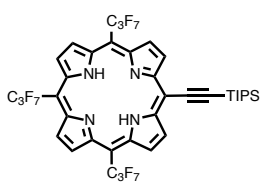

5-Triisopropylsilylethynyl-10,15,20-tris(heptafluoropropyl)porphyrin (MCQ)

Freshly prepared 5,10,15-Tris(heptafluoropropyl)bilane was dissolved in 500 mL of chloroform which had been distilled from CaH_2 under argon.

This solution was purged with argon for two hours. Simultaneously, a solution of 3-triisopropylsilyl-2-propynal (1.34 mL, 5.24 mmol, 1.1 eq) in chloroform (20 mL) was purged with argon for 20 minutes. $BF_3 \bullet OEt_2$ (0.3 mL) was added to the bilane solution, immediately darkening its color, and the propynal solution was then added to this over ~6 hours by syringe pump while stirring under an argon atmosphere in the dark. After stirring for two hours more, DDQ (3.24 g, 14.3 mmol, 3 eq) dissolved in THF (20 mL) was added by syringe. The mixture was left under an argon atmosphere for one hour, then opened to the air, treated with 0.5 mL pyridine, and heated briefly to reflux. Upon cooling to room temperature, the solution was pulled through a plug of silica by suction filtration, and the solvent stripped by rotary evaporation. The residue was chromatographed over silica with CH_2Cl_2:hexanes 1:1, CH_2Cl_2:hexanes 2:8, CH_2Cl_2:hexanes 1:9, to give the title compound as a lustrous purple-black solid (1.091 g, 11.1 mmol, 23% yield).

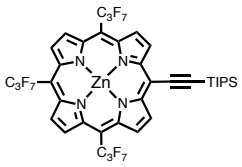

[5-Triisopropylsilylethynyl-10,15,20-tris(heptafluoropropyl)porphinato]zinc(II) (ZnMCQ)

5-Triisopropylsilylethynyl-10,15,20-tris(heptafluoropropyl)porphyrin (1.005 g, 1.24 mmol) and zinc acetate dihydrate (2.73 g, 12.4 mmol, 10 eq) were combined in a 500 mL round-bottomed flask with a stir bar. To this was added CH_2Cl_2:methanol 1:1 (300 mL), and the solution heated at reflux for 16

hours. After cooling to room temperature, the mixture was diluted with water and extracted twice with CH_2Cl_2. The combined organic solutions were dried over Na_2SO_4, and the solvent stripped by rotary evaporation. The residue was purified by silica chromatography; the column was formed from a slurry of silica in THF:hexanes 2:98, and the residue was loaded as a hexanes solution. Elution with hexanes gave one dark purple band which was collected and evaporated down to give the title compound (0.989 g, 0.935 mmol, 75% yield). Analytical samples were further purified by slow evaporation of a CH_2Cl_2:methanol solution to give 0.489 g of sparkling purple-black crystals.

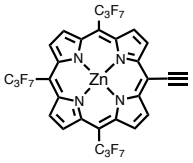

[5-Ethynyl-10,15,20-tris(heptafluoropropyl)porphinato]zinc(II)

[5-Triisopropylsilylethynyl-10,15,20-tris(heptafluoropropyl)porphinato]zinc(II) (0.251 g, 0.237 mmol) was placed in a 50 mL round-bottomed flask with a stir bar. This was sealed with a septum stopper and purged with argon for 20 minutes. Simultaneously, a solution of tetrabutylammonium fluoride (1 M in THF, 0.5 mL, 0.5 mmol, 2 eq) in 30 mL THF was purged with argon while cooling to 0 °C. The solution was cannulated into the flask containing the porphyrin and this mixture was stirred at 0 °C for 10 minutes, at which time TLC indicated that the starting material was exhausted. The solution was pulled through a short plug of silica, and the solvents removed by rotary evaporation. The residue was chromatographed

over silica using a 5:95 THF:hexanes mobile phase; the single purple band was collected and evaporated down to give the title compound (0.205 g, 0.227 mmol, 95% yield).

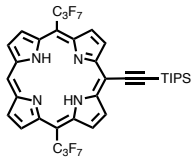

5-Triisopropylsilylethynyl-10,20-bis(heptafluoropropyl)porphyrin (Rf_2E)

Freshly prepared 5,15-bis(heptafluoropropyl)bilane (4.59 g, 7.17 mmol), arong-purged chloroform (500 mL), and a stir bar were brought together in a 500 mL round-bottomed flask wrapped in aluminum foil. In a separate flask, a solution of 3-triisopropylsilyl propynal (2.02 mL, 1.66 g, 7.88 mmol, 1.1 eq) in chloroform (20 mL) was purged with argon for 20 minutes. $BF_3 \bullet OEt_2$ (0.3 mL) was added to the bilane solution, and the propynal solution was then added to this by syringe pump over ~5 hours. After 10 more hours stirring under argon atmosphere, the reaction was unsealed and treated with DDQ (4.88 g, 21.5 mmol, 3 eq) and triethylamine (1 mL), and briefly heated to reflux. The mixture was allowed to cool to room temperature and suction filtered through a plug of silica. After stripping of the solvent by rotary evaporation, the residue was chromatographed several times over silica eluting with chloroform, then chloroform:hexanes 6:4, then chloroform:hexanes 3:7. Following this, the residue was further purified by preparative size exclusion chromatography using SX-1 biobeads with a THF mobile phase. Final purification was accomplished by chromatography over silica eluting with toluene:hexanes 25:75 to give the title compound (0.379 g, 0.458 mmol, 6.4%

yield). Also recovered was 5,15-diethynyl-10,20-bis(heptafluoropropyl)porphyrin (12 mg, 0.014 mmol, 0.2% yield with respect to bilane)

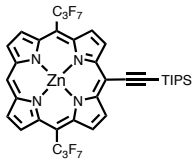

[5-Triisopropylsilylethynyl-10,20-bis(heptafluoropropyl)porphinato]zinc(II) (ZnRf$_2$E)

5-Triisopropylsilylethynyl-10,20-bis(heptafluoropropyl)porphyrin (0.234 g, 0.284 mmol) and zinc acetate dihydrate (0.621 g, 2.83 mmol, 10 eq) were combined in a 250 mL round-bottomed flask. To this was added a stir bar and CH_2Cl_2:methanol 1:1 (150 mL), and the flask was equipped with a condenser and heated at reflux for five hours. At the end of this time, the mixture was cooled to room temperature and diluted with water (300 mL). The organic layer was collected and dried over Na_2SO_4. The solvents were removed by rotary evaporation, and the residue purified by silica chromatography eluting with hexanes:THF 95:5. Further purification was accomplished by preparative size-exclusion chromatography (biobeads SX-1, THF mobile phase) and a final silica column eluting with hexanes:THF 94:6 to give the title compound as a purple solid (0.205 g, 0.230 mmol, 81% yield).

4.5.2 Computational Methods

Starting structures were generated using the Spartan Student package.[237] Two truncations were made in the interest of computational economy; heptafluoropropyl groups were abbreviated as trifluoromethyl, and triisopropylsilyl groups were replaced

with trimethylsilyl groups. In the naming scheme used above, the computational structures are designated with 'prime' after their abbreviation.

Structure optimizations and single-point energy calculations were performed with Density Functional Theory (DFT) using Gaussian 09, Rev C.1.[41] The Becke three-parameter hybrid[42] and the Lee-Yang-Parr correlation functional[43, 44] were employed for all calculations (B3LYP). Optimizations were performed without symmetry constraints (keyword 'nosymm'); initial optimizations used smaller basis sets but the final structures were all produced using tight optimization criteria and the 6-311g basis set[45-53] with two additional d functions (6-311G(2d)) as implemented in Gaussian 09.

Global Fukui functions f^- and f^+ were calculated by generating total electron density cube files for the neutral molecules and the cations (f^-) and anions (f^+) using the coordinates for the neutral species. The cubman[41] utility was used to perform subtraction of the cation density from the neutral (f^-) or the neutral density from the anion (f^+) to yield the Fukui cubes. Global plots of f^- and f^+ were then produced by mapping the neutral electron density calculated with 0.01 isovalue onto these fukui cubes using Gaussview 5.[193]

Condensed to atom Fukui functions f_a^- and f_a^+ were produced for all the porphyrins studied using the Natural Bonding Orbital package within Gaussian 09 (keyword 'pop=nbo').[238] Populations for each atom in the neutral and oxidized or reduced forms were recorded, and the neutral populations subtracted from the anion

populations (f_a^+) or the cation populations subtracted from the neutral populations (f_a^-). For the isobutene and formaldehyde cases, the NBO determined f_a^- and f_a^+ are compared with analogous values determined using Mulliken population analysis as implemented in Gaussian 09.

4.5.3 NMR spectra

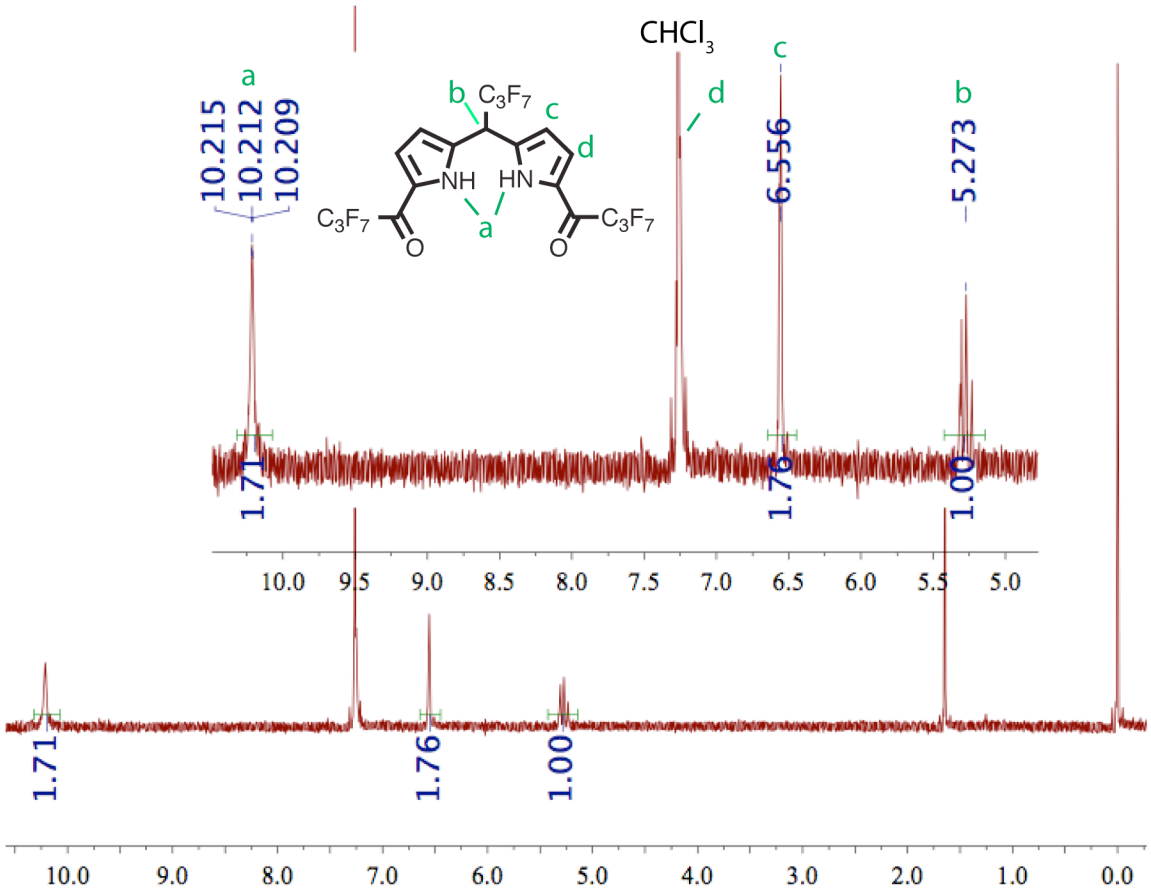

Figure 40. Proton NMR spectrum of dipyrromethane 2 in deuterated chloroform solution.

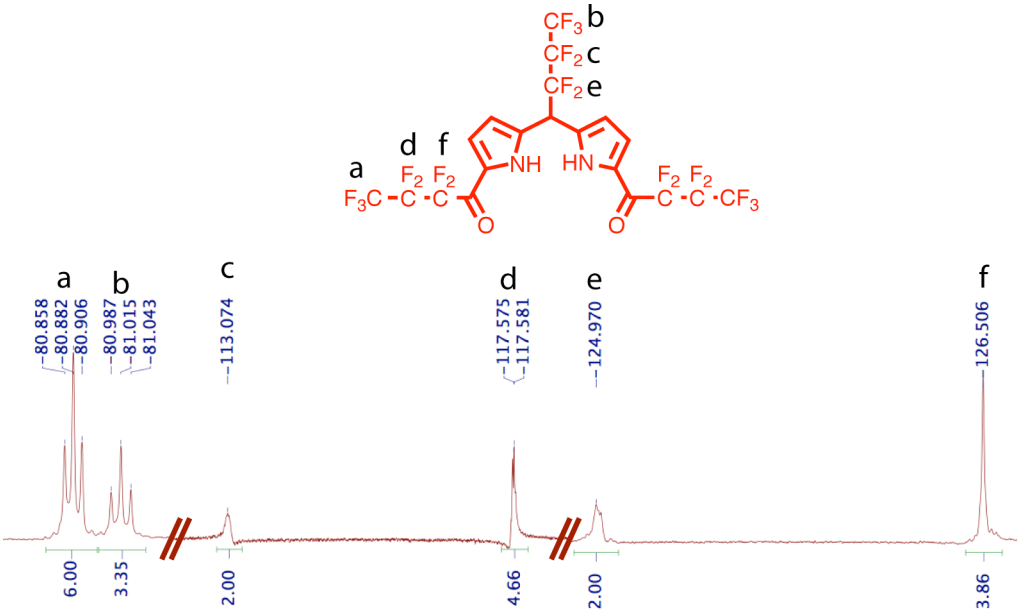

Figure 41. Fluorine NMR spectrum of dipyrromethane 2 in deuterated chloroform solvent.

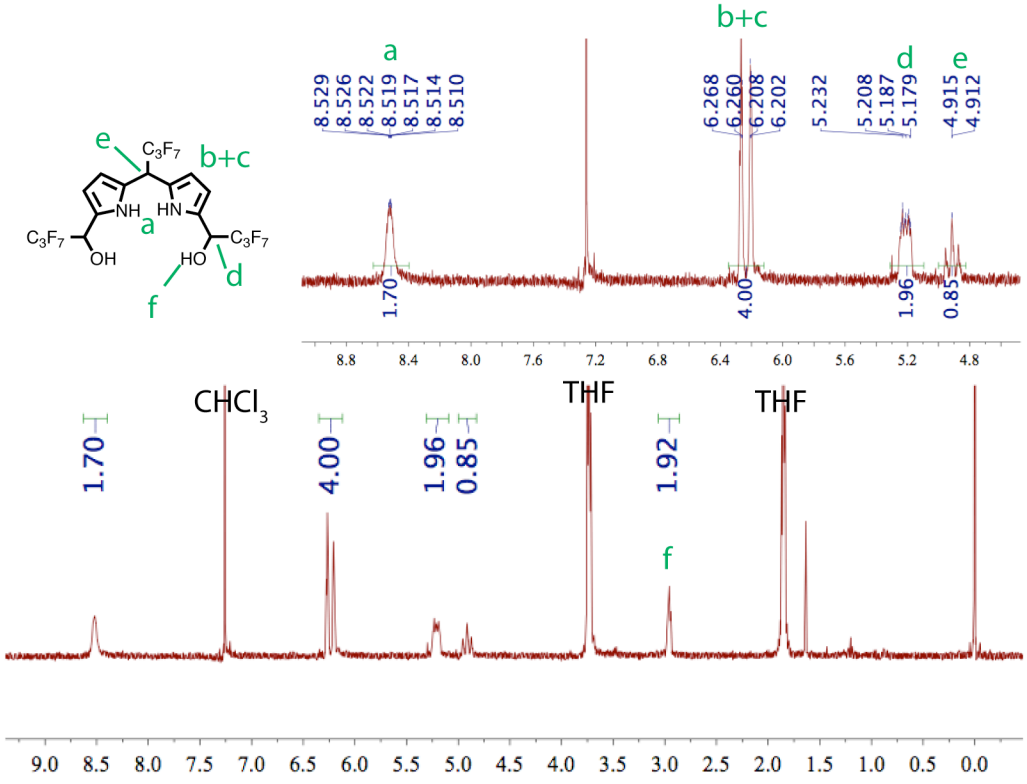

Figure 42. Proton NMR spectrum of dipyrromethane 3 in deuterated chloroform solvent.

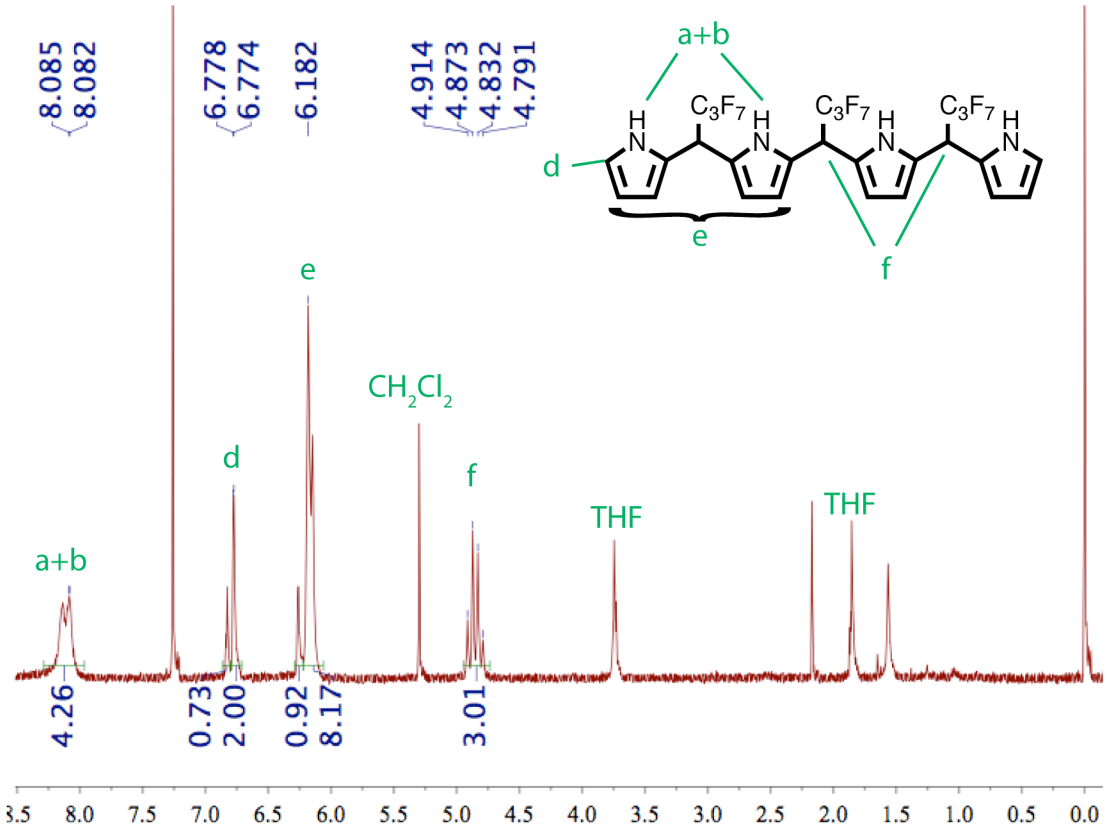

Figure 43. Proton NMR spectrum of bilane 7 in deuterated chloroform solvent.

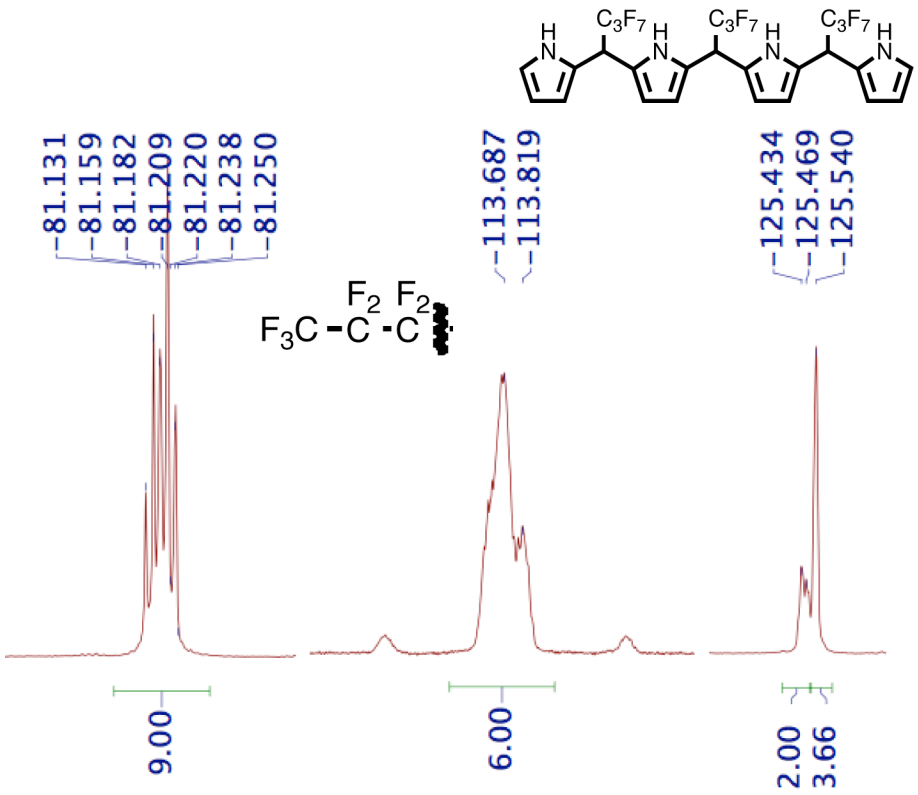

Figure 44. Fluorine NMR spectrum of bilane 7 in deuterated chloroform solvent.

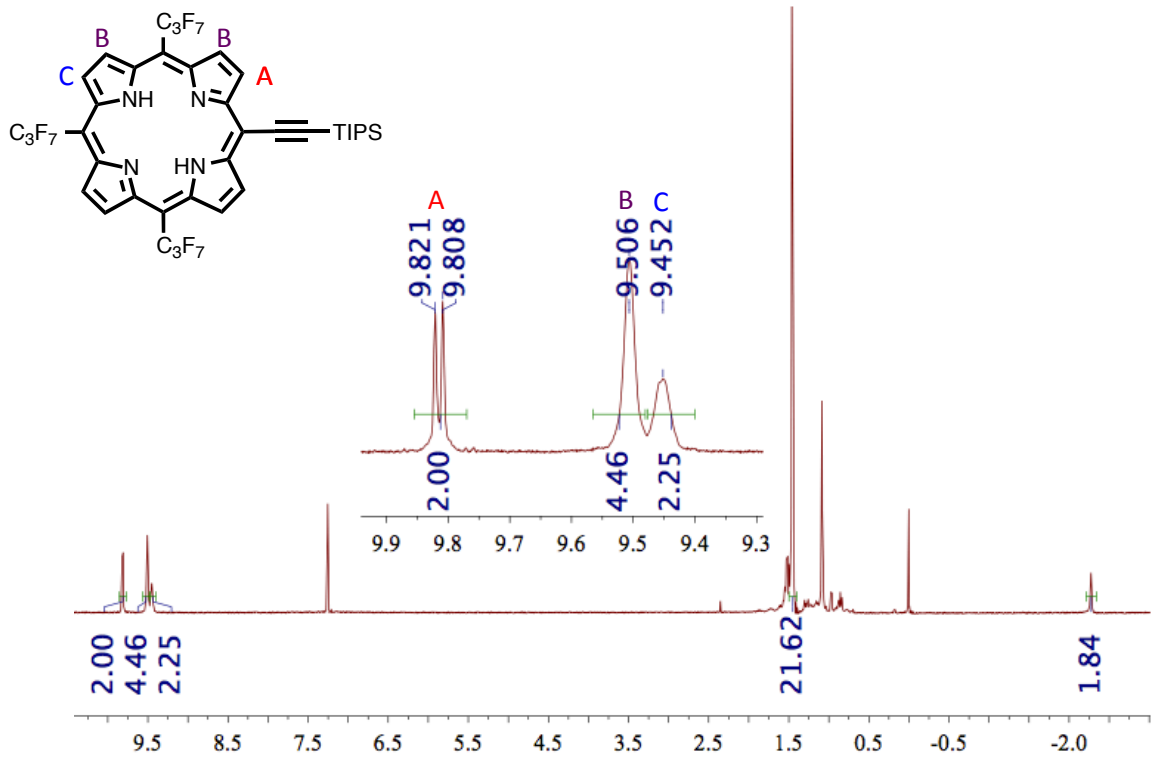

Figure 45. Proton NMR spectrum of porphyrin MCQ in deuterated chloroform solvent.

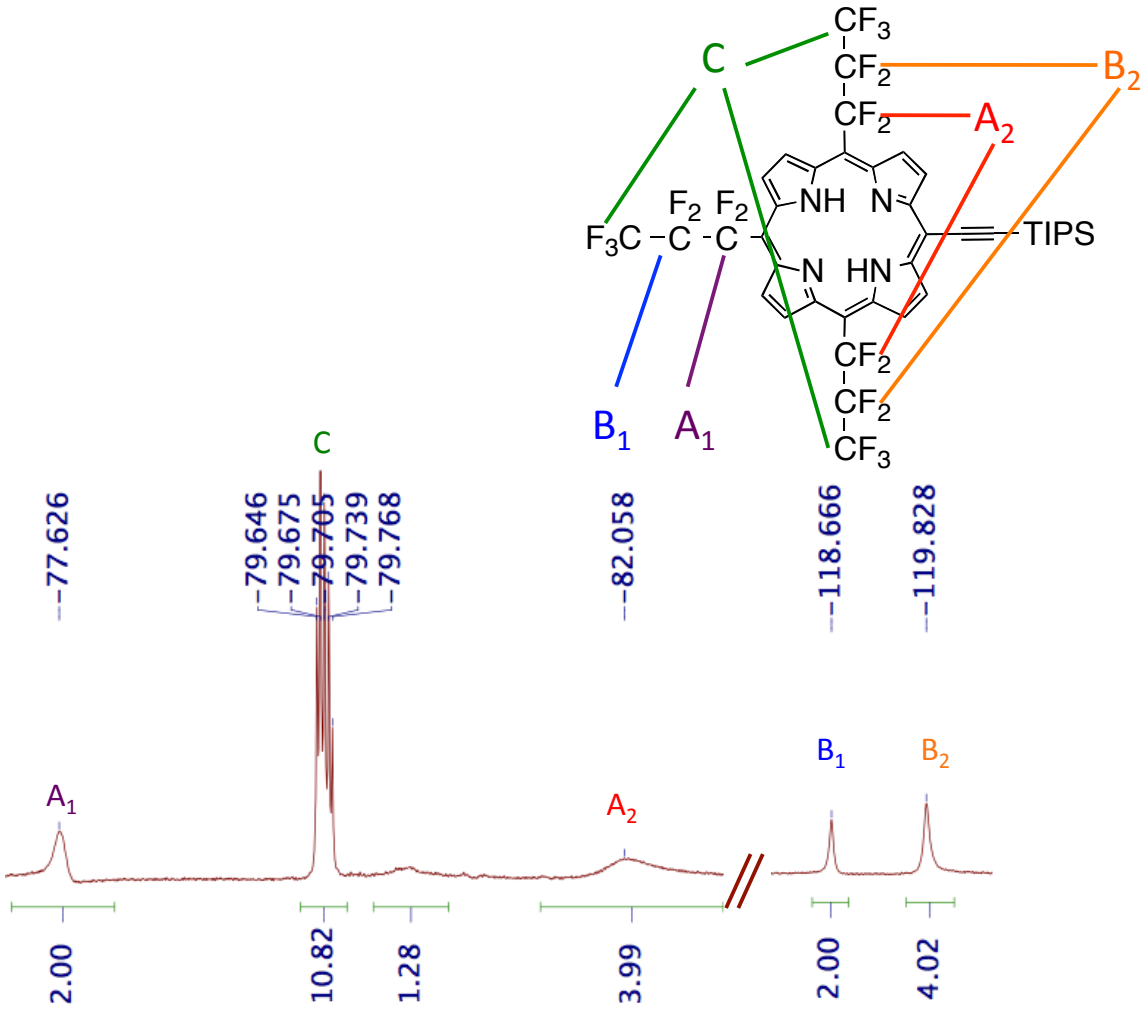

Figure 46. Fluorine NMR spectrum of porphyrin MCQ in deuterated chloroform solvent.

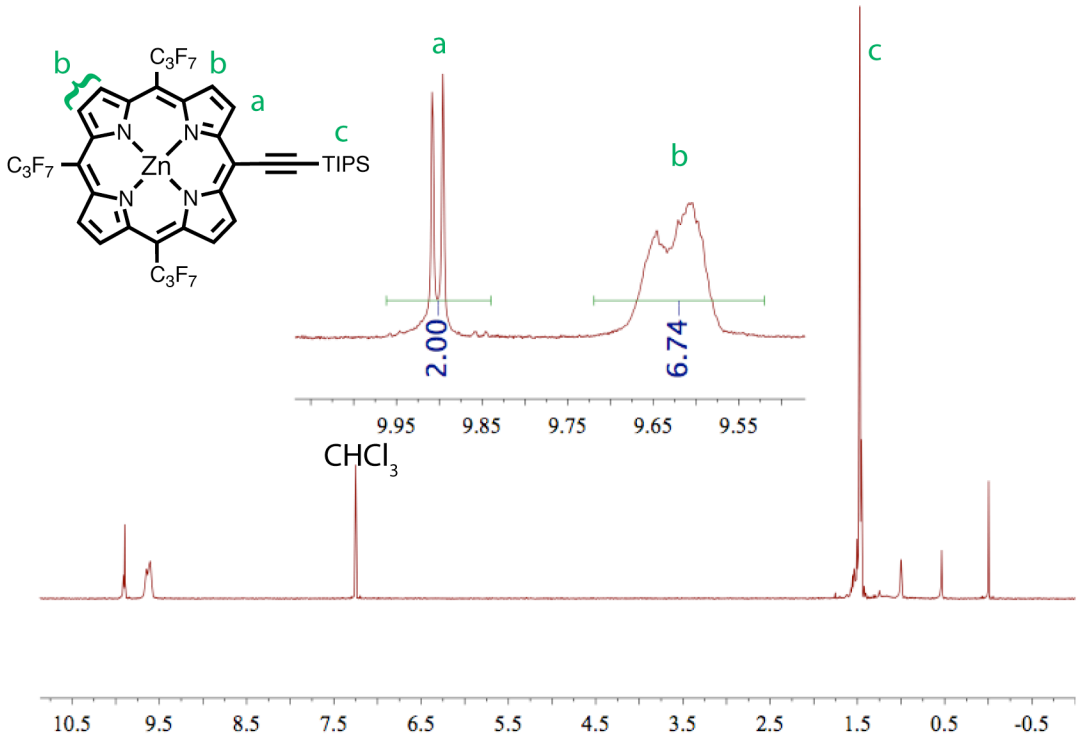

Figure 47. Proton NMR spectrum of porphyrin ZnMCQ in deuterated chloroform solvent.

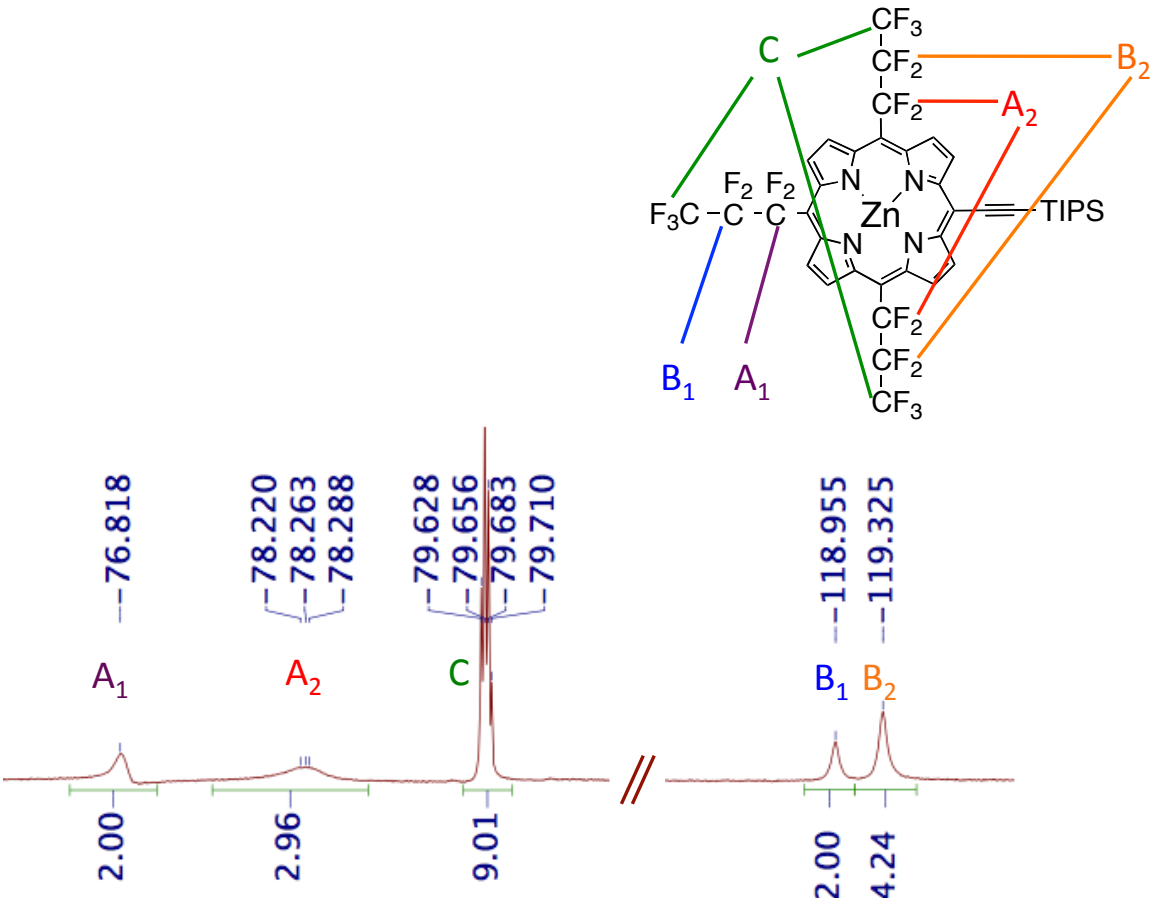

Figure 48. Fluorine NMR spectrum of porphyrin ZnMCQ in deuterated chloroform solvent.

References

1. Lin VS-Y, DiMagno SG, Therien MJ. Highly conjugated, acetylenyl bridged porphyrins: new models for light-harvesting antenna systems. *Science* 1994, **264**(5162)**:** 1105-1111.

2. Uyeda HT, Zhao Y, Wostyn K, Asselberghs I, Clays K, Persoons A, *et al.* Unusual Frequency Dispersion Effects of the Nonlinear Optical Response in Highly Conjugated (Polypyridyl)metal−(Porphinato)zinc(II) Chromophores. *J. Am. Chem. Soc.* 2002, **124**(46)**:** 13806-13813.

3. Susumu K, Duncan TV, Therien MJ. Potentiometric, Electronic Structural, and Ground- and Excited-State Optical Properties of Conjugated Bis[(Porphinato)zinc(II)] Compounds Featuring Proquinoidal Spacer Units. *J. Am. Chem. Soc.* 2005, **127**(14)**:** 5186-5195.

4. Lehn J-M. Supramolecular Chemistry—Scope and Perspectives Molecules, Supermolecules, and Molecular Devices (Nobel Lecture). *Angew. Chem. Int. Ed. Engl.* 1988, **27**(1)**:** 89-112.

5. Connelly NG, Geiger WE. Chemical Redox Agents for Organometallic Chemistry. *Chem. Rev.* 1996, **96**(2)**:** 877-910.

6. Evans DH, O'Connell KM, Petersen RA, Kelly MJ. Cyclic voltammetry. *J. Chem. Educ.* 1983, **60**(4)**:** 290.

7. Geiger WE. Organometallic Electrochemistry: Origins, Development, and Future. *Organomet.* 2007, **26**(24)**:** 5738-5765.

8. Li Y, Hou J. Major Classes of Conjugated Polymers and Synthetic Strategies. In: Sun S-S, Dalton LR (eds). *Introduction to Organic Electronic and Optoelectronic Materials and Devices*. Taylor & Francis Group: Boca Raton, Florida, 2008, pp 173-210.

9. Guo X, Facchetti A, Marks TJ. Imide- and Amide-Functionalized Polymer Semiconductors. *Chem. Rev.* 2014.

10. Frail PR, Susumu K, Huynh M, Fong J, Kikkawa JM, Therien MJ. Modulation of Dark Conductivity over a 1 × 10−12 to 1 × 10−5 S/cm Range Through Ancillary

Group Modification in Amorphous Solids of Ethyne-Bridged (Porphinato)zinc(II) Oligomers. *Chem. Mater.* 2007, **19**(25)**:** 6062-6064.

11. Das R, Harrop P. Printed and organic electronics: forecasts, players, and opportunities 2014-2024. *IDTechEx* 2014.

12. Watanabe S, Ando K, Kang K, Mooser S, Vaynzof Y, Kurebayashi H*, et al.* Polaron spin current transport in organic semiconductors. *Nat. Phys.* 2014, **10**(4)**:** 308-313.

13. Devos A, Lannoo M. Electron-phonon coupling for aromatic molecular crystals: Possible consequences for their superconductivity. *Phys. Rev. B* 1998, **58**(13)**:** 8236-8239.

14. Coropceanu V, Malagoli M, da Silva Filho DA, Gruhn NE, Bill TG, Brédas JL. Hole- and Electron-Vibrational Couplings in Oligoacene Crystals: Intramolecular Contributions. *Phys. Rev. Lett.* 2002, **89**(27)**:** 275503.

15. Zaikowski L, Kaur P, Gelfond C, Selvaggio E, Asaoka S, Wu Q*, et al.* Polarons, Bipolarons, and Side-By-Side Polarons in Reduction of Oligofluorenes. *J. Am. Chem. Soc.* 2012, **134**(26)**:** 10852-10863.

16. Takeda N, Miller JR. Poly(3-decylthiophene) Radical Anions and Cations in Solution: Single and Multiple Polarons and Their Delocalization Lengths in Conjugated Polymers. *J. Phys. Chem. B* 2012, **116**(50)**:** 14715-14723.

17. Bässler H, Köhler A. Charge Transport in Organic Semiconductors. In: Metzger RM (ed). *Unimolecular and Supramolecular Electronics I*, vol. 312. Springer Berlin Heidelberg, 2012, pp 1-65.

18. Moser CC, Keske JM, Warncke K, Farid RS, Dutton PL. Nature of biological electron transfer. *Nature* 1992, **355**(6363)**:** 796-802.

19. Norris JR, Uphaus RA, Crespi HL, Katz JJ. Electron Spin Resonance of Chlorophyll and the Origin of Signal I in Photosynthesis. *Proc. Natl. Acad. Sci. U.S.A.* 1971, **68**(3)**:** 625-628.

20. Marumoto K, Kuroda S-i, Takenobu T, Iwasa Y. Spatial Extent of Wave Functions of Gate-Induced Hole Carriers in Pentacene Field-Effect Devices as Investigated by Electron Spin Resonance. *Phys. Rev. Lett.* 2006, **97**(25)**:** 256603.

21. Tanaka H, Watanabe S-i, Ito H, Marumoto K, Kuroda S-i. Direct observation of the charge carrier concentration in organic field-effect transistors by electron spin resonance. *Appl. Phys. Lett.* 2009, **94**(10)**:** -.

22. Li Z, Park T-H, Rawson J, Therien MJ, Borguet E. Quasi-Ohmic Single Molecule Charge Transport through Highly Conjugated meso-to-meso Ethyne-Bridged Porphyrin Wires. *Nano Lett.* 2012, **12**(6)**:** 2722-2727.

23. Sedghi G, Garcia-Suarez VM, Esdaile LJ, Anderson HL, Lambert CJ, Martin S, *et al.* Long-range electron tunnelling in oligo-porphyrin molecular wires. *Nat. Nano* 2011, **6**(8)**:** 517-523.

24. Susumu K, Frail PR, Angiolillo PJ, Therien MJ. Conjugated Chromophore Arrays with Unusually Large Hole Polaron Delocalization Lengths. *J. Am. Chem. Soc.* 2006, **128**(26)**:** 8380-8381.

25. Yu G, Phillips SD, Tomozawa H, Heeger AJ. Subnanosecond transient photoconductivity in poly(3-hexylthiophene). *Phys. Rev. B* 1990, **42**(5)**:** 3004-3010.

26. Chiang CK, Fincher CR, Park YW, Heeger AJ, Shirakawa H, Louis EJ, *et al.* Electrical Conductivity in Doped Polyacetylene. *Phys. Rev. Lett.* 1977, **39**(17)**:** 1098-1101.

27. Robbins JL, Edelstein N, Spencer B, Smart JC. Syntheses and electronic structures of decamethylmetallocenes. *J. Am. Chem. Soc.* 1982, **104**(7)**:** 1882-1893.

28. Ammeter JH, Swalen JD. Electronic Structure and Dynamic Jahn-Teller Effect of Cobaltocene from EPR and Optical Studies. *J. Chem. Phys.* 1972, **57**(2)**:** 678-698.

29. Closs GL, Closs LE. Negative Ions of Porphin Metal Complexes. *J. Am. Chem. Soc.* 1963, **85**(6)**:** 818-819.

30. Seth J, Bocian DF. Electron paramagnetic resonance studies of metalloporphyrin anion radicals. Effects of solvent, counterion, temperature, and isotopic substitution on the Jahn-Teller active 2Eg ground state. *J. Am. Chem. Soc.* 1994, **116**(1)**:** 143-153.

31. Pawlik J, Gherghel L, Karabunarliev S, Baumgarten M. Characterization of reduced porphyrinatozinc(II) complexes by EPR/ENDOR/TRIPLE and optical absorption spectroscopy. *Chem. Phys.* 1997, **221**(1–2)**:** 121-133.

32. Huber M, Fuhs M. Frontier orbitals of porphyrin electron donors in biomimetic model compounds — partial lifting of orbital degeneracy in asymmetric porphyrins studied by EPR on anion radicals. *Ber. Bunsenges. Phys. Chem.* 1996, **100**(12)**:** 2057-2064.

33. Jaumot J, Gargallo R, de Juan A, Tauler R. A graphical user-friendly interface for MCR-ALS: a new tool for multivariate curve resolution in MATLAB. *Chemometr. Intell. Lab.* 2005, **76**(1)**:** 101-110.

34. Furukawa Y. Reexamination of the assignments of electronic absorption bands of polarons and bipolarons in conducting polymers. *Synth. Met.* 1995, **69**(1–3)**:** 629-632.

35. Fesser K, Bishop AR, Campbell DK. Optical absorption from polarons in a model of polyacetylene. *Phys. Rev. B* 1983, **27**(8)**:** 4804-4825.

36. Vydrov OA, Scuseria GE. Assessment of a long-range corrected hybrid functional. *J. Chem. Phys.* 2006, **125**(23)**:** -.

37. Nelsen SF, Blackstock SC, Kim Y. Estimation of inner shell Marcus terms for amino nitrogen compounds by molecular orbital calculations. *J. Am. Chem. Soc.* 1987, **109**(3)**:** 677-682.

38. Koster LJA, Shaheen SE, Hummelen JC. Pathways to a New Efficiency Regime for Organic Solar Cells. *Adv. Energy Mater.* 2012, **2**(10)**:** 1246-1253.

39. Susumu K, Therien MJ. Decoupling Optical and Potentiometric Band Gaps in π-Conjugated Materials. *J. Am. Chem. Soc.* 2002, **124**(29)**:** 8550-8552.

40. Jaumot J, Tauler R. MCR-BANDS: A user friendly MATLAB program for the evaluation of rotation ambiguities in Multivariate Curve Resolution. *Chemometr. Intell. Lab.* 2010, **103**(2)**:** 96-107.

41. Frisch MJ, Trucks GW, Schlegel HB, Scuseria GE, Robb MA, Cheeseman JR, *et al.* Gaussian 09, Revision C.01. Wallingford CT; 2009.

42. Becke AD. Density-functional thermochemistry. III. The role of exact exchange. *J. Chem. Phys.* 1993, **98**(7)**:** 5648-5652.

43. Lee C, Yang W, Parr RG. Development of the Colle-Salvetti correlation-energy formula into a functional of the electron density. *Phys. Rev. B* 1988, **37**(2)**:** 785-789.

44. Miehlich B, Savin A, Stoll H, Preuss H. Results obtained with the correlation energy density functionals of becke and Lee, Yang and Parr. *Chem. Phys. Lett.* 1989, **157**(3)**:** 200-206.

45. Binning RC, Curtiss LA. Compact contracted basis sets for third-row atoms: Ga–Kr. *J. Comput. Chem.* 1990, **11**(10)**:** 1206-1216.

46. Blaudeau J-P, McGrath MP, Curtiss LA, Radom L. Extension of Gaussian-2 (G2) theory to molecules containing third-row atoms K and Ca. *J. Chem. Phys.* 1997, **107**(13)**:** 5016-5021.

47. Curtiss LA, McGrath MP, Blaudeau J-P, Davis NE, Binning JRC, Radom L. Extension of Gaussian-2 theory to molecules containing third-row atoms Ga--Kr. *J. Chem. Phys.* 1995, **103**(14)**:** 6104-6113.

48. Hay PJ. Gaussian basis sets for molecular calculations. The representation of 3d orbitals in transition-metal atoms. *J. Chem. Phys.* 1977, **66**(10)**:** 4377-4384.

49. Krishnan R, Binkley JS, Seeger R, Pople JA. Self-consistent molecular orbital methods. XX. A basis set for correlated wave functions. *J. Chem. Phys.* 1980, **72**(1)**:** 650-654.

50. McGrath MP, Radom L. Extension of Gaussian-1 (G1) theory to bromine-containing molecules. *J. Chem. Phys.* 1991, **94**(1)**:** 511-516.

51. McLean AD, Chandler GS. Contracted Gaussian basis sets for molecular calculations. I. Second row atoms, Z=11--18. *J. Chem. Phys.* 1980, **72**(10)**:** 5639-5648.

52. Raghavachari K, Trucks GW. Highly correlated systems. Excitation energies of first row transition metals Sc--Cu. *J. Chem. Phys.* 1989, **91**(2)**:** 1062-1065.

53. Wachters AJH. Gaussian Basis Set for Molecular Wavefunctions Containing Third-Row Atoms. *J. Chem. Phys.* 1970, **52**(3)**:** 1033-1036.

54. Peverati R, Truhlar DG. Improving the Accuracy of Hybrid Meta-GGA Density Functionals by Range Separation. *J. Phys. Chem. Lett.* 2011, **2**(21)**:** 2810-2817.

55. NREL. http://rredc.nrel.gov/solar/spectra/am1.5/. [cited 2013 Dec 9th]Available from: http://rredc.nrel.gov/solar/spectra/am1.5/

56. Schlenker CW, Thompson ME. Current challenges in organic photovoltaic solar energy conversion. *Top. Curr. Chem.* 2012, **312:** 175-212.

57. Kirchartz T, Agostinelli T, Campoy-Quiles M, Gong W, Nelson J. Understanding the Thickness-Dependent Performance of Organic Bulk Heterojunction Solar Cells: The Influence of Mobility, Lifetime, and Space Charge. *J. Phys. Chem. Lett.* 2012, **3**(23)**:** 3470-3475.

58. Heeger AJ. 25th Anniversary Article: Bulk Heterojunction Solar Cells: Understanding the Mechanism of Operation. *Adv. Mater.* 2013, **26**(1)**:** 10-28.

59. Ferguson AJ, Kopidakis N, Shaheen SE, Rumbles G. Dark carriers, trapping, and activation control of carrier recombination in neat P3HT and P3HT:PCBM blends. *J. Phys. Chem. C* 2011, **115**(46)**:** 23134-23148.

60. Liu T, Cheung DL, Troisi A. Structural variability and dynamics of the P3HT/PCBM interface and its effects on the electronic structure and the charge-transfer rates in solar cells. *Phys. Chem. Chem. Phys.* 2011, **13**(48)**:** 21461-21470.

61. Jin H, Pivrikas A, Lee KH, Aljada M, Hambsch M, Burn PL, *et al.* Factors Influencing the Efficiency of Current Collection in Large Area, Monolithic Organic Solar Cells. *Adv. Energy Mater.* 2012, **2**(11)**:** 1338-1342.

62. Chen H-Y, Hou J, Zhang S, Liang Y, Yang G, Yang Y, *et al.* Polymer solar cells with enhanced open-circuit voltage and efficiency. *Nat. Photon.* 2009, **3**(11)**:** 649-653.

63. Su M-S, Kuo C-Y, Yuan M-C, Jeng U-S, Su C-J, Wei K-H. Improving Device Efficiency of Polymer/Fullerene Bulk Heterojunction Solar Cells Through Enhanced Crystallinity and Reduced Grain Boundaries Induced by Solvent Additives. *Adv. Mater.* 2011, **23**(29)**:** 3315-3319.

64. Zhou H, Yang L, Stuart AC, Price SC, Liu S, You W. Development of Fluorinated Benzothiadiazole as a Structural Unit for a Polymer Solar Cell of 7 % Efficiency. *Angew. Chem. Int. Ed.* 2011, **50**(13)**:** 2995-2998.

65. He Z, Zhong C, Su S, Xu M, Wu H, Cao Y. Enhanced power-conversion efficiency in polymer solar cells using an inverted device structure. *Nat. Photon.* 2012, **6**(9)**:** 591-595.

66. Small CE, Chen S, Subbiah J, Amb CM, Tsang S-W, Lai T-H, *et al.* High-efficiency inverted dithienogermole-thienopyrrolodione-based polymer solar cells. *Nat. Photon.* 2012, **6**(2)**:** 115-120.

67. Tan Za, Zhang W, Zhang Z, Qian D, Huang Y, Hou J, *et al.* High-Performance Inverted Polymer Solar Cells with Solution-Processed Titanium Chelate as Electron-Collecting Layer on ITO Electrode. *Adv. Mater.* 2012, **24**(11)**:** 1476-1481.

68. You J, Chen C-C, Dou L, Murase S, Duan H-S, Hawks SA, *et al.* Metal Oxide Nanoparticles as an Electron-Transport Layer in High-Performance and Stable Inverted Polymer Solar Cells. *Adv. Mater.* 2012, **24**(38)**:** 5267-5272.

69. You J, Dou L, Yoshimura K, Kato T, Ohya K, Moriarty T, *et al.* A polymer tandem solar cell with 10.6% power conversion efficiency. *Nat. Commun.* 2013, **4:** 1446.

70. Steinmann V, Kronenberg NM, Lenze MR, Graf SM, Hertel D, Meerholz K, *et al.* Simple, Highly Efficient Vacuum-Processed Bulk Heterojunction Solar Cells Based on Merocyanine Dyes. *Adv. Energy Mater.* 2011, **1**(5)**:** 888-893.

71. Wei G, Wang S, Sun K, Thompson ME, Forrest SR. Solvent-Annealed Crystalline Squaraine: PC70BM (1:6) Solar Cells. *Adv. Energy Mater.* 2011, **1**(2)**:** 184-187.

72. Zhou J, Wan X, Liu Y, Long G, Wang F, Li Z, *et al.* A Planar Small Molecule with Dithienosilole Core for High Efficiency Solution-Processed Organic Photovoltaic Cells. *Chem. Mater.* 2011, **23**(21)**:** 4666-4668.

73. Chiu S-W, Lin L-Y, Lin H-W, Chen Y-H, Huang Z-Y, Lin Y-T, *et al.* A donor-acceptor-acceptor molecule for vacuum-processed organic solar cells with a power conversion efficiency of 6.4%. *Chem. Commun.* 2012, **48**(13)**:** 1857-1859.

74. Sun Y, Welch GC, Leong WL, Takacs CJ, Bazan GC, Heeger AJ. Solution-processed small-molecule solar cells with 6.7% efficiency. *Nat. Mater.* 2012, **11**(1)**:** 44-48.

75. Bura T, Leclerc N, Fall S, Leveque P, Heiser T, Retailleau P, *et al.* High-Performance Solution-Processed Solar Cells and Ambipolar Behavior in Organic Field-Effect Transistors with Thienyl-BODIPY Scaffoldings. *J. Am. Chem. Soc.* 2012, **134**(42)**:** 17404-17407.

76. Bura T, Leclerc N, Bechara R, Leveque P, Heiser T, Ziessel R. Triazatruxene-Diketopyrrolopyrrole Dumbbell-Shaped Molecules as Photoactive Electron Donor for High-Efficiency Solution Processed Organic Solar Cells. *Adv. Energy Mater.* 2013, **3**(9)**:** 1118-1124.

77. Kyaw AKK, Wang DH, Wynands D, Zhang J, Nguyen T-Q, Bazan GC, *et al.* Improved Light Harvesting and Improved Efficiency by Insertion of an Optical

Spacer (ZnO) in Solution-Processed Small-Molecule Solar Cells. *Nano Lett.* 2013, **13**(8)**:** 3796-3801.

78. Green MA, Emery K, Hishikawa Y, Warta W, Dunlop ED. Solar cell efficiency tables (version 44). *Prog. Photovoltaics Res. Appl.* 2014, **22**(7)**:** 701-710.

79. Carlé JE, Krebs FC. Technological status of organic photovoltaics (OPV). *Sol. Energy Mater. Sol. Cells* 2013, **119**(0)**:** 309-310.

80. An Z, Odom SA, Kelley RF, Huang C, Zhang X, Barlow S*, et al.* Synthesis and Photophysical Properties of Donor- and Acceptor-Substituted 1,7-Bis(arylalkynyl)perylene-3,4:9,10-bis(dicarboximide)s. *J. Phys. Chem. A* 2009, **113**(19)**:** 5585-5593.

81. Rodríguez-Morgade MS, Claessens CG, Medina A, González-Rodríguez D, Gutiérrez-Puebla E, Monge A*, et al.* Synthesis, Characterization, Molecular Structure and Theoretical Studies of Axially Fluoro-Substituted Subazaporphyrins. *Chem. Eur. J.* 2008, **14**(4)**:** 1342-1350.

82. DiMagno SG, Williams RA, Therien MJ. Facile Synthesis of meso-Tetrakis(perfluoroalkyl)porphyrins: Spectroscopic Properties and X-ray Crystal Structure of Highly Electron-Deficient 5,10,15,20-Tetrakis(heptafluoropropyl)porphyrin. *J. Org. Chem.* 1994, **59**(23)**:** 6943-6948.

83. Goll JG, Moore KT, Ghosh A, Therien MJ. Synthesis, Structure, Electronic Spectroscopy, Photophysics, Electrochemistry, and X-ray Photoelectron Spectroscopy of Highly-Electron-Deficient [5,10,15,20-Tetrakis(perfluoroalkyl)porphinato]zinc(II) Complexes and Their Free Base Derivatives. *J. Am. Chem. Soc.* 1996, **118**(35)**:** 8344-8354.

84. Wertsching AK, Koch AS, DiMagno SG. On the Negligible Impact of Ruffling on the Electronic Spectra of Porphine, Tetramethylporphyrin, and Perfluoroalkylporphyrins. *J. Am. Chem. Soc.* 2001, **123**(17)**:** 3932-3939.

85. Ahmed E, Ren G, Kim FS, Hollenbeck EC, Jenekhe SA. Design of New Electron Acceptor Materials for Organic Photovoltaics: Synthesis, Electron Transport, Photophysics, and Photovoltaic Properties of Oligothiophene-Functionalized Naphthalene Diimides. *Chem. Mater.* 2011, **23**(20)**:** 4563-4577.

86. Huang C, Barlow S, Marder SR. Perylene-3,4,9,10-tetracarboxylic Acid Diimides: Synthesis, Physical Properties, and Use in Organic Electronics. *J. Org. Chem.* 2011, **76**(8)**:** 2386-2407.

87. Mei J, Graham KR, Stalder R, Reynolds JR. Synthesis of isoindigo-based oligothiophenes for molecular bulk heterojunction solar cells. *Org. Lett.* 2010, **12**(4)**:** 660-663.

88. Zhao Y, Wasielewski MR. 3,4:9,10-Perylenebis(dicarboximide) chromophores that function as both electron donors and acceptors. *Tetrahedron Lett.* 1999, **40**(39)**:** 7047-7050.

89. Serin JM, Brousmiche DW, Fréchet JMJ. A FRET-Based Ultraviolet to Near-Infrared Frequency Converter. *J. Am. Chem. Soc.* 2002, **124**(40)**:** 11848-11849.

90. Lin VS-Y, Therien MJ. The Role of Porphyrin-to-Porphyrin Linkage Topology in the Extensive Modulation of the Absorptive and Emissive Properties of a Series of Ethynyl- and Butadiynyl-Bridged Bis- and Tris(porphinato)zinc Chromophores. *Chem. Eur. J.* 1995, **1**(9)**:** 645-651.

91. Kumble R, Palese S, Lin VS-Y, Therien MJ, Hochstrasser RM. Ultrafast Dynamics of Highly Conjugated Porphyrin Arrays. *J. Am. Chem. Soc.* 1998, **120**(44)**:** 11489-11498.

92. Shediac R, Gray MHB, Uyeda HT, Johnson RC, Hupp JT, Angiolillo PJ, *et al.* Singlet and Triplet Excited States of Emissive, Conjugated Bis(porphyrin) Compounds Probed by Optical and EPR Spectroscopic Methods. *J. Am. Chem. Soc.* 2000, **122**(29)**:** 7017-7033.

93. Angiolillo PJ, Susumu K, Uyeda HT, Lin VS-Y, Shediac R, Therien MJ. Trends in triplet excitation delocalization in highly conjugated (porphinato)zinc(II) arrays probed by EPR spectroscopy. *Synth. Met.* 2001, **116**(1–3)**:** 247-253.

94. Rubtsov IV, Susumu K, Rubtsov GI, Therien MJ. Ultrafast Singlet Excited-State Polarization in Electronically Asymmetric Ethyne-Bridged Bis[(porphinato)zinc(II)] Complexes. *J. Am. Chem. Soc.* 2003, **125**(9)**:** 2687-2696.

95. Angiolillo PJ, Uyeda HT, Duncan TV, Therien MJ. Impact of Electronic Asymmetry on Photoexcited Triplet-State Spin Distributions in Conjugated Porphyrin Oligomers Probed via EPR Spectroscopy. *J. Phys. Chem. B* 2004, **108**(32)**:** 11893-11903.

96. Duncan TV, Susumu K, Sinks LE, Therien MJ. Exceptional Near-Infrared Fluorescence Quantum Yields and Excited-State Absorptivity of Highly Conjugated Porphyrin Arrays. *J. Am. Chem. Soc.* 2006, **128**(28)**:** 9000-9001.

97. Duncan TV, Wu SP, Therien MJ. Ethyne-Bridged (Porphinato)Zinc(II)−(Porphinato)Iron(III) Complexes: Phenomenological Dependence of Excited-State Dynamics upon (Porphinato)Iron Electronic Structure. *J. Am. Chem. Soc.* 2006, **128**(32)**:** 10423-10435.

98. Strzalka J, Xu T, Tronin A, Wu SP, Miloradovic I, Kuzmenko I, *et al.* Structural Studies of Amphiphilic 4-Helix Bundle Peptides Incorporating Designed Extended Chromophores for Nonlinear Optical Biomolecular Materials. *Nano Lett.* 2006, **6**(11)**:** 2395-2405.

99. Duncan TV, Frail PR, Miloradovic IR, Therien MJ. Excitation of Highly Conjugated (Porphinato)palladium(II) and (Porphinato)platinum(II) Oligomers Produces Long-Lived, Triplet States at Unit Quantum Yield That Absorb Strongly over Broad Spectral Domains of the NIR. *J. Phys. Chem. B* 2010, **114**(45)**:** 14696-14702.

100. Duncan TV, Rubtsov IV, Uyeda HT, Therien MJ. Highly Conjugated (Polypyridyl)metal−(Porphinato)zinc(II) Compounds: Long-Lived, High Oscillator Strength, Excited-State Absorbers Having Exceptional Spectral Coverage of the Near-Infrared. *J. Am. Chem. Soc.* 2004, **126**(31)**:** 9474-9475.

101. Duncan TV, Ishizuka T, Therien MJ. Molecular Engineering of Intensely Near-Infrared Absorbing Excited States in Highly Conjugated Oligo(porphinato)zinc−(Polypyridyl)metal(II) Supermolecules. *J. Am. Chem. Soc.* 2007, **129**(31)**:** 9691-9703.

102. Duncan TV, Song K, Hung S-T, Miloradovic I, Nayak A, Persoons A, *et al.* Molecular Symmetry and Solution-Phase Structure Interrogated by Hyper-Rayleigh Depolarization Measurements: Elaborating Highly Hyperpolarizable D2-Symmetric Chromophores. *Angew. Chem. Int. Ed.* 2008, **47**(16)**:** 2978-2981.

103. Keinan S, Therien MJ, Beratan DN, Yang W. Molecular Design of Porphyrin-Based Nonlinear Optical Materials. *J. Phys. Chem. A* 2008, **112**(47)**:** 12203-12207.

104. Hu X, Xiao D, Keinan S, Asselberghs I, Therien MJ, Clays K, *et al.* Predicting the Frequency Dispersion of Electronic Hyperpolarizabilities on the Basis of Absorption Data and Thomas−Kuhn Sum Rules. *J. Phys. Chem. C* 2010, **114**(5)**:** 2349-2359.

105. Singh-Rachford TN, Nayak A, Muro-Small ML, Goeb S, Therien MJ, Castellano FN. Supermolecular-Chromophore-Sensitized Near-Infrared-to-Visible Photon Upconversion. *J. Am. Chem. Soc.* 2010, **132**(40)**:** 14203-14211.

106. Kim D. *Multiporphyrin Arrays: Fundamentals and Applications*. Pan Stanford: Singapore, 2012.

107. Panda MK, Ladomenou K, Coutsolelos AG. Porphyrins in bio-inspired transformations: Light-harvesting to solar cell. *Coord. Chem. Rev.* 2012, **256**(21-22)**:** 2601-2627.

108. LeCours SM, DiMagno SG, Therien MJ. Exceptional Electronic Modulation of Porphyrins through meso-Arylethynyl Groups. Electronic Spectroscopy, Electronic Structure, and Electrochemistry of [5,15-Bis[(aryl)ethynyl]- 10,20-diphenylporphinato]zinc(II) Complexes. X-ray Crystal Structures of [5,15-Bis[(4'-fluorophenyl)ethynyl]- 10,20-diphenylporphinato]zinc(II) and 5,15-Bis[(4'-methoxyphenyl)ethynyl]-10,20-diphenylporphyrin. *J. Am. Chem. Soc.* 1996, **118**(47)**:** 11854-11864.

109. LeCours SM, Guan H-W, DiMagno SG, Wang CH, Therien MJ. Push−Pull Arylethynyl Porphyrins: New Chromophores That Exhibit Large Molecular First-Order Hyperpolarizabilities. *J. Am. Chem. Soc.* 1996, **118**(6)**:** 1497-1503.

110. Angiolillo PJ, Rawson J, Frail PR, Therien MJ. The evolution of spin distribution in the photoexcited triplet state of ethyne-elaborated porphyrins. *Chem. Commun.* 2013, **49**(84)**:** 9722-9724.

111. Anderson HL, Wylie AP, Prout K. meso-Tetraalkynylporphyrins. *H. Chem. Soc. Perk. T. 1* 1998(10)**:** 1607-1612.

112. Taylor PN, Wylie AP, Huuskonen J, Anderson HL. Enhanced Electronic Conjugation in Anthracene-Linked Porphyrins. *Angew. Chem. Int. Ed.* 1998, **37**(7)**:** 986-989.

113. Yen W-N, Lo S-S, Kuo M-C, Mai C-L, Lee G-H, Peng S-M, *et al.* Synthesis, Structure, and Optical and Electrochemical Properties of Star-Shaped Porphyrin−Triarylamine Conjugates. *Org. Lett.* 2006, **8**(19)**:** 4239-4242.

114. Kuo M-C, Li L-A, Yen W-N, Lo S-S, Lee C-W, Yeh C-Y. New synthesis of zinc tetrakis(arylethynyl)porphyrins and substituent effects on their redox chemistry. *Dalton Trans.* 2007(14)**:** 1433-1439.

115. Odom SA, Kelley RF, Ohira S, Ensley TR, Huang C, Padilha LA, *et al.* Photophysical Properties of an Alkyne-Bridged Bis(zinc porphyrin)−Perylene Bis(dicarboximide) Derivative. *J. Phys. Chem. A* 2009, **113**(40)**:** 10826-10832.

116. Odom SA, Webster S, Padilha LA, Peceli D, Hu H, Nootz G, *et al.* Synthesis and Two-Photon Spectrum of a Bis(Porphyrin)-Substituted Squaraine. *J. Am. Chem. Soc.* 2009, **131**(22)**:** 7510-7511.

117. Nowak-Król A, Koszarna B, Yoo SY, Chromiński J, Węcławski MK, Lee C-H, *et al.* Synthesis of trans-A2B2-Porphyrins Bearing Phenylethynyl Substituents. *J. Org. Chem.* 2011, **76**(8)**:** 2627-2634.

118. Nowak-Król A, Wilson CJ, Drobizhev M, Kondratuk DV, Rebane A, Anderson HL, *et al.* Amplified Two-Photon Absorption in Trans-A2B2-Porphyrins Bearing Nitrophenylethynyl Substituents. *ChemPhysChem* 2012, **13**(17)**:** 3966-3972.

119. Cho EH, Chae SH, Kim K, Lee SJ, Joo J. Photovoltaic characteristics of organic solar cells using Zn-porphyrin derivatives with controlled π-conjugation structures. *Synth. Met.* 2012, **162**(9-10)**:** 813-819.

120. Hatano J, Obata N, Yamaguchi S, Yasuda T, Matsuo Y. Soluble porphyrin donors for small molecule bulk heterojunction solar cells. *J. Mater. Chem.* 2012, **22**(36)**:** 19258-19263.

121. Huang Y, Li L, Peng X, Peng J, Cao Y. Solution processed small molecule bulk heterojunction organic photovoltaics based on a conjugated donor-acceptor porphyrin. *J. Mater. Chem.* 2012, **22**(41)**:** 21841-21844.

122. Li L, Huang Y, Peng J, Cao Y, Peng X. Enhanced performance of solution-processed solar cells based on porphyrin small molecules with a diketopyrrolopyrrole acceptor unit and a pyridine additive. *J. Mater. Chem. A* 2013, **1**(6)**:** 2144-2150.

123. Yamamoto T, Hatano J, Nakagawa T, Yamaguchi S, Matsuo Y. Small molecule solution-processed bulk heterojunction solar cells with inverted structure using porphyrin donor. *Appl. Phys. Lett.* 2013, **102**(1)**:** 013305/013301-013305/013304.

124. Bessho T, Zakeeruddin SM, Yeh C-Y, Diau EW-G, Grätzel M. Highly Efficient Mesoscopic Dye-Sensitized Solar Cells Based on Donor–Acceptor-Substituted Porphyrins. *Angew. Chem. Int. Ed.* 2010, **49**(37)**:** 6646-6649.

125. Mai C-L, Huang W-K, Lu H-P, Lee C-W, Chiu C-L, Liang Y-R, *et al.* Synthesis and characterization of diporphyrin sensitizers for dye-sensitized solar cells. *Chem. Commun.* 2010, **46**(5)**:** 809-811.

126. Liu Y, Lin H, Dy JT, Tamaki K, Nakazaki J, Nakayama D, *et al.* N-fused carbazole-zinc porphyrin-free-base porphyrin triad for efficient near-IR dye-sensitized solar cells. *Chem. Commun.* 2011, **47**(13)**:** 4010-4012.

127. Li L-L, Diau EW-G. Porphyrin-sensitized solar cells. *Chem. Soc. Rev.* 2013, **42**(1)**:** 291-304.

128. Hamamura T, Dy JT, Tamaki K, Nakazaki J, Uchida S, Kubo T, *et al.* Dye-sensitized solar cells using ethynyl-linked porphyrin trimers. *Phys. Chem. Chem. Phys.* 2014, **16**(10)**:** 4551-4560.

129. Luechai A, Gasiorowski J, Petsom A, Neugebauer H, Sariciftci NS, Thamyongkit P. Photosensitizing porphyrin-triazine compound for bulk heterojunction solar cells. *J. Mater. Chem.* 2012, **22**(43)**:** 23030-23037.

130. Kengthanomma T, Thamyongkit P, Gasiorowski J, Ramil AM, Sariciftci NS. On the potential of porphyrin-spiked triarylamine stars for bulk heterojunction solar cells. *J. Mater. Chem. A* 2013, **1**(35)**:** 10524-10531.

131. Moore KT, Horváth IT, Therien MJ. High-Pressure NMR Studies of (Porphinato)iron-Catalyzed Isobutane Oxidation Utilizing Dioxygen as the Stoichiometric Oxidant. *J. Am. Chem. Soc.* 1997, **119**(7)**:** 1791-1792.

132. Woller EK, DiMagno SG. 2,3,7,8,12,13,17,18-Octafluoro-5,10,15,20-tetraarylporphyrins and Their Zinc Complexes: First Spectroscopic, Electrochemical, and Structural Characterization of a Perfluorinated Tetraarylmetalloporphyrin. *J. Org. Chem.* 1997, **62**(6)**:** 1588-1593.

133. Moore KT, Fletcher JT, Therien MJ. Syntheses, NMR and EPR Spectroscopy, Electrochemical Properties, and Structural Studies of [5,10,15,20-Tetrakis(perfluoroalkyl)porphinato]iron(II) and -iron(III) Complexes. *J. Am. Chem. Soc.* 1999, **121**(22)**:** 5196-5209.

134. Stalder R, Mei J, Graham KR, Estrada LA, Reynolds JR. Isoindigo, a Versatile Electron-Deficient Unit For High-Performance Organic Electronics. *Chem. Mater.* 2014, **26**(1)**:** 664-678.

135. Lei T, Wang J-Y, Pei J. Design, Synthesis, and Structure–Property Relationships of Isoindigo-Based Conjugated Polymers. *Acc. Chem. Res.* 2014, **47**(4)**:** 1117-1126.

136. Wang E, Mammo W, Andersson MR. 25th Anniversary Article: Isoindigo-Based Polymers and Small Molecules for Bulk Heterojunction Solar Cells and Field Effect Transistors. *Adv. Mater.* 2014, **26**(12)**:** 1801-1826.

137. Ashraf RS, Kronemeijer AJ, James DI, Sirringhaus H, McCulloch I. A new thiophene substituted isoindigo based copolymer for high performance ambipolar transistors. *Chem. Commun.* 2012, **48**(33)**:** 3939-3941.

138. Lei T, Dou J-H, Ma Z-J, Yao C-H, Liu C-J, Wang J-Y, *et al.* Ambipolar polymer field-effect transistors based on fluorinated isoindigo: high performance and improved ambient stability. *J. Am. Chem. Soc.* 2012, **134**(49)**:** 20025-20028.

139. Grenier F, Berrouard P, Pouliot J-R, Tseng H-R, Heeger AJ, Leclerc M. Synthesis of new n-type isoindigo copolymers. *Polym. Chem.* 2013, **4**(6)**:** 1836-1841.

140. Lei T, Dou J-H, Ma Z-J, Liu C-J, Wang J-Y, Pei J. Chlorination as a useful method to modulate conjugated polymers: balanced and ambient-stable ambipolar high-performance field-effect transistors and inverters based on chlorinated isoindigo polymers. *Chem. Sci.* 2013, **4**(6)**:** 2447-2452.

141. Liu B, Zou Y, Peng B, Zhao B, Huang K, He Y, *et al.* Low bandgap isoindigo-based copolymers: design, synthesis and photovoltaic applications. *Polym. Chem.* 2011, **2**(5)**:** 1156-1162.

142. Ma Z, Wang E, Vandewal K, Andersson MR, Zhang F. Enhance performance of organic solar cells based on an isoindigo-based copolymer by balancing absorption and miscibility of electron acceptor. *Appl. Phys. Lett.* 2011, **99**(14)**:** 143302.

143. Zhang G, Fu Y, Xie Z, Zhang Q. Synthesis and photovoltaic properties of new low bandgap isoindigo-based conjugated polymers. *Macromol.* 2011, **44**(6)**:** 1414-1420.

144. Wang E, Ma Z, Zhang Z, Vandewal K, Henriksson P, Inganas O, *et al.* An Easily Accessible Isoindigo-Based Polymer for High-Performance Polymer Solar Cells. *J. Am. Chem. Soc.* 2011, **133**(36)**:** 14244-14247.

145. Wang E, Ma Z, Zhang Z, Henriksson P, Inganaes O, Zhang F, *et al.* An isoindigo-based low band gap polymer for efficient polymer solar cells with high photo-voltage. *Chem. Commun.* 2011, **47**(17)**:** 4908-4910.

146. Ma Z, Wang E, Jarvid ME, Henriksson P, Inganaes O, Zhang F, *et al.* Synthesis and characterization of benzodithiophene-isoindigo polymers for solar cells. *J. Mater. Chem.* 2012, **22**(5)**:** 2306-2314.

147. Hu C, Fu Y, Li S, Xie Z, Zhang Q. Synthesis and photovoltaic properties of new conjugated polymers based on syn- and anti-benzodifuran. *Polym. Chem.* 2012, **3**(10)**:** 2949-2955.

148. Stalder R, Grand C, Subbiah J, So F, Reynolds JR. An isoindigo and dithieno[3,2-b:2',3'-d]silole copolymer for polymer solar cells. *Polym. Chem.* 2012, **3**(1)**:** 89-92.

149. Vandewal K, Ma Z, Bergqvist J, Tang Z, Wang E, Henriksson P, *et al.* Quantification of Quantum Efficiency and Energy Losses in Low Bandgap Polymer:Fullerene Solar Cells with High Open-Circuit Voltage. *Adv. Funct. Mater.* 2012, **22**(16)**:** 3480-3490.

150. Cao K, Wu Z, Li S, Sun B, Zhang G, Zhang Q. A low bandgap polymer based on isoindigo and bis(dialkylthienyl)benzodithiophene for organic photovoltaic applications. *J. Polym. Sci., Part A: Polym. Chem.* 2013, **51**(1)**:** 94-100, S194/101-S194/108.

151. Chen MS, Niskala JR, Unruh DA, Chu CK, Lee OP, Fréchet JMJ. Control of Polymer-Packing Orientation in Thin Films through Synthetic Tailoring of Backbone Coplanarity. *Chem. Mater.* 2013, **25**(20)**:** 4088-4096.

152. Dang D, Chen W, Yang R, Zhu W, Mammo W, Wang E. Fluorine substitution enhanced photovoltaic performance of a D-A1-D-A2 copolymer. *Chem. Commun.* 2013, **49**(81)**:** 9335-9337.

153. Ho C-C, Chang S-Y, Huang T-C, Chen C-A, Liao H-C, Chen Y-F, *et al.* Synthesis, characterization and photovoltaic properties of poly(cyclopentadithiophene-alt-isoindigo). *Polym. Chem.* 2013, **4**(20)**:** 5351-5360.

154. Mahmood K, Liu Z-P, Li C, Lu Z, Fang T, Liu X, *et al.* Novel isoindigo-based conjugated polymers for solar cells and field effect transistors. *Polym. Chem.* 2013, **4**(12)**:** 3563-3574.

155. Sonar P, Tan H-S, Sun S, Lam YM, Dodabalapur A. Isoindigo dye incorporated copolymers with naphthalene and anthracene: promising materials for stable organic field effect transistors. *Polym. Chem.* 2013, **4**(6)**:** 1983-1994.

156. Wan M, Zhu H, Deng H, Jin L, Guo J, Huang Y. Low band-gap modulation of isoindigo-based copolymers toward high open-circuit voltage of polymer solar cells. *J. Polym. Sci., Part A: Polym. Chem.* 2013, **51**(16)**:** 3477-3485.

157. Wang C, Zhao B, Cao Z, Shen P, Tan Z, Li X, *et al.* Enhanced power conversion efficiencies in bulk heterojunction solar cells based on conjugated polymer with isoindigo side chain. *Chem. Commun.* 2013, **49**(37)**:** 3857-3859.

158. Xu X, Cai P, Lu Y, Choon NS, Chen J, Hu X, *et al.* Synthesis and characterization of thieno[3,2-b]thiophene-isoindigo-based copolymers as electron donor and hole transport materials for bulk-heterojunction polymer solar cells. *J. Polym. Sci., Part A: Polym. Chem.* 2013, **51**(2)**:** 424-434.

159. Graham KR, Mei J, Stalder R, Shim JW, Cheun H, Steffy F, *et al.* Polydimethylsiloxane as a macromolecular additive for enhanced performance of molecular bulk heterojunction organic solar cells. *ACS Appl. Mater. Interfaces* 2011, **3**(4)**:** 1210-1215.

160. Graham KR, Wieruszewski PM, Stalder R, Hartel MJ, Mei J, So F, *et al.* Improved Performance of Molecular Bulk-Heterojunction Photovoltaic Cells through Predictable Selection of Solvent Additives. *Adv. Funct. Mater.* 2012, **22**(22)**:** 4801-4813.

161. Elsawy W, Lee C-L, Cho S, Oh S-H, Moon S-H, Elbarbary A, *et al.* Isoindigo-based small molecules for high-performance solution-processed organic photovoltaic devices: the electron donating effect of the donor group on photophysical properties and device performance. *Phys. Chem. Chem. Phys.* 2013, **15**(36)**:** 15193-15203.

162. Karakawa M, Aso Y. Narrow-optical-gap π-conjugated small molecules based on terminal isoindigo and thienoisoindigo acceptor units for photovoltaic application. *RSC Adv.* 2013, **3**(37)**:** 16259-16263.

163. Liu Q, Du Z, Chen W, Sun L, Chen Y, Sun M, *et al.* Low HOMO isoindigo based small molecule for high open-circuit voltage 1.0 V solution processed organic solar cells. *Synth. Met.* 2013, **178:** 38-43.

164. Wang T, Chen Y, Bao X, Du Z, Guo J, Wang N, *et al.* A new isoindigo-based molecule with ideal energy levels for solution-processable organic solar cells. *Dyes Pigm.* 2013, **98**(1)**:** 11-16.

165. Yang M, Chen X, Zou Y, Pan C, Liu B, Zhong H. A solution-processable D-A-D small molecule based on iso-indigo for organic solar cells. *J. Mater. Sci.* 2013, **48**(3)**:** 1014-1020.

166. Yassin A, Leriche P, Allain M, Roncali J. Donor-acceptor-donor (D-A-D) molecules based on isoindigo as active material for organic solar cells. *New J. Chem.* 2013, **37**(2)**:** 502-507.

167. Stalder R, Mei J-G, Subbiah J, Grand C, Estrada LA, So F, *et al.* n-Type Conjugated Polyisoindigos. *Macromol.* 2011, **44**(16)**:** 6303-6310.

168. Lunak S, Jr., Horakova P, Lycka A. Absorption and fluorescence of arylmethylidenoxindoles and isoindigo. *Dyes Pigm.* 2010, **85**(3)**:** 171-176.

169. Wienk MM, Kroon JM, Verhees WJH, Knol J, Hummelen JC, van Hal PA, *et al.* Efficient Methano[70]fullerene/MDMO-PPV Bulk Heterojunction Photovoltaic Cells. *Angew. Chem. Int. Ed.* 2003, **42**(29)**:** 3371-3375.

170. Xu T, Wu SP, Miloradovic I, Therien MJ, Blasie JK. Incorporation of Designed Extended Chromophores into Amphiphilic 4-Helix Bundle Peptides for Nonlinear Optical Biomolecular Materials. *Nano Lett.* 2006, **6**(11)**:** 2387-2394.

171. Gouterman M. Spectra of porphyrins. *J. Mol. Spectrosc.* 1961, **6**(0)**:** 138-163.

172. Takacs CJ, Sun Y, Welch GC, Perez LA, Liu X, Wen W, *et al.* Solar Cell Efficiency, Self-Assembly, and Dipole–Dipole Interactions of Isomorphic Narrow-Band-Gap Molecules. *J. Am. Chem. Soc.* 2012, **134**(40)**:** 16597-16606.

173. Weller A. Photoinduced Electron Transfer in Solution: Exciplex and Radical Ion Pair Formation Free Enthalpies and their Solvent Dependence. *Z. Phys. Chem.* 1982, **133**(1)**:** 93-98.

174. Juris A, Balzani V, Barigelletti F, Campagna S, Belser P, von Zelewsky A. Ru(II) polypyridine complexes: photophysics, photochemistry, eletrochemistry, and chemiluminescence. *Coord. Chem. Rev.* 1988, **84**(0)**:** 85-277.

175. Rand BP, Burk DP, Forrest SR. Offset energies at organic semiconductor heterojunctions and their influence on the open-circuit voltage of thin-film solar cells. *Phys. Rev. B* 2007, **75**(11)**:** 115327.

176. Veldman D, Meskers SCJ, Janssen RAJ. The Energy of Charge-Transfer States in Electron Donor–Acceptor Blends: Insight into the Energy Losses in Organic Solar Cells. *Adv. Funct. Mater.* 2009, **19**(12)**:** 1939-1948.

177. Dimitrov SD, Durrant JR. Materials Design Considerations for Charge Generation in Organic Solar Cells. *Chem. Mater.* 2014, **26**(1)**:** 616-630.

178. Several competing values for the Fc/Fc+ work function are prevalent in the literature. By selecting one and applying it uniformly to our own potentiometric data referenced to an internal standard we hope to minimize ambiguity. For more, see Cardona, C. M.; Li, W.; Kaifer, A. E.; Stockdale, D.; Bazan, G. C. Adv. Mater. 2011, 23, 2367.

179. Bloking JT, Han X, Higgs AT, Kastrop JP, Pandey L, Norton JE*, et al.* Solution-Processed Organic Solar Cells with Power Conversion Efficiencies of 2.5% using Benzothiadiazole/Imide-Based Acceptors. *Chem. Mater.* 2011, **23**(24)**:** 5484-5490.

180. Zhou Y, Dai Y-Z, Zheng Y-Q, Wang X-Y, Wang J-Y, Pei J. Non-fullerene acceptors containing fluoranthene-fused imides for solution-processed inverted organic solar cells. *Chem. Commun.* 2013, **49**(51)**:** 5802-5804.

181. Winzenberg KN, Kemppinen P, Scholes FH, Collis GE, Shu Y, Birendra Singh T, *et al.* Indan-1,3-dione electron-acceptor small molecules for solution-processable solar cells: a structure-property correlation. *Chem. Commun.* 2013, **49**(56)**:** 6307-6309.

182. Yan Q, Zhou Y, Zheng Y-Q, Pei J, Zhao D. Towards rational design of organic electron acceptors for photovoltaics: a study based on perylenediimide derivatives. *Chem. Sci.* 2013, **4**(12)**:** 4389-4394.

183. Kim HU, Kim J-H, Suh H, Kwak J, Kim D, Grimsdale AC*, et al.* High open circuit voltage organic photovoltaic cells fabricated using 9,9[prime or minute]-bifluorenylidene as a non-fullerene type electron acceptor. *Chem. Commun.* 2013, **49**(93)**:** 10950-10952.

184. Douglas JD, Chen MS, Niskala JR, Lee OP, Yiu AT, Young EP*, et al.* Solution-Processed, Molecular Photovoltaics that Exploit Hole Transfer from Non Fullerene, n-Type Materials. *Adv. Mater.* 2014, **26**(27)**:** 4606-4606.

185. Mao Z, Senevirathna W, Liao J-Y, Gu J, Kesava SV, Guo C*, et al.* Azadipyrromethene-Based Zn(II) Complexes as Nonplanar Conjugated Electron Acceptors for Organic Photovoltaics. *Adv. Mater.* 2014, **26**(36)**:** 6290-6294.

186. Zhang Y, Pandey AK, Tandy K, Dutta GK, Burn PL, Meredith P, *et al.* Channel II photocurrent quantification in narrow optical gap polymer-fullerene solar cells with complimentary acceptor absorption. *Appl. Phys. Lett.* 2013, **102**(22)**:** 223302.

187. Fang Y, Pandey AK, Nardes AM, Kopidakis N, Burn PL, Meredith P. A Narrow Optical Gap Small Molecule Acceptor for Organic Solar Cells. *Adv. Energy Mater.* 2013, **3**(1)**:** 54-59.

188. Pho TV, Toma FM, Tremolet de Villers BJ, Wang S, Treat ND, Eisenmenger ND, *et al.* Decacyclene Triimides: Paving the Road to Universal Non-Fullerene Acceptors for Organic Photovoltaics. *Adv. Energy Mater.* 2014, **4**(5)**:** 1301007.

189. Brabec CJ, Winder C, Sariciftci NS, Hummelen JC, Dhanabalan A, van Hal PA, *et al.* A Low-Bandgap Semiconducting Polymer for Photovoltaic Devices and Infrared Emitting Diodes. *Adv. Funct. Mater.* 2002, **12**(10)**:** 709-712.

190. Brédas J-L, Beljonne D, Coropceanu V, Cornil J. Charge-Transfer and Energy-Transfer Processes in π-Conjugated Oligomers and Polymers: A Molecular Picture. *Chem. Rev.* 2004, **104**(11)**:** 4971-5004.

191. Scharber MC, Mühlbacher D, Koppe M, Denk P, Waldauf C, Heeger AJ, *et al.* Design Rules for Donors in Bulk-Heterojunction Solar Cells—Towards 10 % Energy-Conversion Efficiency. *Adv. Mater.* 2006, **18**(6)**:** 789-794.

192. Su Y-W, Lan S-C, Wei K-H. Organic photovoltaics. *Mater. Today* 2012, **15**(12)**:** 554-562.

193. Dennington R, Keith T, Millam J. Gaussview, Version 5. Shawnee Mission, KS: Semichem Inc.; 2009.

194. O'Boyle NM, Tenderholt AL, Langner KM. cclib: A library for package-independent computational chemistry algorithms. *J. Comput. Chem.* 2008, **29**(5)**:** 839-845.

195. Mulliken RS. Electronic Population Analysis on LCAO[Single Bond]MO Molecular Wave Functions. I. *J. Chem. Phys.* 1955, **23**(10)**:** 1833-1840.

196. Humphrey W, Dalke A, Schulten K. VMD: visual molecular dynamics. *J. Mol. Graph.* 1996, **14**(1)**:** 33-38, 27-38.

197. Fletcher JT, Therien MJ. Extreme Electronic Modulation of the Cofacial Porphyrin Structural Motif. *J. Am. Chem. Soc.* 2002, **124**(16)**:** 4298-4311.

198. Tse MK, Zhou Z-y, Mak TCW, Chan KS. Regioselective Bromination and Subsequent Suzuki Cross-Coupling of Highly Electron Deficient 5,10,15,20-Tetrakis(trifluoromethyl)porphyrin. *Tetrahedron* 2000, **56**(39)**:** 7779-7783.

199. Shimizu S, Aratani N, Osuka A. meso-Trifluoromethyl-Substituted Expanded Porphyrins. *Chem. Eur. J.* 2006, **12**(18)**:** 4909-4918.

200. Wijesekera TP. 5-Perfluoroalkyldipyrromethanes and porphyrins derived therefrom. *Can. J. Chem.* 1996, **74**(10)**:** 1868-1871.

201. Laha JK, Dhanalekshmi S, Taniguchi M, Ambroise A, Lindsey JS. A Scalable Synthesis of Meso-Substituted Dipyrromethanes. *Org. Process Res. Dev.* 2003, **7**(6)**:** 799-812.

202. Saito S, Osuka A. N-Fusion Reaction Sequence of Heptaphyrin(1.1.1.1.1.1.1): Singly, Doubly, and Quadruply N-Fused Heptaphyrins. *Chem. Eur. J.* 2006, **12**(35)**:** 9095-9102.

203. Mori H, Aratani N, Osuka A. Synthesis of A2B6-Type [36]Octaphyrins: Copper(II)-Metalation-Induced Fragmentation Reactions to Porphyrins and N-Fusion Reactions of meso-(3-Thienyl) Substituents. *Chem. Asian J.* 2012, **7**(6)**:** 1340-1346.

204. Nudy LR, Hutchinson HG, Schieber C, Longo FR. A study of bromoporphins. *Tetrahedron* 1984, **40**(12)**:** 2359-2363.

205. Chumakov DE, Khoroshutin AV, Anisimov AV, Kobrakov KI. Bromination of Porphyrins. *Chem. Heterocycl. Compd.* 2009, **45**(3)**:** 259-283.

206. Callot HJ, Schaeffer E. *J. Chem. Res., Synop.* 1978, **1978:** 51.

207. Bonnett R, Campion-Smith IH, Kozyrev AN, Mironov AF. The Bromination and Iodination of Porphyrins. *J. Chem. Res., Synop.* 1990, **1990:** 138-139.

208. Bonnett R, Campion-Smith IH, Kozyrev AN, Mironov AF. Bromination and Iodination of Porphyrins. *Journal of Chemical Research (M)* 1990, **1990:** 1015-1043.

209. Parr RG, Yang W. Density functional approach to the frontier-electron theory of chemical reactivity. *J. Am. Chem. Soc.* 1984, **106**(14)**:** 4049-4050.

210. Bultinck P, Fias S, Alsenoy CV, Ayers PW, Carbo-Dorca R. Critical thoughts on computing atom condensed Fukui functions. *J. Chem. Phys.* 2007, **127**(3)**:** 034102.

211. Yang W, Mortier WJ. The use of global and local molecular parameters for the analysis of the gas-phase basicity of amines. *J. Am. Chem. Soc.* 1986, **108**(19)**:** 5708-5711.

212. Langenaeker W, Demel K, Geerlings P. Quantum-chemical study of the Fukui function as a reactivity index: Part 2. Electrophilic substitution on mono-substituted benzenes. *J. Mol. Struct.-THEOCHEM* 1991, **234**(0)**:** 329-342.

213. Anderson JSM, Melin J, Ayers PW. Conceptual Density-Functional Theory for General Chemical Reactions, Including Those That Are Neither Charge- nor Frontier-Orbital-Controlled. 2. Application to Molecules Where Frontier Molecular Orbital Theory Fails. *J. Chem. Theory Comput.* 2007, **3**(2)**:** 375-389.

214. Anderson JSM, Melin J, Ayers PW. Conceptual Density-Functional Theory for General Chemical Reactions, Including Those That Are Neither Charge- nor Frontier-Orbital-Controlled. 1. Theory and Derivation of a General-Purpose Reactivity Indicator. *J. Chem. Theory Comput.* 2007, **3**(2)**:** 358-374.

215. Foster JP, Weinhold F. Natural hybrid orbitals. *J. Am. Chem. Soc.* 1980, **102**(24)**:** 7211-7218.

216. Reed AE, Curtiss LA, Weinhold F. Intermolecular interactions from a natural bond orbital, donor-acceptor viewpoint. *Chem. Rev.* 1988, **88**(6)**:** 899-926.

217. Reed AE, Weinhold F. Natural bond orbital analysis of near-Hartree--Fock water dimer. *J. Chem. Phys.* 1983, **78**(6)**:** 4066-4073.

218. Reed AE, Weinstock RB, Weinhold F. Natural population analysis. *J. Chem. Phys.* 1985, **83**(2)**:** 735-746.

219. Beck ME. Do Fukui Function Maxima Relate to Sites of Metabolism? A Critical Case Study. *J. Chem. Inf. Model.* 2005, **45**(2)**:** 273-282.

220. Cárdenas-Jirón GI. Reactivity descriptors applied to the study of cobalt porphyrin and their aza derivatives. *Int. J. Quantum Chem.* 2003, **91**(3)**:** 389-397.

221. Feng X-T, Yu J-G, Liu R-Z, Lei M, Fang W-H, Proft FD, *et al.* Why Iron? A Spin-Polarized Conceptual Density Functional Theory Study on Metal-Binding Specificity of Porphyrin. *J. Phys. Chem. A* 2010, **114**(21)**:** 6342-6349.

222. Zhao L, Qi D, Zhang L, Bai M, Cai X. Electronic structures, spectroscopic properties, and reaction activities of porphyrins with alkali metal ions: density

functional theory approach to the central metal effects. *J. Porphyr. Phthalocya.* 2012, **16**(07n08)**:** 927-934.

223. Kolling OW. Comparison of donor-acceptor parameters in nonaqueous solvents. *Anal. Chem.* 1982, **54**(2)**:** 260-264.

224. Nappa M, Valentine JS. The influence of axial ligands on metalloporphyrin visible absorption spectra. Complexes of tetraphenylporphinatozinc. *J. Am. Chem. Soc.* 1978, **100**(16)**:** 5075-5080.

225. Wang MYR, Hoffman BM. Systematic trends in metalloporphyrin optical spectra. *J. Am. Chem. Soc.* 1984, **106**(15)**:** 4235-4240.

226. Stephan D, Gorgues A, Belyasmine A, Le Coq A. Acetylenedicarbaldehyde: isolation and some examples of exclusive dienophilicity under neutral conditions. *J. Chem. Soc. Chem. Comm.* 1988(4)**:** 263-264.

227. Gorgues A, Simon A, Le Coq A, Hercouet A, Corre F. Versatilite de reactivite de l`acetylene dicarbaldehyde et des aldehydes α-acetyleniques a l'egard des dienes conjugues cycliques et heterocycliques en milieu acide. *Tetrahedron* 1986, **42**(1)**:** 351-370.

228. Poncini L. A Convenient Synthesis of Phenylpropargylaldehyde Diethyl Acetal. *Liebigs Ann. Chem.* 1984, **1984**(8)**:** 1529-1530.

229. Cavaleiro JAS, Smith KM. Transformation of chlorins into bile pigment analogues. *H. Chem. Soc. Perk. T. 1* 1973(0)**:** 2149-2155.

230. Bonnett R, Dimsdale MJ, Stephenson GF. The meso-reactivity of porphyrins and related compounds. Part IV. Introduction of oxygen functions. *J. Chem. Soc. C* 1969(4)**:** 564-570.

231. Barnett GH, Evans B, Smith KM. Meso-oxidation of some metalloporphyrins. *Tetrahedron* 1975, **31**(21)**:** 2711-2717.

232. Clezy P, Smythe G. The chemistry of pyrrolic compounds. VIII. Dipyrrylthiones. *Aust. J. Chem.* 1969, **22**(1)**:** 239-249.

233. Plater MJ, Aiken S, Bourhill G. A new synthetic route to donor–acceptor porphyrins. *Tetrahedron* 2002, **58**(12)**:** 2405-2413.

234. Clezy P, Liepa A, Smythe G. The chemistry of pyrrolic compounds. X. A contribution to the chemistry of the oxyporphyrins. *Aust. J. Chem.* 1970, **23**(3)**:** 603-618.

235. Khoury RG, Jaquinod L, Paolesse R, Smith KM. New chemistry of oxophlorins (oxyporphyrins) and their π-radicals. *Tetrahedron* 1999, **55**(22)**:** 6713-6732.

236. John Plater M, Aiken S, Bourhill G. Metallated porphyrins containing lead(II), copper(II) or zinc(II). *Tetrahedron* 2002, **58**(12)**:** 2415-2422.

237. Wavefunction I. Spartan Student. Irvine, CA; 2010.

238. Glendening ED, Reed AE, Carpenter JE, Weinhold F. NBO Version 3.1.

Biography

Jeff Rawson was born in Metarie, LA in December of 1978. He grew up in St. Petersburg, Florida, where he attended the Canterbury School and graduated valedictorian. As a student at Bard College, he won the Charles and June Patrick Award, but note that winning an athletic award at Bard College is akin to being voted 'cleverest moron'. Jeff's undergraduate career was otherwise undistinguished, but he did discover a love of organic chemistry and, through an REU fellowship in the lab of David Bergbreiter at Texas A&M, a love of research. At the University of Vermont, Jeff worked in the lab of Thomas Hughes, eventually earning a Master's degree. He has also worked as a substitute teacher, a painter, a carpenter, and a janitor.

At Duke University, Jeff has studied under the mentorship of Michael Therien. He has enjoyed the generous support of a Zielek Fellowship for three semesters, and his poster entitled 'Tailoring porphyrin-based electron acceptors for organic photovoltaics' was selected for the Sci-Mix session at the ACS National Meeting in Philadelphia in August 2012. He eagerly anticipates moving with his wife Rachael and his son Julius to Germany to work with Paul Kögerler at Forschungszentrum Jülich in early 2015.